



**IAEA**  
International Atomic Energy Agency

**INDC(NDS)-0608**  
Distr. AI+MN+NM

# **INDC International Nuclear Data Committee**

Summary Report

Second Research Coordination Meeting on

## **Prompt Fission Neutron Spectra of Major Actinides**

IAEA Headquarters  
Vienna, Austria

13 – 16 December 2011

Prepared by

R. Capote Noy  
IAEA Nuclear Data Section  
Vienna, Austria

September 2013

Selected INDC documents may be downloaded in electronic form from  
<https://www-nds.iaea.org/publications/>  
or sent as an e-mail attachment.

Requests for hardcopy or e-mail transmittal should be directed to  
[NDS.Contact-Point@iaea.org](mailto:NDS.Contact-Point@iaea.org)

or to:

Nuclear Data Section  
International Atomic Energy Agency  
Vienna International Centre  
PO Box 100  
A-1400 Vienna  
Austria

Produced by the IAEA in Austria

September 2013

Summary Report  
Second Research Coordination Meeting on  
**Prompt Fission Neutron Spectra of Major Actinides**

IAEA Headquarters  
Vienna, Austria

13 – 16 December 2011

Prepared by

R. Capote Noy  
IAEA Nuclear Data Section  
Vienna, Austria

### **Abstract**

A summary is given of the Second Research Coordination Meeting on *Prompt Fission Neutron Spectra of Actinides*. Experimental data and modelling methods on prompt fission neutron spectra were reviewed. Extensive technical discussions held on theoretical methods to calculate prompt fission spectra. Detailed coordinated research proposals have been agreed. Summary reports of selected technical presentations at the meeting are given. The resulting work plan of the Coordinated Research Programme is summarized, along with actions and deadlines.

September 2013



## TABLE OF CONTENTS

1. Introduction.....	7
2. Experimental data .....	8
3. Theory & Modeling .....	8
4. Evaluations.....	9
5. Benchmarking and dosimetry .....	9
6. Conclusions.....	9

### APPENDICES:

AGENDA.....	11
LIST OF PARTICIPANTS .....	13
MEETING PHOTO .....	15
ADDITIONAL DOCUMENTS .....	17



## 1. Introduction

The energy spectrum of prompt neutrons emitted in fission plays an important role in many applications in nuclear science. In particular, accurate predictions of nuclear criticality using neutron transport codes are dependent on the underlying nuclear data, especially the fission spectrum. While the accuracy of fission cross sections and neutron multiplicities (nubar) in the relevant energy range have been steadily improved, we are faced with the situation that existing measured prompt fission neutron spectra (PFNS) are in many cases discrepant, and that different PFNS theoretical models give differing predictions.

In November 2008, a Consultants' Meeting (CM) was organised in Vienna to review and discuss the adequacy and quality of the recommended prompt fission neutron spectra to be found in existing nuclear data applications libraries<sup>1</sup>. These prompt fission neutron spectra were judged to be inadequate. Therefore, the meeting participants strongly recommended initiating a new IAEA Coordinated Research Project (CRP) on prompt fission neutron spectra evaluations. The proposed goal was to determine the prompt fission neutron spectra and covariance matrices for actinides in the energy range from thermal to 20 MeV, including validation against integral critical assembly (k-eff) and dosimetry data.

The Coordinated Research Project (CRP) "Prompt Fission Neutron Spectra for Actinides" started in 2010. Its first Research Coordination Meeting (RCM) was held at IAEA Headquarters, Vienna, Austria 6–9 April 2010. Experimental data and modelling methods on prompt fission neutron spectra were reviewed. The programme to compile and evaluate prompt fission spectra including uncertainty information over the neutron energy range from thermal to 20 MeV was proposed. Validation of the resulting data against integral critical assembly and dosimetry data was foreseen. A summary report of that meeting was published as an IAEA(NDS)-0571 technical report<sup>2</sup> (available online at <https://www-nds.iaea.org/publications/indc/indc-nds-0571.pdf>).

The second RCM of the CRP was held at IAEA Headquarters, Vienna, Austria 13–16 December 2011 and was attended by fifteen CRP participants. The IAEA was represented by N. Otsuka and R. Capote, who served as Scientific Secretary. T. Ohsawa (Kinki University, Japan) was elected Chairman of the meeting and P. Talou (LANL, USA) as the rapporteur. The approved Agenda is attached as an Appendix 1 and the list of participants with affiliations as an Appendix 2. Summary reports of presentations given by meeting participants including relevant figures can be found in Appendix 3. All presentations from the meeting are available online at <https://www-nds.iaea.org/index-meeting-crp/PFNS-2RCM/>.

Within the CRP following nuclei have been studied:

- major actinides <sup>235,238</sup>U and <sup>239</sup>Pu;
- <sup>232</sup>Th, <sup>233</sup>U, and <sup>234</sup>U of relevance to the Th-U fuel cycle;

In addition, evaluations will also be available for all remaining nuclei in the uranium, and plutonium isotopic chains.

---

<sup>1</sup> R. Capote, V. Maslov, E. Bauge, T. Ohsawa, A. Vorobyev, M.B. Chadwick and S. Oberstedt, *Summary Report of Consultants' Meeting on Prompt Fission Neutron Spectra of Major Actinides*, INDC(NDS)-0541 (IAEA, Vienna, Austria, January 2009)

<sup>2</sup> R. Capote Noy, *Summary Report of the First Research Coordination Meeting on Prompt Fission Neutron Spectra of Major Actinides*, INDC(NDS)-0571 (IAEA, Vienna, Austria, December 2010)

The structure of the final document of the CRP was discussed and it was agreed that it should contain following chapters:

- 1- Introduction/overview
- 2- Experiments
- 3- Modeling (Los Alamos Model, Monte Carlo methods, ...)
- 4- Evaluations (spectrum + covariances)
- 5- Benchmarks
- 6- Open Questions

Participants also recommended holding a satellite meeting to review the progress of the project and outstanding issues at International Conference on Nuclear Data for Science and Technology-ND2013, New York in March 2013.

The actions to be undertaken prior to the final RCM which will be held in the fall of 2013 were agreed together with their relative time-schedule and deadlines (default deadline for all actions is the next RCM, if not otherwise stated). The assigned actions together with deadlines and recommendations as agreed by all CRP participants are summarized below.

## 2. Experimental data

Goal: Finalize experimental database of PFNS, in complement of what has been done so far for  $n+^{235}\text{U}$ ,  $n+^{239}\text{Pu}$ , and  $^{252}\text{Cf}(sf)$ . The database should contain tables of spectrum values (energy- midpoint or bin limits, spectrum, uncertainty) and correlation information if possible.

Experimentalists in charge of the following isotopes:

- **Vorobyev**  $^{233}\text{U}$
- **Kornilov**  $^{235}\text{U}$
- **Oberstedt**  $^{238}\text{U}$
- **Granier**  $^{239}\text{Pu}$
- **Nuclear Data Section**  $^{232}\text{Th}$

Data should cover incident neutron energies from thermal up to 20 MeV.

Other Actions:

- **Vorobyev** - send preliminary data on  $^{233}\text{U}$  to IAEA
- **Vorobyev** - send  $^{252}\text{Cf}(sf)$  data for fixed angles to IAEA
- **Granier** - send preliminary data on  $^{238}\text{U}$  to IAEA
- **Capote** - add memo CP-D/635 (list of EXFOR entries) from Otsuka to web site.

## 3. Theory & Modeling

- **Talou, Vogt, Serot, Schmidt, Shu, Kornilov** - Monte Carlo calculations to be performed for  $n_{\text{th}}+^{235}\text{U}$ ,  $n_{\text{th}}+^{239}\text{Pu}$  and  $^{252}\text{Cf}(sf)$ .
- Pre-neutron emission fission fragment yields  $Y(A,Z,TKE)$  to be sent to IAEA by **Talou** -  $n_{\text{th}}+^{239}\text{Pu}$ ; **Serot** -  $^{252}\text{Cf}(sf)$ ; and **Schmidt** -  $n_{\text{th}}+^{235}\text{U}$ .
- **Talou, Vogt, Serot, Schmidt, Shu, Kornilov** - Provide results of MC calculations for PFNS,  $\langle v \rangle$ ,  $\langle v \rangle(A)$ ,  $\langle v \rangle(TKE)$ ,  $P(v)$ , lab PFNS at different angles (**2 months before final RCM**)
- **Schmidt** - write draft of introduction text on Monte Carlo approach.

#### 4. Evaluations

- Evaluations to be performed for  $n+^{233}\text{U}$ ,  $^{235}\text{U}$ ,  $^{238}\text{U}$ ,  $^{239}\text{Pu}$ , and  $^{232}\text{Th}$  for incident neutron energies from thermal up to 20 MeV, and for outgoing energies from 1 keV to 20 MeV. Both mean values and uncertainties if possible (**all evaluators**).
- Provide PFNS covariance matrices for  $^{235}\text{U}$ ,  $^{238}\text{U}$  and  $^{239}\text{Pu}$  for thermal incident neutron energy (**Talou**).

#### 5. Benchmarking and dosimetry

- Compile list of benchmarks (with documentation) to be used in CRP
- Provide whole dosimetry files (IRDF-2002 + new IRDFF) on CRP web site (NDS)
- Provide code to compute C/E spectrum-averaged cross sections (NDS)
- Provide Excel file of integral experimental data from Mannhart (NDS)

#### 6. Conclusions

Presentations and discussions during the meeting showed a good progress of on-going CRP work. Much work needs to be done in the next 15 months so that the CRP goals can be achieved. Co-ordinated programme of work was agreed among the participants, leading to several additional actions to be undertaken. Technical issues related to the fission physics to be considered in employed models were extensively debated. The output of the CRP in terms of expected evaluations was defined, including an updated set of PFNS evaluations for major and selected minor actinides.





**2<sup>nd</sup> Research Coordination Meeting on**

***“Prompt Fission Neutron Spectra of Actinides”***

IAEA Headquarters, Vienna, Austria  
13 – 16 December 2011

Conference Room A0531

**AGENDA**

**Tuesday, 13 December**

- 08:30 - 09:30**      **Registration** (IAEA Registration desk, Gate 1)
- 09:30 - 10:00**      **Opening Session**  
Welcoming address  
Introductory Remarks (R. Capote Noy)  
Election of Chairman and Rapporteur  
Adoption of Agenda
- 10:00 - 10:45*      *Administrative and Financial Matters related to participants, Coffee break*
- 10:45 - 12:30**      **Session 1: Presentations**
- 1) *Global approach to fission-fragment prompt-neutron and gamma emission (Schmidt)*
  - 2) *Prompt Fission Neutron Spectrum: Ongoing Theoretical and Experimental Efforts at LANL (Talou)*
  - 3) *New evaluation and theoretical model of fission neutron emission (Kornilov)*
- 12:30 – 14:00**      **Lunch**
- 14:00 – 18:00**      **Session 1 (cont'd)**
- 1) *Monte Carlo simulation of prompt neutron emission during acceleration in fission (Ohsawa)*
  - 2) *Investigation of the prompt neutron characteristics from a Monte Carlo simulation of the fission fragment de-excitation (Serot)*
  - 3) *Modeling the prompt fission neutron spectrum with FREYA (Vogt)*
  - 4) *Model calculations of prompt fission neutron spectra mainly of  $^{235}\text{U}(n,f)$  and also of  $^{232}\text{Th}(n,f)$  and  $^{238}\text{U}(n,f)$  (Tudora)*
  - 5) *Calculation of Prompt fission neutron spectra for  $^{235}\text{U}(n,f)$  ( $E_n < 6$  MeV) with semi-empirical model (Shu)*
  - 6) *Processing and intercomparison of Pu-239 fission spectra covariances from LANL, JENDL-4, SCALE-6 and IAEA-IJS (Kodeli)*

*Coffee break as needed*

## Wednesday, 14 December

- 09:00 - 12:30**      **Session 2**
- 1) *Ongoing experimental activities at CEA (Granier)*
  - 2) *Ongoing experimental activities at IRMM (Oberstedt)*
  - 3) *Ongoing experimental activities at PNPI, Russia (Vorobyev)*
  - 4) *Results of implementation of new prompt fission neutron spectra data in ROSFOND (Manturov)*
  - 5) *Testing the ENDF-B/VII.1 and JENDL-4  $^{235}\text{U}(n_{\text{th}},f)$  prompt fission neutron spectra using updated dosimetry cross sections – IRDFF-beta1 (Capote)*
- Coffee break as needed*
- 12:30 - 14:00**      **Lunch**
- 14:00 – 18:00**      **Session 2 (cont'd)**  
**Discussion on available experimental data that could be used to improve existing evaluations, possible new data to be considered.**
- Coffee break as needed*
- 19:00**              **Dinner at a restaurant in the city**

## Thursday, 15 December

- 09:00 - 12:30**      **Session 3**  
**Discussion on modelling and uncertainty estimates, evaluations**
- Coffee break as needed*
- 12:30 - 14:00**      **Lunch**
- 14:00 – 18:00**      **Session 4**  
**Coordination of required work, outputs, formatting**  
**Drafting the structure of the (final) Technical Report and expected outputs**
- Coffee break as needed*

## Friday, 16 December

- 09:00 - 12:30**      **Drafting of the Summary Report of the Meeting**
- Coffee break as needed*
- 12:30 - 14:00**      **Lunch**
- 14:00 – 17:30**      **Review and Approval of the Summary Report**  
**Closing of the Meeting**



**Second Research Coordination Meeting on  
“Prompt Fission Neutron Spectra of Actinides”**

IAEA Headquarters, Vienna, Austria  
13 – 16 December 2011

**LIST OF PARTICIPANTS**

**CHINA**

Chen Yongjing  
Department of Physics  
China Institute of Atomic Energy (CIAE)  
China National Nuclear Corp. (CNNC)  
P.O. Box 275-41  
Beijing 102413  
Tel. +86 10 69 35 84 10  
e-mail: [cyj@ciae.ac.cn](mailto:cyj@ciae.ac.cn)

**CHINA**

Nengchuan Shu  
Department of Physics  
China Institute of Atomic Energy (CIAE)  
China National Nuclear Corp. (CNNC)  
P.O. Box 275-41  
Beijing 102413  
Tel. +86 10 69 35 84 10  
e-mail: [nshu2007@gmail.com](mailto:nshu2007@gmail.com)  
[nshu@ciae.ac.cn](mailto:nshu@ciae.ac.cn)

**FRANCE**

Thierry Granier  
Service de Physique Nucleaire  
DAM Ile-de-France  
Commissariat a l'Energie Atomique  
B.P. 12  
91680 Bruyeres le Chatel  
Tel. +33 1 69 26 57 86  
e-mail: [thierry.granier@cea.fr](mailto:thierry.granier@cea.fr)

**JAPAN**

Takaaki Ohsawa  
Department of Electric and Electronic  
Engineering  
Faculty of Science and Engineering  
Kinki University  
3-4-1 Kowakae  
Higashi-Osaka-shi  
Osaka-fu 577-8502  
Tel. +81 6 6730 5880 4425  
e-mail: [ohsawa@ele.kindai.ac.jp](mailto:ohsawa@ele.kindai.ac.jp)

**ROMANIA**

Anabella C. Tudora  
Dept of Nuclear Physics  
Faculty of Physics  
Bucharest University  
P.O. Box MG-11  
76900 Bucharest-Magurele  
Tel. +40 21 4574666  
e-mail: [anabellatudora@hotmail.com](mailto:anabellatudora@hotmail.com)

**RUSSIA**

Gennady Manturov and Gleb Lomakov  
Institute of Physics and Power Engineering  
(IPPE)  
Bondarenko Sq. 1  
249033 Obninsk, Kaluga Region  
Tel. +7 4843994958  
e-mail: [mant@ippe.ru](mailto:mant@ippe.ru)

**Germany**

Karl-Heinz Schmidt  
Rheinstrasse 4  
Erzhausen 64390  
e-mail: [schmidt-erzhausen@t-online.de](mailto:schmidt-erzhausen@t-online.de)

**SLOVENIA**

Ivan Kodeli  
Institut Jozef Stefan  
Jamova 39  
1000 Ljubljana  
Tel.  
e-mail: [ivan.kodeli@ijs.si](mailto:ivan.kodeli@ijs.si)

**USA**

Patrick Talou  
Group T-2, MS-B283  
Theoretical Division  
Los Alamos National Laboratory  
Los Alamos, NM 87545  
Tel. +1 505 665-0993  
Fax +1 505 667-1931  
e-mail: [talou@lanl.gov](mailto:talou@lanl.gov)

**INTERNATIONAL ORGANIZATION**

Stephan Oberstedt  
EC-JRC-IRMM  
Neutron Physics Unit  
Retieseweg 111  
2440 Geel  
Belgium  
Tel. +32 14 57 1351  
e-mail: [stephan.oberstedt@ec.europa.eu](mailto:stephan.oberstedt@ec.europa.eu)

**IAEA**

Roberto Capote Noy  
Nuclear Data Section  
Division of Physical and Chemical Sciences  
Vienna International Centre  
PO Box 100  
1400 Vienna  
Tel. +43-1-2600-21713  
Fax +43-1-26007  
e-mail: [r.capotenoy@iaea.org](mailto:r.capotenoy@iaea.org)

**RUSSIA**

Alexander S. Vorobyev  
St. Petersburg Nuclear Physics Institute  
(PNPI)  
Russian Academy of Sciences  
188350 Gatchina  
St. Petersburg Oblast  
Tel. + 7 8137146444  
e-mail: [alexander.vorobyev@pnpi.spb.ru](mailto:alexander.vorobyev@pnpi.spb.ru)

**USA**

Nikolay Kornilov  
Accelerator Lab.  
Physics and Astronomy Department  
Ohio University  
Athens, OH 45701  
USA  
Tel. +1 740 593-0992  
e-mail: [kornilov@phy.ohiou.edu](mailto:kornilov@phy.ohiou.edu)

**USA**

Ramona Vogt  
Livermore National Laboratory  
P.O. Box 808  
LIVERMORE, CA 94551  
USA  
Tel. +1 505 667-4835  
e-mail: [vogt@lbl.gov](mailto:vogt@lbl.gov)

**FRANCE**

Olivier Serot  
Commissariat a l'Energie Atomique  
CEA-Cadarache, Bldg 230  
Saint Paul lez Durance F-13108  
Tel. +33 44 2257630  
e-mail: [olivier.serot@cea.fr](mailto:olivier.serot@cea.fr)

**IAEA**

Naohiko Otsuka  
Nuclear Data Section  
Division of Physical and Chemical Sciences  
Vienna International Centre  
PO Box 100  
1400 Vienna  
Tel. +43-1-2600-21715  
Fax +43-1-26007  
e-mail: [r.capotenoy@iaea.org](mailto:r.capotenoy@iaea.org)

**MEETING PHOTO**





## ADDITIONAL DOCUMENTS

1. *Model Calculations of prompt fission neutron spectra of  $^{235}\text{U}(n,f)$  and  $^{232}\text{Th}(n,f)$*   
by A. Tudora 19
2. *Monte Carlo Simulation of prompt fission emission during acceleration of fission fragments* by T. Ohsawa 23
3. *Calculation of prompt fission neutron spectra for the fission of  $^{235}\text{U}+n(E_n < 5 \text{ MeV})$*   
by Chen Yong-Jing, *et al.* 25
4. *Non-equilibrium? Maxwell's Demon? A Chairman's note* by T. Ohsawa 43
5. *Prompt-neutron spectra from a general description of the fission process*  
by K.-H. Schmidt and B. Jurado 47
6. *Preliminary remarks on some correlations of prompt-neutron multiplicities with properties of the fission fragments* by K.-H. Schmidt 59
7. *Correlation between prompt-neutron multiplicities and fission-fragment total kinetic energies further investigated with the GEF code* by K.-H. Schmidt 62
8. *Reply to "Comments about the partition of excitation energy between complementary fission fragments in connection with - A Chairman's note"* by T. Ohsawa 65



# 1. Model calculations of prompt fission neutron spectra of $^{235}\text{U}(n,f)$ and $^{232}\text{Th}(n,f)$

Anabella Tudora, University of Bucharest, Faculty of Physics

The Point by Point (PbP) model was applied to the neutron-induced fission of  $^{235}\text{U}$  with focus on prompt fission neutron spectra (PFNS). Prompt neutron and gamma-ray quantities as a function of fragment obtained from the multi-parametric matrix  $\nu(Z,A,TKE)$  (provided by the PbP model) such as  $\nu(A)$ ,  $E\gamma(A)$ ,  $\nu(TKE)$ ,  $P(\nu)$  describe very well all existing experimental data, see details in [1-3] and references therein.

Two methods of total excitation energy (TXE) partition between complementary FF were investigated. The first one, described in [4] has the advantage to be independent on models and assumptions made at scission and in this sense it can be taken as a possible reference method. The second method is based on: *i*) the calculation of the additional deformation energy of fragments (meaning the difference between the fragment deformation energies at scission and at full acceleration) and *ii*) the partition of the available excitation energy at scission (obtained by subtracting the additional deformation energies from TXE) assuming the statistical equilibrium at scission.

Total average PFNS, prompt neutron multiplicity (PFNM) and prompt gamma-ray energy  $\langle E\gamma \rangle$  obtained by averaging the respective fragment quantities over the experimental fission fragment (FF) distributions  $Y(A,TKE)$  of [5] describe well the existing experimental data proving again the consistency of the present calculations.

The sensitivity of the PFNS shape to different optical model parameterizations used to calculate the compound nucleus (CN) cross-section of the inverse process of neutron evaporation from fragments was studied. The anisotropy effect and a possible contribution of scission neutrons were investigated, too.

Two examples of PFNS results in very good agreement with experimental data are given in Fig. 1.

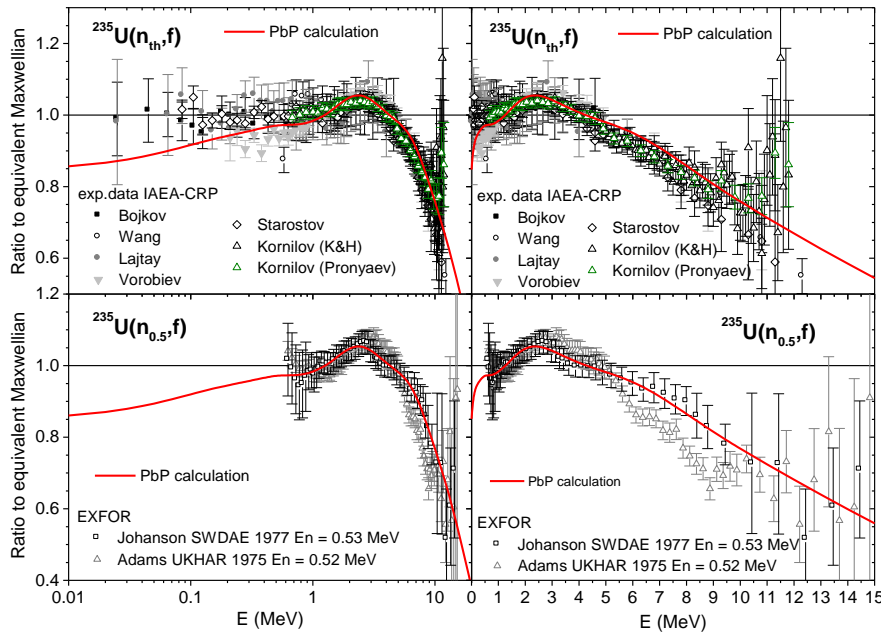


**Fig. 1:** PbP spectrum calculations of  $^{235}\text{U}$  at thermal  $E_n$  (upper part) and at  $E_n=0.5$  MeV (lower part) in comparison with experimental data (provided by the IAEA-CRP for thermal  $E_n$  and taken from EXFOR for  $E_n=0.5$  MeV).

At higher incident neutron energies ( $E_n$ ) where multiple fission chances are involved the most probable fragmentation approach was used with average values of model parameters obtained from the PbP treatment in the case of the main compound  $^{236}\text{U}$  and of the third chance  $^{234}\text{U}$ . For other fissioning U nuclei involved in the reaction, the average input parameters are provided by the systematic of [6]. The behavior of spread and scarce experimental data at the spectrum queue, measured at  $E_n$  of about

14-15 MeV for a few nuclei ( $^{235}\text{U}$ ,  $^{238}\text{U}$ ,  $^{232}\text{Th}$ ), shows a spectrum increase at around 7-8 MeV emitted neutron energies (where the pre-equilibrium peak is present). In the case of  $^{235}\text{U}(n,f)$  at  $E_n=14.7$  MeV the behavior of experimental data around 8 MeV is very well described by our calculation of Ref. [7] when the  $(n,xn)$  spectra provided by GNASH calculation are used for the neutrons evaporated prior to the scission, see the solid line in Fig. 2. This fact proves that  $(n,xn)$  spectra obtained from nuclear reaction code calculations such as EMPIRE, GNASH, or TALYS (from which the contribution of neutrons leading to excitation energies of the residual nucleus less than the fission barrier height were subtracted) seem to be more appropriated to describe neutrons evaporated prior to the scission than the traditional Weisskopf-Ewing spectra.

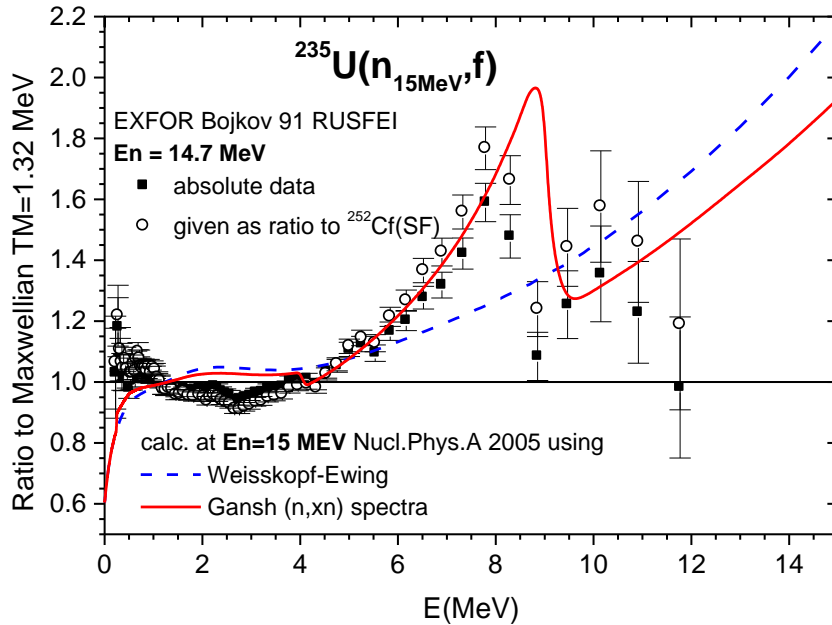


**Fig. 2:** PFNS calculations of  $^{235}\text{U}(n,f)$  at  $E_n=14.7$  MeV in comparison with experimental data from EXFOR, using for neutrons evaporated prior to the scission the  $(n,xn)$  spectra of GNASH (solid line) and the Weisskopf-Ewing spectra (dashed line)

For the first time prompt neutron and gamma-ray quantities of  $^{232}\text{Th}(n,f)$  are calculated in the frame of the PbP model (for incident energies up to about 6 MeV) and the most probable fragmentation approach (up to  $E_n=20$  MeV). Preliminary results are briefly given below.

In the case of PbP model calculations total average PFNS, PFNM and  $\langle E_\gamma \rangle$  were obtained by averaging the fragment quantities over the experimental FF distributions  $Y(A)$  and  $\text{TKE}(A)$  available in the EXFOR library [8]. At higher  $E_n$  where more fission chances are participating the most probable fragmentation approach is used, with average input parameters obtained from the PbP treatment in the case of the main compound  $^{233}\text{Th}$  and from the systematic of Ref.[6] in the case of other fission chances  $^{232-230}\text{Th}$ . The fission cross-section ratios (RF) are obtained from recent  $^{232}\text{Th}$  evaluations (JEFF3.1.1. and JENDL4).

The very good agreement with experimental data of prompt neutron and  $\gamma$ -ray quantities proves the consistency of the present calculations. Two examples are given in Fig.3. In the upper part of the figure, the PbP result of PFNM (plotted with full red circles) describes very well the experimental data. At higher  $E_n$  the most probable fragmentation PFNM obtained by using RF from JEFF3.1 (plotted with red solid line) describes very well the experimental data over the entire  $E_n$  range up to 20 MeV. In the case of RF from JENDL4 the PFNM result (plotted with blue dashed line) agrees very well with the experimental data up to 17 MeV, above this energy it slightly underestimates the experimental data but remaining in the error bar limit. In the lower part of Fig. 3 the total average  $\langle E_\gamma \rangle$  result is given in comparison with the unique experimental data measured by Fréhaut [9] (plotted with full squares). The PbP result of  $\langle E_\gamma \rangle$  (plotted with red open circles) succeeds to give an overall good description of experimental data. The most probable fragmentation result (plotted with blue dashed line) agrees well with the experimental data, too.

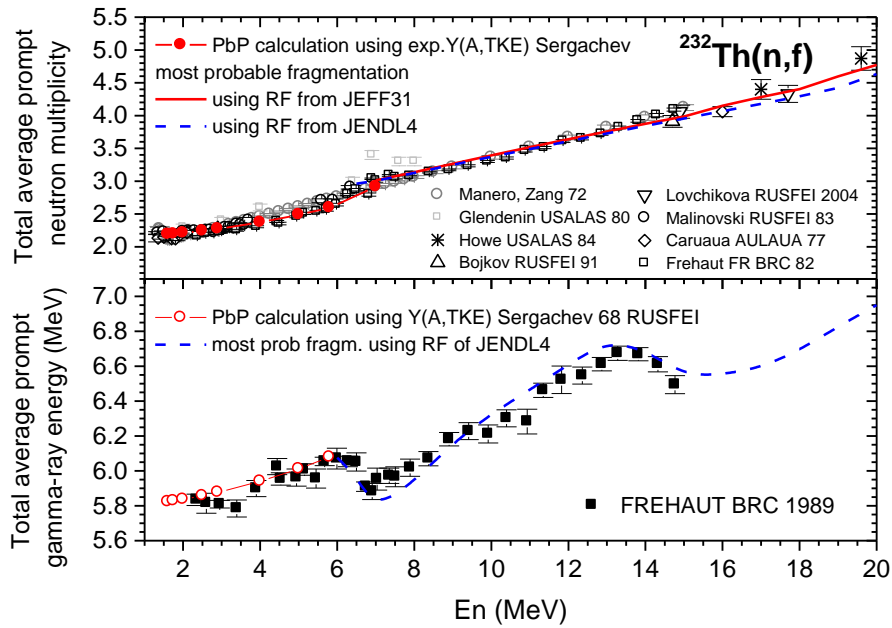


**Fig. 3:**  $^{232}\text{Th}(n,f)$  Results of PbP model and most probable fragmentation approach regarding the PFNM (upper part) and  $\langle E_\gamma \rangle$  (lower part) in comparison with experimental data.

PFNS of  $^{232}\text{Th}(n,f)$  obtained concomitantly with other prompt fission quantities in the frame of PbP and most probable fragmentation approaches describe well the existing experimental data. An example is given in Fig. 4 where the PbP spectrum results at  $E_n = 2$  MeV (upper part) and  $E_n = 2.9$  MeV (lower part) are obtained in very good agreement with the experimental data of EXFOR [10].

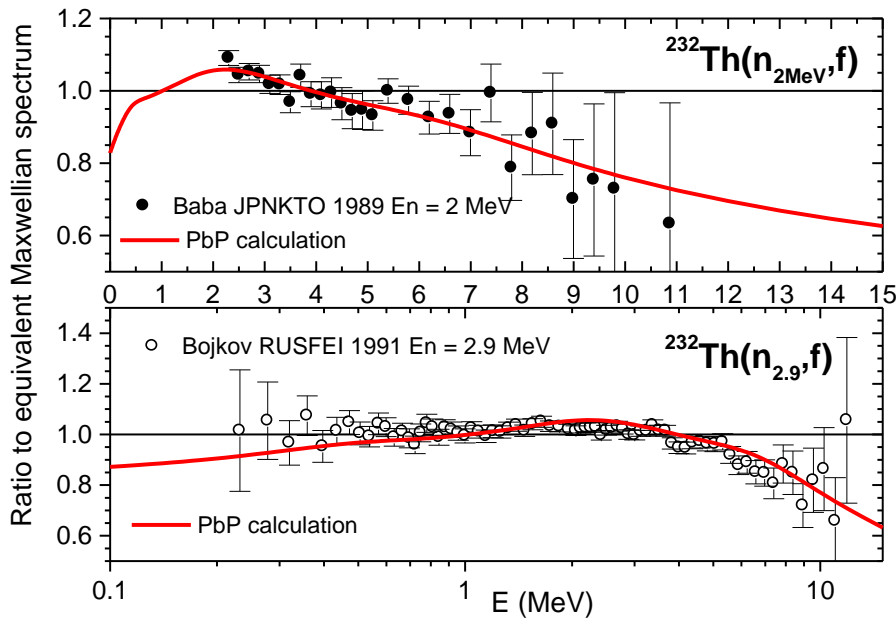


**Fig. 4:**  $^{232}\text{Th}(n,f)$  PbP spectrum calculations at  $E_n=2$  MeV (upper part) and  $E_n=2.9$  MeV (lower part) in comparison with experimental data from EXFOR.

The PbP and most probable fragmentation approaches can be considered as adequate tools for PFNS evaluation purposes. The consistent description of available experimental data, regarding both types of prompt neutron and gamma-ray quantities (as a function of fragment and total average), proves that the average values of input parameters resulted from the PbP treatment are reliable. The average input parameters provided by systematics can be also taken as starting values of parameters (in some cases slight adjustments to improve the agreement with experimental data being needed).

Model refinements such as the inclusion of the anisotropy effect or of a possible contribution of scission neutrons can improve in some cases the description of PFNS experimental data at low prompt neutron energies.

Different optical model parameterizations used to calculate the CN cross-section of the inverse process of neutron evaporation from FF lead to visible changes of the PFNS shape. In the majority of cases the Becchetti-Greenless parameterization gives the best agreement of spectrum shape with experimental data.

At incident neutron energies where multiple fission chances are involved, the fission cross-section ratios as well as the evaporation spectra of neutrons emitted prior to the scission are important ingredients of the model.

For a given actinide in many cases the fission cross-section ratios provided by recent evaluations differ considerably each other leading to visible differences in the resulted PFNM and PFNS. This fact can affect the prediction possibilities of the model in the absence of any PFNS experimental data.

At incident energies of about 14-15 MeV the behavior of scarce PFNS experimental data suggests that evaporation spectra of neutrons emitted prior to the scission obtained from the (n,xn) spectra provided by nuclear reaction codes like EMPIRE, GNASH, TALYS are more adequate than the traditional Weisskopf-Ewing spectra. This fact made the evaluation of PFNS dependent on detailed calculations performed by modern nuclear reaction codes.

#### References:

- [1] A. Tudora, *Ann. Nucl. Energy* **33** (11-12) (2006) 1030-1038.
- [2] A. Tudora, *Ann. Nucl. Energy* **35** (1) (2008) 1-10.
- [3] A. Tudora, F.-J. Hamsch, *Ann. Nucl. Energy* **37** (6) (2010) 771-777.
- [4] C. Manailescu, A. Tudora, F.-J. Hamsch, C. Morariu, S. Oberstedt, *Nucl. Phys. A* **867** (2011) 12-40.
- [5] Ch. Straede, C. Budtz-Jorgensen, H.H. Knitter, *Nucl. Phys. A* **462** (1987) 85-108.
- [6] A. Tudora, *Ann. Nucl. Energy* **36** (1) (2009) 72-84.
- [7] A. Tudora, B. Morillon, F.-J. Hamsch, G. Vladuca, S. Oberstedt, *Nucl. Phys. A* **756** (1-2) (2005) 176-191.
- [8] EXFOR Experimental Nuclear Reaction Data Base 2011, target Th-232, reaction (n,f), quantity MASS, PRE FY, data sets of Sergachev *et al.*, RUSFEI 1978. Available online <http://www-nds.iaea.org/EXFOR>.
- [9] J. Fréhaut, IAEA-INDC(NDS)-220, 1989, 99-111.
- [10] Experimental Nuclear Reaction Data Base 2011, target Th-232, reaction (n,f), quantity DE. Available online <http://www-nds.iaea.org/EXFOR>.

## 2. Monte Carlo Simulation of Prompt Neutron Emission During Acceleration of Fission Fragments

Takaaki Ohsawa

School of Science and Engineering, Kinki University, Higashi-osaka, Japan

### 1. Introduction

Possible reasons for apparent discrepancy in the prompt fission neutron spectra (PFNS) in the low-energy region, say <0.5 MeV, have been discussed. There are five possibilities: (1) uncertainty in the measured data in the low energy region, (2) neutron emission during acceleration (NEDA), instead of after full acceleration, (3) angular anisotropy in neutron emission in the CM-system of fission fragments (FF), (4) possible effect of “yrast levels”, and (5) possible existence of scission neutrons.

In this report we examined the possibility (2) and (3) as well. It has been considered that the most of the prompt fission neutrons are emitted after full acceleration of fission fragments due to rapid acceleration by strong Coulomb repulsion working between them. On the other hand, however, there has also been a discussion on a possibility of neutron emission during acceleration. This phenomenon is interesting from physics point of view, as it provides knowledge on the timescale of de-excitation of excited nuclei and on possible competition with the Coulomb acceleration of FFs. It is also interesting from application point of view, since neutron emission from FFs before full acceleration implies an enhancement of low-energy component of the PFNS, because the NEDA neutrons receive smaller linear momentum from the FF. This possibility was examined by using Monte Carlo simulation.

### 2. Method

In order to examine the NEDA effect, we have to analyze the competition of neutron emission from excited fragments and Coulomb acceleration of the FFs.

#### (1) Neutron Emission from Excited FFs

The average lifetime  $\tau_k$  for the  $k$ -th emitted neutron was calculated with the Ericson formula<sup>1)</sup>:

$$\tau_k = \frac{(2\pi\hbar)^3}{16m_n\pi} \frac{\rho_C(E_k^*)}{\int_0^{\varepsilon_{\max,k}} \varepsilon \sigma_C(\varepsilon) \rho_R(E_k - S_{n,k} - \varepsilon) d\varepsilon} \quad (1)$$

where  $m_n$  is the neutron mass, and  $\rho_C(E_k^*)$  and  $\rho_R(E_k - S_{n,k} - \varepsilon)$  the level densities of the compound and residual nucleus, respectively. The inverse reaction cross section  $\sigma_C(\varepsilon)$  was calculated using the spherical optical model potential of Becchetti and Greenlees. From eq.(1), we see that the average lifetime varies according to the excitation energy, neutron separation energy and level density, which are significantly influenced by the shell and pairing effects.

#### (2) Coulomb Acceleration of FFs

It has been known<sup>2)</sup> from point-charge model that the relation

$$t_{acc} = \frac{l}{v_{final}} \left[ \frac{\sqrt{\chi}}{1-\chi} + \frac{1}{2} \ln \frac{1+\sqrt{\chi}}{1-\sqrt{\chi}} \right] \quad (2)$$

holds between the acceleration time  $t_{acc}$  after scission and the relative acceleration  $\chi = KE/KE_{final}$  of fragments at the time  $t_{acc}$ , where  $v_{final}$  is the final velocity,  $l$  the charge-center distance at scission, given by  $l = Z_L Z_H e^2 / TKE$  with consideration of fluctuation in TKE. It is to be noted here that the quantity  $l$  here is a stochastic quantity randomly sampled in accordance with the TKE distribution. The probability of emission of the first neutron at time  $t$  after scission is expressed by  $P(t) = 1 - \exp(-t/\tau)$ . Using eq. (2), we can describe the probability  $P(\chi)$  of neutron emission at the moment when the relative acceleration is  $\chi$ :

$$P(\chi) = 1 - \exp \left[ -\frac{l}{\tau v_{final}} \left\{ \frac{\sqrt{\chi}}{1-\chi} + \frac{1}{2} \ln \left( \frac{1+\sqrt{\chi}}{1-\sqrt{\chi}} \right) \right\} \right] \quad (3)$$

### (3) PFNS with Consideration of NEDA Effect

The PFNS was calculated with the Madland-Nix model<sup>3)</sup>. Here, the multimode model in fission was considered<sup>4)</sup>. The *modal* PFNS was given by weighted average of spectra from LF and HF:

$$N_i(E) = [v_{i,L} N_{i,L}(E, E_{f,i,L}, T_{m,i,L}) + v_{i,H} N_{i,H}(E, E_{f,i,H}, T_{m,i,H})] / (v_{i,L} + v_{i,H}). \quad (4)$$

The *total* PFNS was calculated by averaging the *modal* PFNS with mode branching ratio  $w_i$  and neutron multiplicity  $v_i$  as weightings:

$$N(E) = \sum_i w_i v_i N_i(E) / \sum_i w_i v_i \quad (5)$$

The PFNS with consideration of NEDA effect was obtained by integrating the total PFNS over distribution of  $P(\chi)$ :

$$\langle N(E, E_f, T_m) \rangle = \int_0^1 N(E, \chi E_f, T_m) P(\chi) d\chi. \quad (6)$$

## 3. Results

### (1) Basic Input Data

In the present study, the multimodal random neck-rapture (MM-RNR) model<sup>4)</sup> was used as a framework of representation of the primary distribution, since it provides best account of the two-dimensional distributions of mass and TKE of the FFs for many actinides.<sup>5,6)</sup> In the present model the fission process is considered to proceed along three definite deformation paths, symbolically named Standard-1 (S1), Standard-2 (S2), Standard-X (SX) and Superlong (SL). The multimodal parameters were determined from experimental data<sup>5,6,8-10)</sup>, or taken from systematics<sup>11,12)</sup> when adequate measured data were not available.

### (2) Calculated Results

#### (a) Neutron Emission Lifetime and NEDA Probability

The neutron emission lifetime calculated with eq. (10) for FF from  $^{235}\text{U}(n_{\text{th}}, f)$  is shown as a function of fragment mass in Fig. 1.

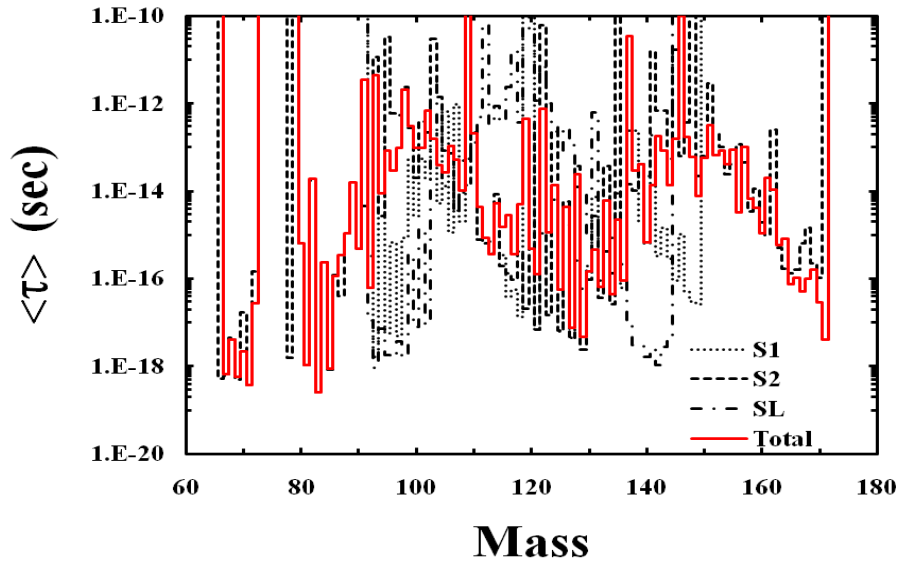


Fig. 1 The neutron emission lifetime for FF as a function of fragment mass for  $^{235}\text{U}(n_{\text{th}}, f)$ .

It can readily be observed that (i) the lifetime varies over 6 orders of magnitude from fragment to fragment, (ii) it fluctuates greatly between neighboring FF due to even-odd effect, and (iii) the gross structure is determined by shell effect on the LDP and  $S_n$  and do not depend strongly on the hypotheses on TXE between the FFs.

#### (b) The NEDA Probability as a Function of Relative TKE

The NEDA probability calculated with MC method for  $^{235}\text{U}(n_{\text{th}}, f)$  is plotted in Fig. 2. We confirm that, although neutron emission probability is high in the final stage of acceleration ( $\chi \approx 1$ ), a certain fraction of neutrons are certainly emitted before full acceleration. It was found that the probability of NEDA

integrated up to 90% of  $E_{\text{final}}$  is  $\sim 10\%$  for  $^{235}\text{U}(n_{\text{th}},f)$  and  $\sim 16\%$  for  $^{252}\text{Cf}(s.f)$ , because of the greater fission Q-values for the last case.

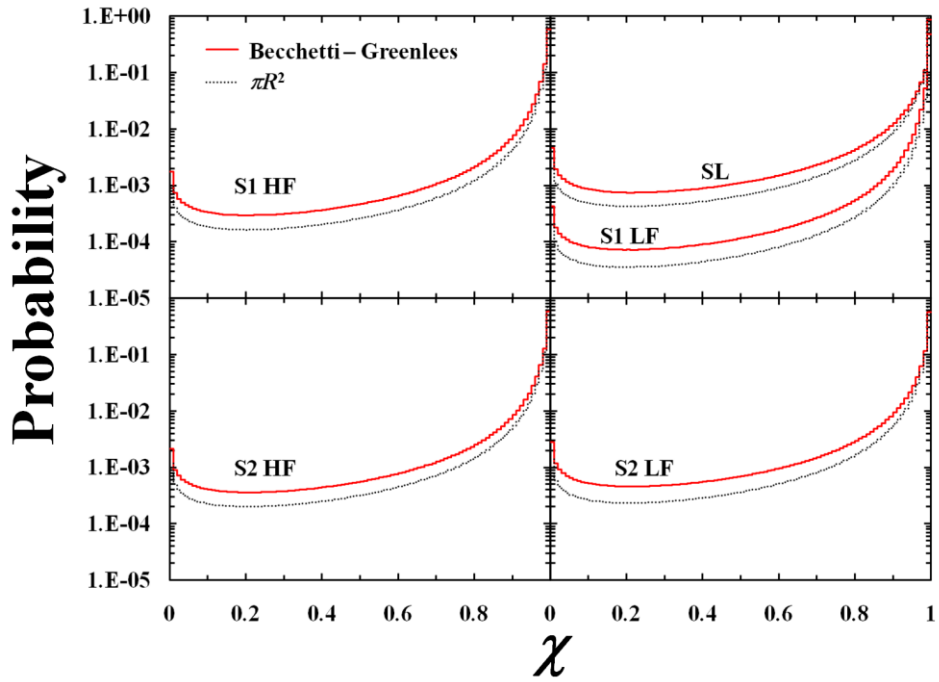


Fig. 2. NEDA probability as a function of relative acceleration  $\chi$  for different fission modes calculated with energy-dependent<sup>(21)</sup> and constant inverse reaction cross sections for  $^{235}\text{U}(n_{\text{th}},f)$ .

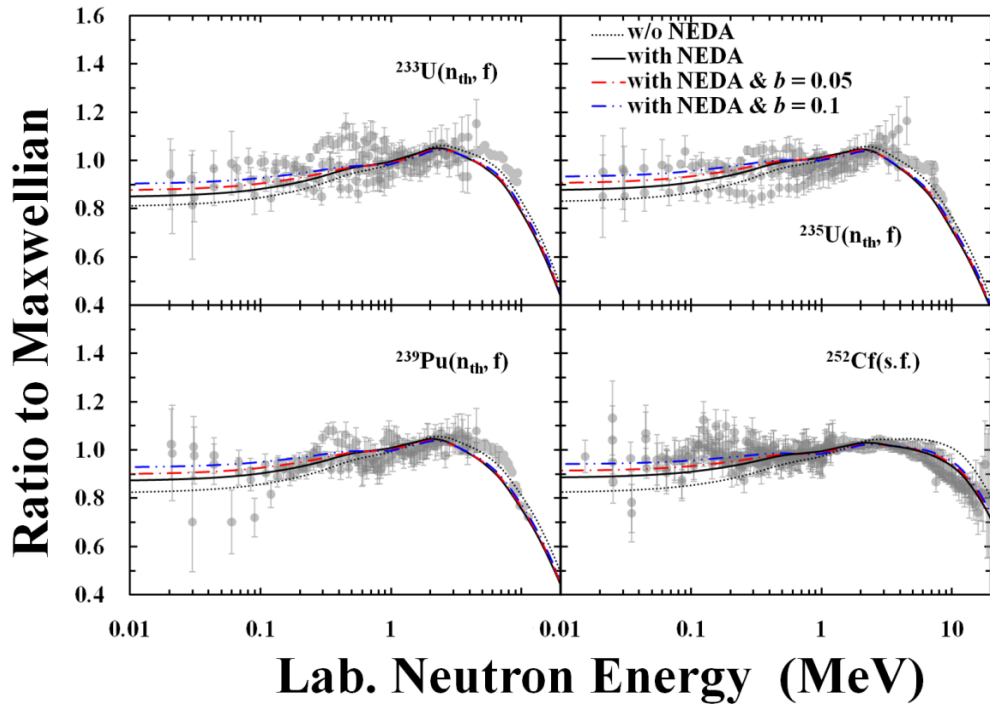


Fig. 3. Prompt fission neutron spectra calculated with and without NEDA effect. Calculations with consideration of CM-angular anisotropy of neutron emission are also shown.

(c) Prompt Fission Neutron Spectra

Results of calculation of PFNS with and without consideration of NEDA effects are compared in Fig. 3. Results are also shown for anisotropic emission of neutrons calculated by the equation<sup>(7)</sup>

$$N(E, E_f, \sigma_c) = \frac{1}{4\sqrt{E_f}} \int_{(\sqrt{E}-\sqrt{E_f})^2}^{(\sqrt{E}+\sqrt{E_f})^2} \frac{\phi(\varepsilon, \sigma_c) [1 + b(E - \varepsilon - E_f)^2 / 4\varepsilon E_f]}{\sqrt{\varepsilon}(1 + b/3)} d\varepsilon \quad (6)$$

with anisotropic parameter  $b=0.05$ <sup>8)</sup> and  $b=0.1$ <sup>9)</sup>. Note that the spectra are represented as the ratio to the Maxwellian distribution with temperature parameters  $T_M=1.324$  MeV, 1.324 MeV, 1.38 MeV, and 1.42 MeV for  $^{233}\text{U}(\text{n}_{\text{th}},\text{f})$ ,  $^{235}\text{U}(\text{n}_{\text{th}},\text{f})$ ,  $^{239}\text{Pu}(\text{n}_{\text{th}},\text{f})$ ,  $^{252}\text{Cf}(\text{sf})$ , respectively.

Consideration of NEDA effect were found to enhance the low-energy (<1 MeV) part and reduce the high-energy (>3 MeV) part of the spectrum, because of less boosting to NEDA-neutrons. Consideration of angular anisotropy of neutron emission has the effect of enhancing both the low-energy (<0.6 MeV) and high-energy (>4 MeV) parts of the spectrum. One of our interests was to examine what would be the result if both effects are considered simultaneously. The present result shows that the agreement between calculation and experiments is improved at the lowest energies. On the other hand, the agreement seems to be worsened a bit at energies over 3 MeV, except for the case of  $^{252}\text{Cf}(\text{sf})$ . One of the reasons would be that, since the overall integral of the spectrum is normalized to unity, an increase at lower energies leads to a decrease at higher energies. A remedy for this discrepancy remains to be studied.

#### 4. Conclusion

By applying the MC method to simulate the NEDA phenomena in the fission process, we obtained the results that, (a) the NEDA probability before acceleration up to 90% of final TKE of the fragments varies according to the fission mode, due to different excitation energy pertinent to the fission mode, and (b) the NEDA probability ranges from 2.2% at minimum (LF in the S1-mode) to 18.1% at maximum (SL-mode), the average being around 10% for  $^{235}\text{U}(\text{n}_{\text{th}},\text{f})$ . The NEDA probability for  $^{252}\text{Cf}(\text{sf})$  is higher, ranging from 15.3% (LF in the S1-mode) to 18.0% (SL-mode), the average being 16%. This is due to the fact that the average emission time  $\tau$ , as given by Ericson<sup>20)</sup>, depends strongly to the excitation energy of the FF.

The NEDA-phenomenon has an effect of enhancing the low-energy part and reducing the high-energy part of the PFNS. Thus, taking into account the NEDA-effect, together with accounting for CM-anisotropy of neutron emission in the multimodal Madland-Nix model significantly enhances the low-energy part and improves the agreement with experimental data in the region less than 0.6 MeV. The apparent discrepancy observed at energies over 3 MeV for the cases except for  $^{252}\text{Cf}(\text{sf})$  remains to be remedied in the future.

#### References

- 1) T. Ericson, *Adv. Phys.* **9**, 425 (1960).
- 2) V.P. Eismont, *Atomnaya Energiya* **19**, 113 (1965) [*Sov. At. Energy* **19**, 1000 (1965)].
- 3) D.G. Madland and J.R. Nix, *Nucl. Sci. Eng.* **81**, 213 (1982).
- 4) U. Brosa, S. Grossman and A. Müller, *Phys. Rep.* **197**, 167 (1990).
- 5) H.-H. Knitter, F.-J. Hamsch, C. Budtz-Jørgensen, J.P. Theobald, *Z. Naturforsch.* **42a**, 786 (1987).
- 6) P. Siegler, F.-J. Hamsch, and S. Oberstedt and J.P. Theobald, *Nucl. Phys.* **A594**, 45 (1995).
- 7) T. Ohsawa *et al.*, *Summary Report of Consultants' Meeting on Prompt Fission Neutron Spectra of Major Actinides*, INDC(NDS)-0541, p.71 (2009), IAEA.
- 8) C. Budtz-Jørgensen and H.-H. Knitter, *Proc. of a Consultants' Meeting on Physics of Neutron Emission in Fission*, INDC(NDS)-220, p.181 (1989) IAEA.
- 9) V.F. Gerasimenko and V.A. Rubchenya, *ibid.*, p.283 (1989) IAEA.

# Calculation of prompt fission neutron spectra for the fission of $^{235}\text{U}+\text{n}$ ( $E_n < 5$ MeV)

CHEN Yong-Jing, SHU Neng-Chuan, LIU Ting-Jin

*China Nuclear Data Center, China Institute of Atomic Energy, Beijing 102413, China*

The prompt fission neutron spectra for neutron-induced fission of  $^{235}\text{U}$  at  $E_n < 5$  MeV are calculated using the nuclear evaporation theory with a semi-empirical model, in which non-constant temperature and constant temperature related to the Fermi gas model are taken into account. The results reproduce the experimental data well. For  $\text{n}(\text{thermal})+^{235}\text{U}$  reaction, the average nuclear temperature of fission fragment and the probability distribution of the nuclear temperature are discussed and compared with the Los Alamos model. The energy carried away by  $\gamma$  rays emitted of each fragment is also obtained and the results are in good agreement with the existing experimental data.

PACS numbers: 25.85.Ec, 24.10.Ca, 24.75.+i

## I. INTRODUCTION

The prompt fission neutron spectra (PFNS) from neutron-induced fissions plays an important role in various nuclear engineering and technologies, both in energy and non-energy applications. From a more fundamental point of view, studying the prompt fission neutron spectrum in detail can reveal some interesting properties of the nuclear fission process itself. The early representations of the prompt fission neutron spectrum, in which many physical effects were covered up, are the Maxwellian and Watt spectrum representations with one or two parameters that are adjusted to reproduce the experimental spectrum. The Los Alamos (LA) model [1] is one of the most successful models for predicting PFNS with an assumption of the same triangular-shaped initial nuclear temperature distribution for both light and heavy fragments. However, further study is needed to describe more specific physical quantities for a given fission fragment.

In recent years, the concept of the multi-modal random neck-rupture model [2, 3] and multi-modal Los Alamos model (MMLA) have been used to quantitatively predict the fission fragment properties, and applied to some calculations of PFNS and multiplicity of actinide nuclei isotopes [4, 5]. But the nuclear temperature adopted in these two models is still the triangular distribution.

In the present work, the PFNS for neutron induced fission of  $^{235}\text{U}$  with a semi-empirical model was calculated, which is very different from the LA model, more physical quantities are taken into account, such as the initial excitation energy of every fission fragment, the nuclear temperature of each fragment and the prompt fission neutron multiplicity distribution. We are only concerned with low-energy (0-5.0 MeV) fission in this paper, for which only the first-chance fission compound is formed. The present work is the continuation of Refs. [6, 7], where only the prompt fission neutron multiplicity of  $\text{n}+^{235}\text{U}$  was studied.

## II. FORMULATION

The total excitation energy  $E_{\text{TXE}}(A_L + A_H)$  of fission fragment pair is given as follows:

$$E_{\text{TXE}}(A_L + A_H) = E_r^*(A_L + A_H) + B_n(A_c) + E_n - E_{\text{TKE}}(A_L + A_H), \quad (1)$$

where  $B_n(A_c)$  is the neutron binding energy of the fission compound nucleus, and the subscript  $c$  refers to the compound nucleus.  $E_n$  is the kinetic energy of the neutron inducing fission.  $E_{\text{TKE}}(A_L + A_H)$  is the total kinetic energy of both light and heavy fragments, and is taken from experimental data.  $E_r^*(A_L + A_H)$  is the energy released in the fission process, which can be calculated with the following:

$$E_r^*(A_L + A_H) = M(Z_c, A_c) - M(Z_L, A_L) - M(Z_H, A_H). \quad (2)$$

Where,  $M(Z_c, A_c)$ ,  $M(Z_L, A_L)$  and  $M(Z_H, A_H)$  are the mass of the compound nucleus, the light fragment and the heavy fragment, respectively.

For a given fragment pair, the  $E_{\text{TXE}}(A_L + A_H)$  is distributed among the light and heavy fragments by means of the energy partition  $R_{E_n}$ , as in Ref. [7]. Then,  $E^*(A)$ , the excitation energy for a given fission fragment can be obtained:

$$E^*(A) = R_{E_n}(A) \times E_{\text{TXE}}(A_L + A_H). \quad (3)$$

Within the Fermi gas model, the initial fission fragment energy  $E^*(A)$  is simply related to the nuclear temperature  $T$ . The probability for the fission fragment to emit a neutron at a given kinetic energy is obtained by Weisskopf spectrum at this particular temperature [8]. Assuming a constant value of the cross section of inverse process of compound nucleus formation, the normalized prompt fission neutron spectrum  $\phi(\varepsilon)$  in the center of mass system is

$$\phi(A, T, \varepsilon) = \frac{\varepsilon}{T^2} \exp(-\varepsilon/T), \quad (4)$$

where  $\varepsilon$  is the center-of-mass neutron energy, and  $T$  is the residual nuclear temperature of fission fragment. There is a matching energy ( $E_{\text{match}}(A)$ ) for every nucleus in Fermi gas model. At higher nuclear excitation energies ( $E^*(A) > E_{\text{match}}(A)$ ), the nuclear temperature  $T$  is simply written as:

$$T = \sqrt{\frac{E^*(A) - B_n(A)}{a_{A-1}}}, \quad (5)$$

with  $a_{A-1}$  the level density parameter of the  $(A - 1)$  nucleus.  $B_n(A)$  is the neutron separation energy of the given fragment. When the excitation energies is lower than the matching energy, a constant temperature was taken for neutron evaporation.

For a fragment with excitation energy  $E^*(A)$ , it could de-excite through emitting neutrons and  $\gamma$  rays. Here we assumed that the neutrons are emitted firstly, and only in the case that the excitation energy is lower than the neutron binding energy, i.e., the neutron could not be emitted again, then the  $\gamma$  rays are emitted. The excitation energy of fragment will decrease after a neutron is emitted from a fragment, this will decrease the nuclear temperature  $T$  as well. The PFNSs at different temperature  $T$  were calculated by using the Eq. (4) for each fragment. The total prompt fission neutron spectrum of every fragment is obtained by summing all of them up. The following shows how these spectra are weighted.

Usually the  $\bar{\nu}$  is the average total prompt neutron number. Actually, there have distributions for neutrons emission, i.e. the prompt neutron multiplicity distribution  $P(\nu)$ . The average value of this distribution is  $\bar{\nu}$ . Considering the neutron emission of every fission fragment as a Poisson process [9], the neutron multiplicity distribution  $P(N)$  of fragment A can be obtained:

$$P(N) = \frac{\bar{\nu}^N(A)}{N!} e^{-\bar{\nu}(A)}, \quad (6)$$

where  $P(N)$  is the probability of  $N$  neutron emitting by fragment A and  $\bar{\nu}(A)$  is the mean prompt fission neutron number emitted by the fragment A [6]. Then the number of emitting the  $i$ -th neutron for emitting total  $N$  neutrons can be written as:

$$P_N''(i) = NP(N) \times \frac{P'(i)}{\sum_i P'(i)}. \quad (7)$$

where,

$$P'(i) = \frac{P(i)}{P(i-1)}, P'(0) = P(0). \quad (8)$$

For a given fragment A, the sum of  $P_N''(i)$  ( $i = 1, N$ ) is equal to  $\bar{\nu}(A)$ .

According to the statistical theory, a fragment can emit  $N$  neutrons, only the probability of each neutron is different. In this work, 11 neutron emissions were considered for every fragment, regardless of its average prompt neutron number  $\bar{\nu}(A)$ . Therefore there have 11 excitation energies and 11 nuclear temperatures for every fragment. These mean that 11 neutron spectra should be considered for every fragment. The total prompt fission neutron spectrum of each fragment in the center-of-mass system is written as  $\phi(A, \varepsilon)$ , and calculated as a superposition of 11 neutron spectra by weighting with the  $P_N''(i)$ ,

$$\phi(A, \varepsilon) = \sum_{i=1}^{11} \frac{\varepsilon}{T_i^2} \exp(-\varepsilon/T_i) \times P_N''(i). \quad (9)$$

$T_i$  is the nuclear temperature corresponding to the  $i$ -th neutron emitting by a fragment.

Given the center-of-mass neutron energy spectra of every fragment, the corresponding neutron energy spectra  $\Phi(A, E)$  in the laboratory system can be obtained by assuming that neutrons are emitted isotropically in the center of mass frame of a fission fragment. The total PFNS of all fragments can be expressed as:

$$N(E) = \sum_j Y(A_j) \bar{\nu}(A_j) \Phi(A_j, E), \quad (10)$$

where  $j$  stands for all fission fragments.  $Y(A)$  is the chain yield, and  $\bar{\nu}(A)$  is the average prompt fission neutron number.

### III. RESULTS AND DISCUSSIONS

For every fission fragment, 11 center-of-mass neutron energy spectra are calculated using Eq. (4), then the normalized center-of-mass neutron energy spectra are calculated from Eq. (9). Fig. 1 shows the neutron energy spectra for the fission of  $^{235}\text{U}$  induced by thermal neutrons, and the fragment mass number A is 88. The dash curves indicate

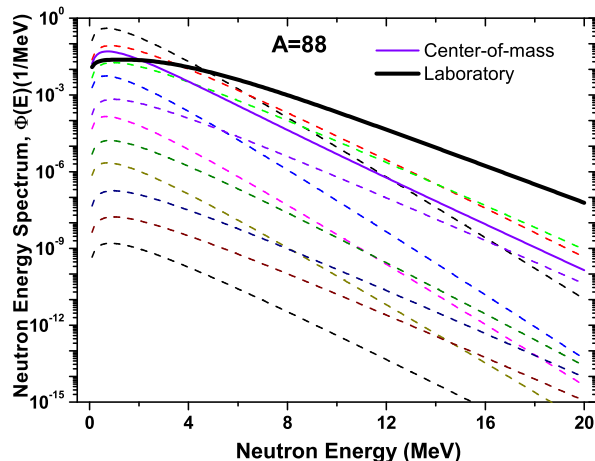


FIG. 1: The PFNSs for a given fragment ( $A=88$ ) of  $^{235}\text{U}+n(\text{thermal})$  fission calculated with 11 temperatures ( $T_1, T_2, \dots, T_{11}$  from top to bottom).

the 11 center-of-mass neutron energy spectra with their weight  $P_N''(i)$ , and the thin solid curve indicates the total normalized center-of-mass neutron energy spectrum. Transformation to the laboratory system yields the thick solid curve shown in Fig. 1.

In Fig. 1, the dash spectra are corresponding to  $T_1, T_2, \dots$  and  $T_{11}$  from top to bottom. It is clear that the neutron energy spectra (dash curves) become overall softer with the neutron emission. This is because that the neutron emissions lead to the decrease of the excitation energy as well as the nuclear temperature. In addition, it can be seen in Fig. 1 that the normalized neutron spectra in the center-of-mass system is dominantly contributed by the first few neutron emissions by fragment, and this is due to the neutron emission probability decreases very fast with the number of emitted neutrons.

The total PFNS in the laboratory system are calculated with Eq. (10), and the mass number range of fragment is  $78 \leq A \leq 158$ . Fig. 2 gives the total PFNS in the laboratory system for the  $n(\text{thermal})+^{235}\text{U}$  fission. The solid curve indicates the calculated neutron energy spectrum, and the other symbols are the experimental data. The present calculation agrees well with the experimental data. At the spectrum tail the calculation spectrum is a little harder relative to the experiment, but remaining within the experimental error limits.

Figure 3 shows the calculated results for the  $n+^{235}\text{U}$  reaction with the incident neutron energy is 0.4 MeV, 0.53 MeV, 1.5 MeV and 2.9 MeV, respectively. It can be seen that the calculated spectra are in good agreement with the experiment data when the incident neutron energy is 0.4 MeV, 0.53 MeV and 1.5 MeV. For the case of  $E_n=0.53$  MeV, the calculated spectrum shows a little bit harder than the experiment in the region from 5.5 MeV to 10 MeV, but agrees with experiment well above 10 MeV and below 5.5 MeV. While for  $E_n=2.9$  MeV, the calculated data disagree with the experimental data above  $\sim 5.0$  MeV, where the calculated spectrum appears to be too hard. We compare the experimental spectra at 0.53 MeV and 2.9 MeV and show in Fig. 4. It can be seen that the two spectra have the same shape below 6.5 MeV. While at above 6.5 MeV region, the spectrum with 2.9 MeV incident neutron energy is even softer than that of 0.53 MeV. This may be not proper since the PFNS should become harder with the

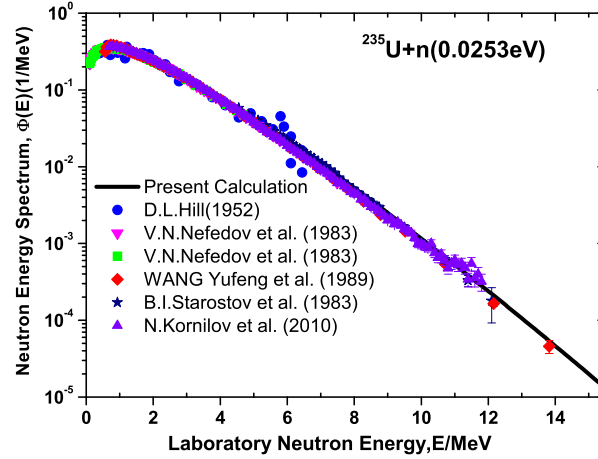


FIG. 2: The total PFNS for  $n(\text{thermal})+^{235}\text{U}$  reaction. The solid curve is calculated results. The other symbols are the experimental data from EXFOR [10].

increasing of the incident energy physically .

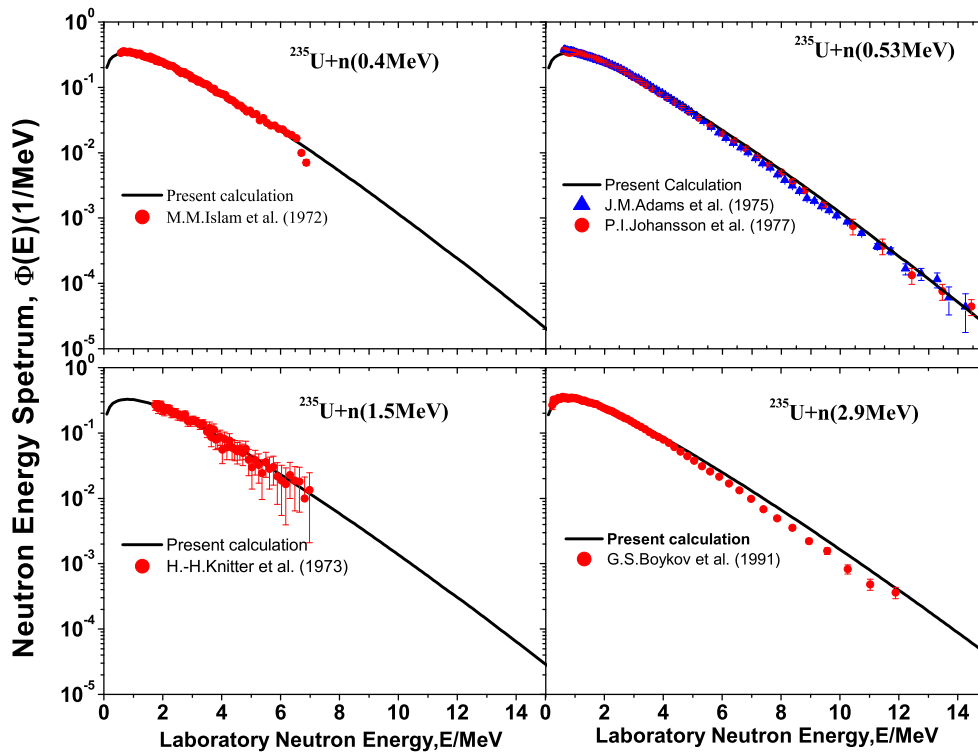


FIG. 3: The total PFNS for  $n+^{235}\text{U}$  reaction. The incident neutron energy is 0.4 MeV, 0.53 MeV, 1.5 MeV and 2.9 MeV, respectively. The solid curve is calculated results. The other symbols are the experimental data from EXFOR [10].

In the case of  $n(\text{thermal})+^{235}\text{U}$  reaction, the following quantities were calculated and discussed for cross checking

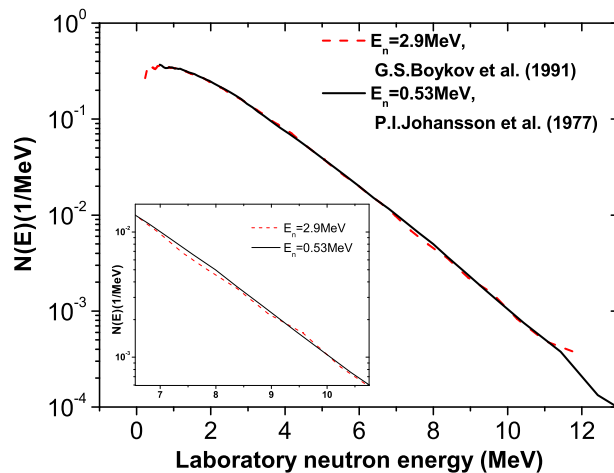


FIG. 4: Experimental data at  $E_n=2.9$  MeV in comparison with experimental data at 0.53 MeV.

and making insight into some properties of the fragment.

1. the nuclear temperature

In this work, 11 excitation energies and 11 nuclear temperatures were considered for every fragment. For a given fragment A, the average nuclear temperature can be obtained by weighting with the  $P_N''(i)$ , and was shown in Fig. 5 as a function of fragment mass A. It is shown that the average nuclear temperature of the light and heavy fission fragments is different, specially in the symmetric fission region, where appears a considerable symmetric variation.

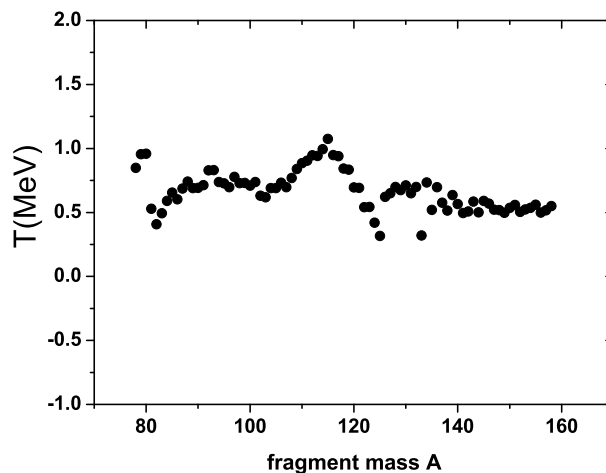


FIG. 5: The average nuclear temperature of fission fragment for  $n(\text{thermal})+^{235}\text{U}$  reaction.

By the use of Fermi gas model, Terrell transformed the distributions of residual fragment energies to the distributions of nuclear temperature ( $P(T)$ ) shown in the upper part of Fig. 6 [11]. The calculated distributions of the nuclear temperature in this work are also shown in the lower part of Fig. 6. It can be seen that both have the same trends, i.e. an approximately Gaussian distribution, but with the different FWHM. The FWHM is 0.385 in

this work, and is 0.772 in Ref. [11]. The probability of nuclear temperature of 0.6 to 0.8 MeV in this work is larger than that of the Ref. [11]. This is because some constant temperatures were used for some fragments in this work, and the nuclear temperatures in Ref. [11] are transformed according to the estimated distributions of the residual fragment energies. The distribution of the nuclear temperature in this work was calculated one fragment by one fragment exactly with the excitation energy partitioning, so it is more reasonable.

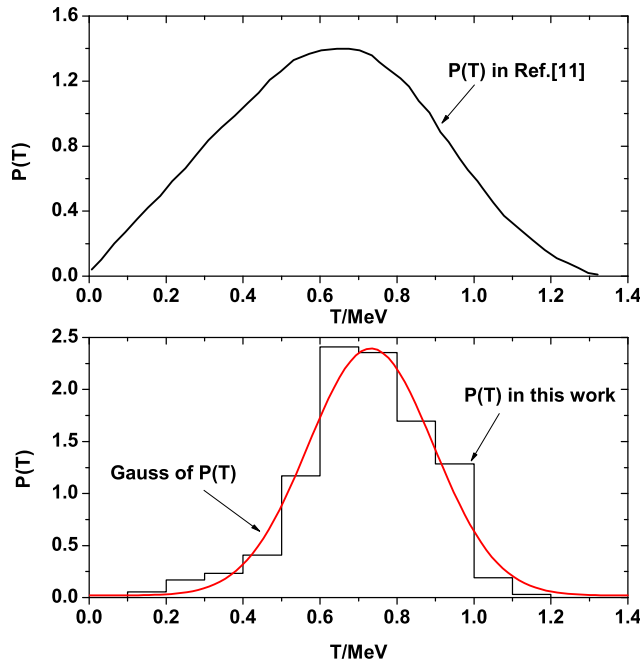


FIG. 6: The distributions of the nuclear temperature of fission fragments. The upper part of the figure shows the temperature distributions given in Ref. [11].

The average nuclear temperature  $\bar{T}$  of all fission fragments was also calculated and compared. In this work, the  $\bar{T}$  is given as superposition of each fragment temperature, taking the chain yield  $Y(A)$  and the average prompt fission neutron number  $\bar{\nu}(A)$  as weight. In the LA model, the average nuclear temperature  $\bar{T}$  of all fragments is  $\frac{2}{3}T_m$ , and  $T_m$  is the maximum temperature. For  $n(\text{thermal})+^{235}\text{U}$  reaction, the  $\bar{T}$  is 0.663 MeV for the LA model, and is 0.652 MeV for this work. The average nuclear temperature given in Ref. [11] is 0.6 to 0.7 MeV. They are in good agreement. But in this work, the average nuclear temperature for light fragments is 0.72 MeV, while for the heavy fragments is 0.56 MeV. They are very different, and the ratio is 1.28, while they are assumed as the same in the LA model and Ref. [11]. In Ref. [12], the dependence of nuclear temperature  $T$  with the nucleus mass number  $A$  ( $T \propto 1/A^{2/3}$ ) has been obtained by fitting available data on nuclear densities, indicating that the heavy fragment has the lower temperature  $T$ , and this is in agreement with our result qualitatively.

## 2. the average neutron kinetic energy $\langle \varepsilon \rangle$

The average neutron kinetic energy  $\langle \varepsilon \rangle$  for neutron emission from a given initial fission fragment used in Ref. [6] is the experimental data. While in this work, the  $2T$  is the mean energy of neutron emitted with an evaporation spectrum distribution corresponding to the average temperature  $T$  of fission fragment. Fig. 7 shows comparisons of

$\langle \varepsilon \rangle$  values for  $n+^{235}\text{U}$  reaction. The solid circles are the experimental data, the open circles are the calculated values in this work, and the triangular symbols are the calculated results in Ref. [13]. The values obtained for the light fragments are good agreement with the experimental data. For the heavy fragments, the calculated  $\langle \varepsilon \rangle$  values are lower than the experimental data. There are no experimental data between  $113 \leq A \leq 125$ , we give the same trend as the Ref. [13] in this mass region.

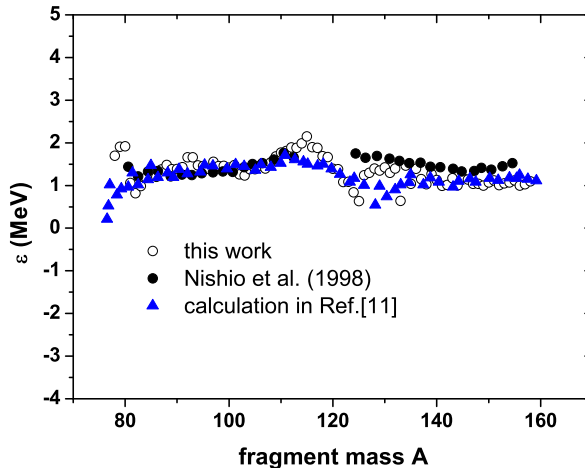


FIG. 7: Average neutron kinetic energy  $\langle \varepsilon \rangle$  for  $n(\text{thermal})+^{235}\text{U}$  reaction.

### 3. $E_\gamma(A)$ : the energy carried away by $\gamma$ rays

Another quantity of interest is  $E_\gamma(A)$ , the energy carried away by  $\gamma$  rays emission from a fragment.  $E_\gamma(A)$  used in Ref. [6] is the experimental data. While in this work, the average total energy carried away by  $\gamma$  rays ( $E_\gamma(A)$ ) is considered as the average excitation energy left when no further neutron emission. Fig. 8 gives the experimental  $E_\gamma(A)$  values used in Ref. [6] and the calculated results for  $n(\text{thermal})+^{235}\text{U}$  reaction in this work. The closed circles show the experimental data and the open circles are the calculated values. One can see that the experimental  $E_\gamma$  trend as a function of fragment mass  $A$  is well reproduced, although there are somewhat difference for heavy fragments. This indicates that the calculation of this work is reasonable in physics and programming.

### 4. the average fission fragment neutron separation energy $B_n(A)$

In Ref. [6], the average fission fragment neutron separation energy  $B_n(A)$  is determined by weighting with the independent fission-fragment yields of the same mass chain. While in this work, it is obtained by weighting with  $P'_N(i)$ . In generally, the agreement is good (Fig. 9).

### 5. the energy conservation

For  $n(\text{thermal})+^{235}\text{U}$  fission reaction,  $E_{\text{fission}}$ , the total energy of fission system is given by

$$E_{\text{fission}} = E_r^*(A_L + A_H) + B_n(A_c) + E_n, \quad (11)$$

which is distributed between the total excitation energy  $E_{\text{TXE}}$  and the total kinetic energy  $E_{\text{TKE}}$ . Then the  $E_{\text{TXE}}$  is divided into a pair of fission fragments, i.e., the excitation energy of each initial fission fragment,  $E^*(A_L)$  and  $E^*(A_H)$ , and they could de-excite through emitting neutrons and  $\gamma$  rays. So, the  $E_{\text{fission}}$  also can be expressed using the following formula:

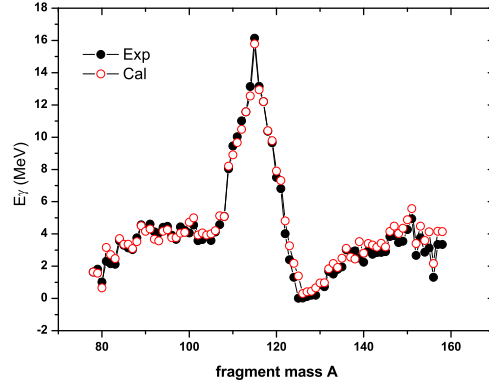


FIG. 8:  $\bar{E}_\gamma(A)$  for  $n+^{235}\text{U}$  reaction.

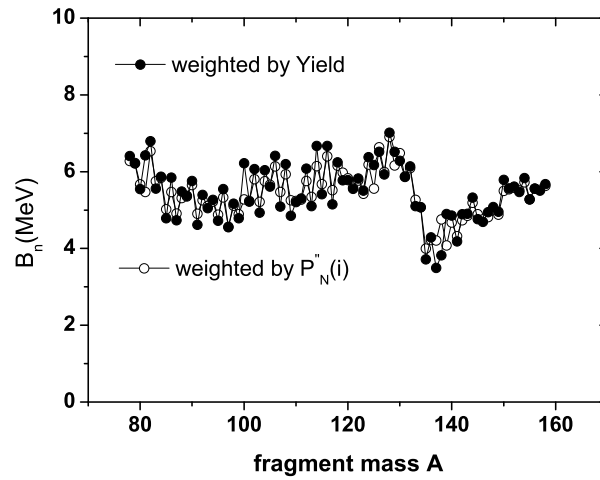


FIG. 9:  $B_n$  as a function of fission fragment mass for  $n+^{235}\text{U}$  reaction.

$$\begin{aligned}
 E_{\text{fission}} &= E_{\text{TKE}}(A_L + A_H) + E_{\text{TXE}}(A_L + A_H) \\
 &= E_{\text{TKE}}(A_L) + E_{\text{TKE}}(A_H) + E^*(A_L) + E^*(A_H) \\
 &= E_{\text{TKE}}(A_L) + E_\gamma(A_L) + \bar{\nu}(A_L) \times [\langle \varepsilon \rangle(A_L) + \langle B_n \rangle(A_L)] \\
 &\quad + E_{\text{TKE}}(A_H) + E_\gamma(A_H) + \bar{\nu}(A_H) \times [\langle \varepsilon \rangle(A_H) + \langle B_n \rangle(A_H)].
 \end{aligned} \tag{12}$$

In this work, the  $\langle \varepsilon \rangle(A)$ ,  $E_\gamma(A)$  and  $B_n(A)$  are the calculated results shown in Figs.(7-9),  $E_{\text{TKE}}$  is the experimental data and the  $\bar{\nu}(A)$  is calculated results with the Ref. [6]. In physics, the  $E_{\text{fission}}$  from Eq.(11) and Eq.(12) should be equal, i.e., the energy should be conserved in the calculation. Fig. 10 gives the both calculated results. It can be seen that the energy is conserved very well in the present work.

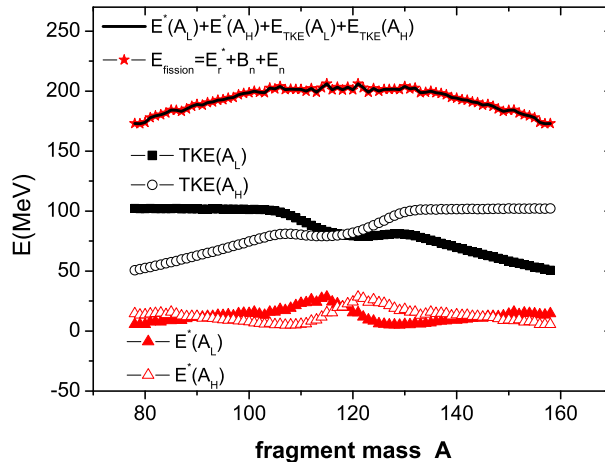


FIG. 10: The energy conservation for  $n(\text{thermal})+^{235}\text{U}$  reaction.

#### IV. CONCLUSION

In conclusion, we calculated the PFNS for neutron-induced fission of  $^{235}\text{U}$  at  $E_n = 0.0253$  eV, 0.4 MeV, 0.53 MeV, 1.5 MeV and 2.9 MeV with a semi-empirical method. The prompt fission neutron multiplicity distribution and non-constant and constant temperatures were taken into account. The calculated neutron spectra display is in good agreement with the experimental spectra except for the case of  $n(2.9 \text{ MeV})+^{235}\text{U}$  reaction for which the experimental data may be not reasonable. The average nuclear temperature of fission fragment and the probability distribution of the nuclear temperature were calculated and compared with the LA model. The energy carried away by  $\gamma$  rays for the case of  $n(\text{thermal})+^{235}\text{U}$  reaction was also calculated and compared with the experimental data.

Due to the prompt fission neutron spectrum was calculated according to the excitation energy of each fragment, and there is no any adjusted parameter in the present work, so the results reported could shed some light on the fission fragment properties:

- (1) The evaporation mechanism is the main mechanism for neutron emission from fission fragment.
- (2) The nuclear temperature of the two fission fragments are different. Therefore the hypothesis of two fission fragment have the same nuclear temperature is not reasonable. The ratio of average nuclear temperature for light fragments and the heavy fragments is 1.28 in this work, and it is very close to the  $R_T=1.2$  or 1.4 used in Ref. [14]. Also the nuclear temperature in the symmetric fission region varies considerably, from 1.07 MeV to 0.31 MeV.
- (3) The calculated energy carried away by  $\gamma$  rays is in good agreement with experimental data, which proves that the two steps model of the fragment de-excitation is reasonable: first neutron emitting, and then, only in the case that the excitation energy is not enough to emitting neutron, emitting  $\gamma$  rays. During neutron emitting, there is few competition from  $\gamma$  ray emitting.

## V. ACKNOWLEDGEMENT

This work is partially supported by IAEA CRP (No. 15905), NSFC (91126010) and State Key Lab. of Nuclear Physics and Technology of Peking University.

---

- [1] Madland D C, Nix J R. Nucl. Sci. Eng., 1982, **81**: 213
- [2] Brosa U, Grossmann S, Muller A. Phys. Rep., 1990, **197**: 167
- [3] Fan T S, Hu J M, Bao S L. Nucl. Phys. A, 1995, **591**: 161
- [4] Ohsawa T, Horiguchi T, Hayashi H. Nucl. Phys. A, 1999, **653**: 17
- [5] Ohsawa T, Horiguchi T, Mitsunashi M. Nucl. Phys. A, 2000, **665**: 3
- [6] CHEN Yong-Jing, LIU Ting-Jin, SHU Neng-Chuan. Chin. Phys. C, 2010, **34**: 953
- [7] CHEN Yong-Jing, LIU Ting-Jin. Chin. Phys. C, 2011, **35**: 344
- [8] Weisskopf V. Phys. Rev., 1937, **52**: 295
- [9] Bogomolova E S, Grashin A F, Efimenko A D et al. IAEA-INDC(CRP)-404, 26
- [10] [www-nds.iaea.org/exfor/](http://www-nds.iaea.org/exfor/), Experimental Nuclear Reaction Data (EXFOR)(2011)
- [11] Terrell J. Phys. Rev., 1959, **113**: 527
- [12] T. von Egidy and D.Bucuresu, Phys. Rev. C, 2005, **72**: 044311
- [13] Lemaire S, Talou P, Kawano T et al. Phys. Rev. C, 2006, **73**: 014602
- [14] Talou P, Kawano T. EPJ Web of Conferences, 2010, **2**: 08005

TABLE I: The calculated neutron energy spectrum  $\Phi(E)$ .

E(MeV)	$\Phi(E)$				
	$E_n=0.0253\text{eV}$	$E_n=0.4\text{MeV}$	$E_n=0.53\text{MeV}$	$E_n=1.5\text{MeV}$	$E_n=2.9\text{MeV}$
0.1	0.19552	0.19995	0.19818	0.19307	0.18856
0.2	0.25384	0.25997	0.25615	0.25046	0.24374
0.3	0.28582	0.29215	0.28781	0.28212	0.27425
0.4	0.3055	0.31162	0.30722	0.30155	0.29327
0.5	0.31839	0.32427	0.3199	0.3142	0.30594
0.6	0.32657	0.33219	0.328	0.32233	0.31411
0.7	0.33078	0.33599	0.33223	0.32673	0.31862
0.8	0.33166	0.33629	0.33322	0.32804	0.32012
0.9	0.32973	0.33356	0.3315	0.32672	0.31909
1.0	0.32565	0.32866	0.32764	0.32332	0.31611
1.1	0.3202	0.32258	0.32228	0.31835	0.31173
1.2	0.31375	0.31573	0.31584	0.31223	0.30624
1.3	0.30646	0.3081	0.30842	0.30515	0.29979
1.4	0.29845	0.29979	0.30018	0.29724	0.29251
1.5	0.2899	0.29093	0.29132	0.28868	0.28455
1.6	0.28087	0.28158	0.28193	0.27962	0.27602
1.7	0.27144	0.27182	0.27213	0.27016	0.26702
1.8	0.26172	0.26176	0.26202	0.26041	0.25769
1.9	0.2518	0.25149	0.25172	0.25047	0.24817
2.0	0.24176	0.24111	0.24134	0.24045	0.23857
2.1	0.23169	0.23073	0.23096	0.23042	0.22896
2.2	0.22164	0.22041	0.22064	0.22045	0.2194
2.3	0.21167	0.2102	0.21045	0.21058	0.20994
2.4	0.20184	0.20016	0.20045	0.20087	0.20062
2.5	0.19219	0.19034	0.19066	0.19135	0.19148
2.6	0.18276	0.18077	0.18113	0.18206	0.18255
2.7	0.17357	0.17148	0.17189	0.17302	0.17385
2.8	0.16465	0.16249	0.16294	0.16426	0.16539
2.9	0.15602	0.15383	0.15432	0.15578	0.1572
3.0	0.1477	0.14549	0.14602	0.14761	0.14929
3.1	0.1397	0.13749	0.13806	0.13975	0.14165
3.2	0.13201	0.12983	0.13043	0.1322	0.1343
3.3	0.12465	0.12251	0.12314	0.12497	0.12724
3.4	0.11761	0.11552	0.11618	0.11805	0.12046
3.5	0.11089	0.10886	0.10954	0.11145	0.11398
3.6	0.10449	0.10253	0.10322	0.10515	0.10777
3.7	0.0984	0.09651	0.09722	0.09915	0.10185
3.8	0.09261	0.0908	0.09151	0.09344	0.0962
3.9	0.08711	0.08539	0.0861	0.08802	0.09082
4.0	0.0819	0.08026	0.08098	0.08287	0.08569
4.1	0.07696	0.07541	0.07612	0.07799	0.08082
4.2	0.07229	0.07082	0.07153	0.07337	0.0762
4.3	0.06787	0.06648	0.06718	0.06899	0.07181
4.4	0.0637	0.06239	0.06308	0.06485	0.06765
4.5	0.05976	0.05852	0.0592	0.06093	0.0637

E(MeV)	$\Phi(E)$				
	$E_n=0.0253\text{ev}$	$E_n=0.4\text{MeV}$	$E_n=0.53\text{MeV}$	$E_n=1.5\text{MeV}$	$E_n=2.9\text{MeV}$
4.6	0.05604	0.05488	0.05555	0.05724	0.05996
4.7	0.05253	0.05144	0.0521	0.05375	0.05643
4.8	0.04923	0.04821	0.04885	0.05045	0.05308
4.9	0.04611	0.04516	0.04579	0.04734	0.04992
5.0	0.04318	0.04229	0.0429	0.04441	0.04693
5.1	0.04043	0.0396	0.04019	0.04165	0.04411
5.2	0.03783	0.03706	0.03763	0.03905	0.04145
5.3	0.03539	0.03468	0.03523	0.03661	0.03894
5.4	0.0331	0.03244	0.03297	0.03431	0.03657
5.5	0.03095	0.03033	0.03085	0.03214	0.03434
5.6	0.02893	0.02836	0.02886	0.0301	0.03223
5.7	0.02703	0.0265	0.02699	0.02819	0.03025
5.8	0.02526	0.02476	0.02523	0.02639	0.02838
5.9	0.02359	0.02313	0.02358	0.0247	0.02662
6.0	0.02202	0.0216	0.02204	0.02311	0.02497
6.1	0.02056	0.02017	0.02059	0.02162	0.02341
6.2	0.01918	0.01883	0.01923	0.02022	0.02195
6.3	0.01789	0.01757	0.01795	0.01891	0.02057
6.4	0.01669	0.01639	0.01676	0.01768	0.01928
6.5	0.01556	0.01529	0.01564	0.01652	0.01806
6.6	0.01451	0.01425	0.01459	0.01544	0.01692
6.7	0.01352	0.01329	0.01361	0.01442	0.01584
6.8	0.01259	0.01239	0.01269	0.01347	0.01483
6.9	0.01173	0.01154	0.01183	0.01258	0.01389
7.0	0.01092	0.01075	0.01103	0.01175	0.013
7.1	0.01017	0.01001	0.01028	0.01097	0.01216
7.2	0.00947	0.00932	0.00958	0.01023	0.01138
7.3	0.00881	0.00868	0.00892	0.00955	0.01065
7.4	0.00819	0.00808	0.00831	0.00891	0.00996
7.5	0.00762	0.00751	0.00774	0.00831	0.00931
7.6	0.00709	0.00699	0.0072	0.00775	0.00871
7.7	0.00659	0.0065	0.0067	0.00723	0.00814
7.8	0.00612	0.00604	0.00623	0.00674	0.00761
7.9	0.00569	0.00562	0.0058	0.00628	0.00711
8.0	0.00529	0.00522	0.00539	0.00585	0.00664
8.1	0.00491	0.00485	0.00502	0.00545	0.0062
8.2	0.00456	0.00451	0.00466	0.00508	0.0058
8.3	0.00423	0.00419	0.00433	0.00473	0.00541
8.4	0.00393	0.00389	0.00403	0.0044	0.00505
8.5	0.00364	0.00361	0.00374	0.0041	0.00472
8.6	0.00338	0.00335	0.00347	0.00381	0.0044
8.7	0.00314	0.00311	0.00323	0.00355	0.00411
8.8	0.00291	0.00288	0.003	0.0033	0.00383
8.9	0.0027	0.00268	0.00278	0.00307	0.00358
9.0	0.0025	0.00248	0.00258	0.00286	0.00334

$\Phi(E)$					
E(MeV)	$E_n=0.0253\text{ev}$	$E_n=0.4\text{MeV}$	$E_n=0.53\text{MeV}$	$E_n=1.5\text{MeV}$	$E_n=2.9\text{MeV}$
9.1	0.00232	0.0023	0.0024	0.00266	0.00311
9.2	0.00215	0.00213	0.00222	0.00247	0.0029
9.3	0.00199	0.00198	0.00206	0.0023	0.00271
9.4	0.00184	0.00183	0.00191	0.00213	0.00252
9.5	0.00171	0.0017	0.00177	0.00198	0.00235
9.6	0.00158	0.00157	0.00164	0.00184	0.00219
9.7	0.00146	0.00146	0.00152	0.00171	0.00204
9.8	0.00135	0.00135	0.00141	0.00159	0.0019
9.9	0.00125	0.00125	0.00131	0.00148	0.00177
10.0	0.00116	0.00116	0.00121	0.00137	0.00165
10.1	0.00107	0.00107	0.00112	0.00127	0.00154
10.2	9.90327E-4	9.89169E-4	0.00104	0.00118	0.00143
10.3	9.15667E-4	9.15081E-4	9.6159E-4	0.0011	0.00133
10.4	8.46486E-4	8.46394E-4	8.9014E-4	0.00102	0.00124
10.5	7.82391E-4	7.82725E-4	8.23857E-4	9.43131E-4	0.00115
10.6	7.23023E-4	7.23721E-4	7.62382E-4	8.7482E-4	0.00107
10.7	6.68051E-4	6.69057E-4	7.05384E-4	8.11337E-4	9.98836E-4
10.8	6.17152E-4	6.18417E-4	6.5254E-4	7.52346E-4	9.29205E-4
10.9	5.70034E-4	5.71514E-4	6.03556E-4	6.97537E-4	8.64308E-4
11.0	5.26423E-4	5.28079E-4	5.58158E-4	6.46622E-4	8.0383E-4
11.1	4.86067E-4	4.87867E-4	5.16094E-4	5.99335E-4	7.47483E-4
11.2	4.48761E-4	4.5068E-4	4.77164E-4	5.55465E-4	6.95036E-4
11.3	4.14239E-4	4.16244E-4	4.41082E-4	5.14711E-4	6.46163E-4
11.4	3.82329E-4	3.84389E-4	4.07678E-4	4.76897E-4	6.00672E-4
11.5	3.53015E-4	3.5507E-4	3.76926E-4	4.42007E-4	5.58559E-4
11.6	3.26195E-4	3.28112E-4	3.4856E-4	4.09772E-4	5.19586E-4
11.7	3.01711E-4	3.03533E-4	3.22683E-4	3.80281E-4	4.83751E-4
11.8	2.79873E-4	2.81744E-4	2.99963E-4	3.5409E-4	4.51685E-4
11.9	2.58868E-4	2.60901E-4	2.77985E-4	3.28893E-4	4.2084E-4
12.0	2.39376E-4	2.41286E-4	2.57274E-4	3.05151E-4	3.91748E-4
12.1	2.21163E-4	2.23142E-4	2.381E-4	2.83099E-4	3.64615E-4
12.2	2.0411E-4	2.0609E-4	2.20086E-4	2.62322E-4	3.38966E-4
12.3	1.88367E-4	1.90303E-4	2.03396E-4	2.43022E-4	3.15048E-4
12.4	1.73614E-4	1.755E-4	1.87743E-4	2.24879E-4	2.92517E-4
12.5	1.60028E-4	1.61883E-4	1.73331E-4	2.08143E-4	2.71674E-4
12.6	1.47487E-4	1.49275E-4	1.59974E-4	1.9259E-4	2.52236E-4
12.7	1.35897E-4	1.37632E-4	1.47631E-4	1.78184E-4	2.34171E-4
12.8	1.25194E-4	1.26868E-4	1.3621E-4	1.64817E-4	2.17348E-4
12.9	1.15313E-4	1.16927E-4	1.25653E-4	1.52429E-4	2.01705E-4
13.0	1.06197E-4	1.07751E-4	1.15898E-4	1.40959E-4	1.87181E-4
13.1	9.77885E-5	9.92792E-5	1.06885E-4	1.30331E-4	1.73669E-4
13.2	9.00352E-5	9.1465E-5	9.85643E-5	1.20499E-4	1.61133E-4
13.3	8.28866E-5	8.42567E-5	9.08814E-5	1.11402E-4	1.49498E-4
13.4	7.62951E-5	7.76038E-5	8.37835E-5	1.02966E-4	1.38661E-4
13.5	7.02183E-5	7.14663E-5	7.72294E-5	9.51541E-5	1.28586E-4

$\Phi(E)$					
E(MeV)	$E_n=0.0253\text{ev}$	$E_n=0.4\text{MeV}$	$E_n=0.53\text{MeV}$	$E_n=1.5\text{MeV}$	$E_n=2.9\text{MeV}$
13.6	6.46177E-5	6.58065E-5	7.11797E-5	8.7925E-5	1.1923E-4
13.7	5.94564E-5	6.05876E-5	6.55961E-5	8.12357E-5	1.10543E-4
13.8	5.47016E-5	5.57769E-5	6.04445E-5	7.50481E-5	1.02479E-4
13.9	5.03216E-5	5.13426E-5	5.56916E-5	6.93245E-5	9.49943E-5
14.0	4.62878E-5	4.72565E-5	5.13077E-5	6.40313E-5	8.80476E-5
14.1	4.25713E-5	4.34894E-5	4.72623E-5	5.91347E-5	8.15994E-5
14.2	3.9152E-5	4.00187E-5	4.35317E-5	5.46074E-5	7.56164E-5
14.3	3.60017E-5	3.68206E-5	4.0091E-5	5.04212E-5	7.00649E-5
14.4	3.31E-5	3.38745E-5	3.69183E-5	4.65511E-5	6.49146E-5
14.5	3.04292E-5	3.11611E-5	3.39933E-5	4.29739E-5	6.01373E-5
14.6	2.79709E-5	2.8662E-5	3.12971E-5	3.96679E-5	5.57067E-5
14.7	2.57082E-5	2.63606E-5	2.88116E-5	3.66125E-5	5.15974E-5
14.8	2.36258E-5	2.42411E-5	2.65205E-5	3.37886E-5	4.77862E-5
14.9	2.17102E-5	2.229E-5	2.44094E-5	3.11798E-5	4.42527E-5
15.0	1.99477E-5	2.04939E-5	2.24641E-5	2.87696E-5	4.09765E-5
15.1	1.83265E-5	1.88407E-5	2.06719E-5	2.65433E-5	3.79396E-5
15.2	1.68355E-5	1.73193E-5	1.90209E-5	2.4487E-5	3.51246E-5
15.3	1.54641E-5	1.5919E-5	1.75E-5	2.25877E-5	3.25153E-5
15.4	1.42031E-5	1.46307E-5	1.60992E-5	2.0834E-5	3.00975E-5
15.5	1.30437E-5	1.34455E-5	1.48093E-5	1.92148E-5	2.7857E-5
15.6	1.1978E-5	1.23552E-5	1.36215E-5	1.77199E-5	2.57812E-5
15.7	1.09982E-5	1.13521E-5	1.25279E-5	1.63398E-5	2.3858E-5
15.8	1.00976E-5	1.04297E-5	1.1521E-5	1.50659E-5	2.20764E-5
15.9	9.27E-6	9.5814E-6	1.05942E-5	1.38902E-5	2.04263E-5
16.0	8.50946E-6	8.80129E-6	9.74109E-6	1.28051E-5	1.88979E-5
16.1	7.81063E-6	8.084E-6	8.95593E-6	1.18039E-5	1.74825E-5
16.2	7.16855E-6	7.4246E-6	8.23337E-6	1.088E-5	1.61718E-5
16.3	6.57872E-6	6.81845E-6	7.5685E-6	1.00277E-5	1.49583E-5
16.4	6.03692E-6	6.26121E-6	6.95673E-6	9.24134E-6	1.38347E-5
16.5	5.53925E-6	5.74903E-6	6.39389E-6	8.51597E-6	1.27945E-5
16.6	5.08222E-6	5.27841E-6	5.87616E-6	7.84701E-6	1.18317E-5
16.7	4.66253E-6	4.84594E-6	5.39992E-6	7.23002E-6	1.09405E-5
16.8	4.27717E-6	4.44852E-6	4.96192E-6	6.66104E-6	1.01157E-5
16.9	3.92333E-6	4.08338E-6	4.55906E-6	6.13635E-6	9.3524E-6
17.0	3.59848E-6	3.74796E-6	4.18861E-6	5.6526E-6	8.64609E-6
17.1	3.3003E-6	3.43986E-6	3.84799E-6	5.20664E-6	7.99259E-6
17.2	3.02661E-6	3.15682E-6	3.53482E-6	4.79549E-6	7.38794E-6
17.3	2.77538E-6	2.89686E-6	3.24687E-6	4.41647E-6	6.82853E-6
17.4	2.54483E-6	2.65814E-6	2.98218E-6	4.06715E-6	6.31108E-6
17.5	2.33328E-6	2.43894E-6	2.7389E-6	3.74524E-6	5.83252E-6
17.6	2.13917E-6	2.23764E-6	2.51529E-6	3.44854E-6	5.38984E-6
17.7	1.96105E-6	2.05281E-6	2.30975E-6	3.17512E-6	4.98041E-6
17.8	1.79765E-6	1.88315E-6	2.12088E-6	2.92321E-6	4.60182E-6
17.9	1.64776E-6	1.7274E-6	1.94734E-6	2.69112E-6	4.25177E-6
18.0	1.51027E-6	1.58441E-6	1.78788E-6	2.4773E-6	3.9281E-6

$\Phi(E)$						
E(MeV)	$E_n=0.0253\text{ev}$	$E_n=0.4\text{MeV}$	$E_n=0.53\text{MeV}$	$E_n=1.5\text{MeV}$	$E_n=2.9\text{MeV}$	
18.1	1.38416E-6	1.45317E-6	1.64137E-6	2.28031E-6	3.62884E-6	
18.2	1.26849E-6	1.33274E-6	1.50677E-6	2.09887E-6	3.35217E-6	
18.3	1.16243E-6	1.2222E-6	1.38312E-6	1.93175E-6	3.09645E-6	
18.4	1.06517E-6	1.12076E-6	1.26955E-6	1.77783E-6	2.86005E-6	
18.5	9.75985E-7	1.02769E-6	1.16523E-6	1.63608E-6	2.64156E-6	
18.6	8.94208E-7	9.4229E-7	1.06941E-6	1.50554E-6	2.43963E-6	
18.7	8.19238E-7	8.63939E-7	9.81422E-7	1.38535E-6	2.25301E-6	
18.8	7.50521E-7	7.92056E-7	9.0063E-7	1.27469E-6	2.08058E-6	
18.9	6.8753E-7	7.26119E-7	8.26443E-7	1.1728E-6	1.92124E-6	
19.0	6.29781E-7	6.65639E-7	7.58316E-7	1.07899E-6	1.774E-6	
19.1	5.76855E-7	6.10165E-7	6.95771E-7	9.92651E-7	1.638E-6	
19.2	5.28355E-7	5.59283E-7	6.38359E-7	9.1317E-7	1.51234E-6	
19.3	4.83909E-7	5.12622E-7	5.85655E-7	8.4002E-7	1.39628E-6	
19.4	4.43177E-7	4.69837E-7	5.37273E-7	7.72691E-7	1.28906E-6	
19.5	4.05851E-7	4.30598E-7	4.92858E-7	7.10717E-7	1.19E-6	
19.6	3.71656E-7	3.94617E-7	4.52101E-7	6.53697E-7	1.09854E-6	
19.7	3.40328E-7	3.61625E-7	4.14696E-7	6.01223E-7	1.01407E-6	
19.8	3.11626E-7	3.31385E-7	3.80367E-7	5.52939E-7	9.36053E-7	
19.9	2.85331E-7	3.03664E-7	3.48866E-7	5.08522E-7	8.64036E-7	
20.0	2.61247E-7	2.78246E-7	3.19962E-7	4.67653E-7	7.9752E-7	

#### 4. Non-equitemperature? Maxwell's Demon? A Chairman's Note

Takaaki Ohsawa

School of Science and Engineering, Kinki University, Higashi-osaka, Japan

One of the foci of discussions at the RCM, according to the author, was the question of partition of the excitation energy between the two fragments, or the equitemperature/non-equitemperature issue. This theme is one of the essential problems in understanding the fission process, so it would be worthwhile to briefly review and summarize the relevant discussions.

- O. Serot proposed to treat the nuclear temperature ratio  $R_T = T_L/T_H$  as a function of fragment mass (Fig.1). This was necessary to reproduce the total neutron multiplicity  $\nu_{\text{tot}}$  and the saw-tooth structure of  $\nu(A)$ ; equitemperature assumption  $T_L = T_H$  did not work successfully in reproducing the quantities.

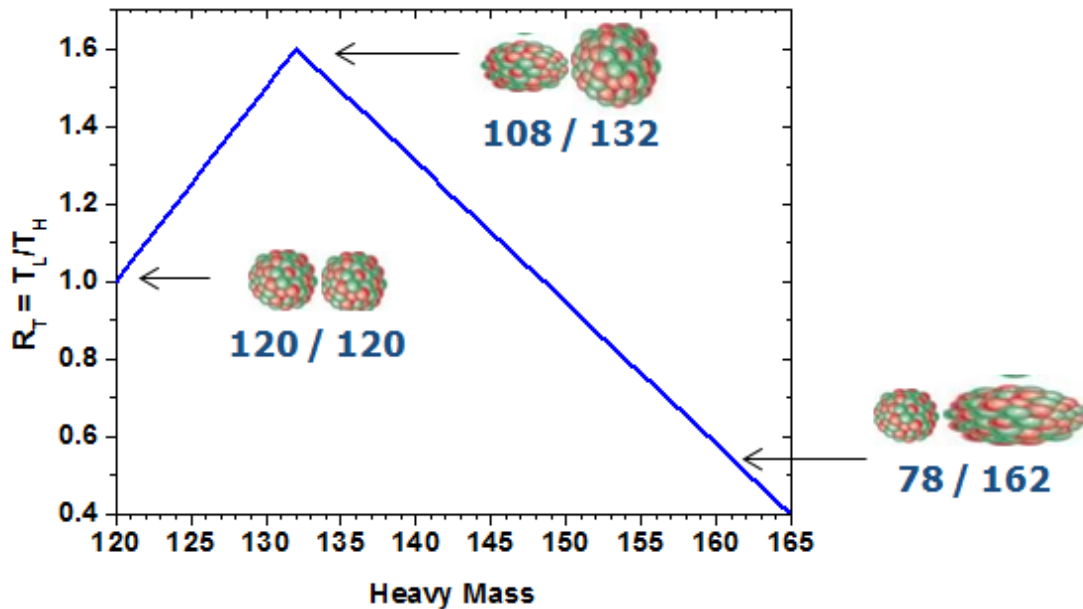


Fig. 1. Nuclear temperature ratio as a function of HF mass for  $^{239}\text{Pu}(n_{\text{th}}, f)$  (after Serot)

- A. Tudora used equitemperature assumption  $E_L^*/E_H^* = a_L/a_H$  in her point-by-point calculation of the PFNS, using different models (Gilbert-Cameron, Ignatyuk, Egidy) for level density parameters (LDP). Her calculation of  $\nu(A)$  agreed well with saw-tooth behavior of the experimental data, irrespective of the choice of the LDP model.

- N.-C. Shu reported that, in his calculation based on multimodal model of fission and sequential neutron evaporation, energy partition was assumed to be proportional to  $\langle \nu \rangle \langle \eta \rangle + \langle E_\nu \rangle$  for standard-1 and -2 modes,  $\langle \eta \rangle$  being the average energy carried away by a neutron. Egidy's formula<sup>1)</sup> says that the nuclear temperature with consideration of the shell effects  $S$  is given by the equation

$$T = A^{-2/3} [17.45 - 0.515S + 0.051S^2]. \quad (1)$$

According to Shu, the average temperature ratio was obtained to be  $R_T = \langle T_L \rangle / \langle T_H \rangle = 1.28$  for  $^{235}\text{U}(n, f)$ . This value seems to be approximately consistent with Fig.1 averaged over fragment mass distribution.

- K.-H. Schmidt discussed, on the basis of Egidy's formula (1), that the temperature of HF is lower than that of LF unless the shell effect  $S$  is large, which explained the experimental fact of Naqvi

*et al.*<sup>2)</sup> that, comparing the  $\bar{\nu}(A)$ -data for incident neutron energies 0.8 and 5.5 MeV, the increase in  $\bar{\nu}_{\text{tot}}$  is totally accounted for only by  $\bar{\nu}_{\text{H}}$ . This can be interpreted by energy sorting in a superfluid system due to temperature difference  $T_{\text{L}} > T_{\text{H}}$ .

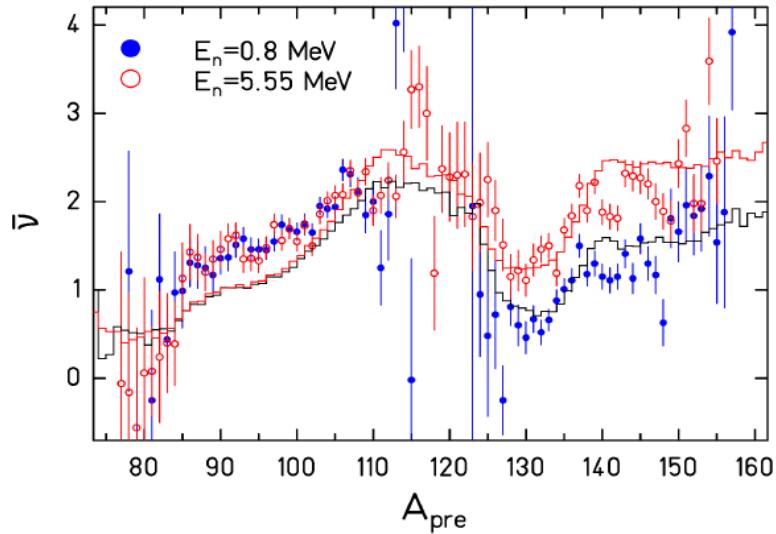


Fig. 2.  $\bar{\nu}(A)$ -values for incident neutron energies 0.8 and 5.5 MeV for  $^{237}\text{Np}(n,f)$ . The stepwise curves show the calculation by K.-H. Schmidt.

• O. Serot compared the  $\bar{\nu}(A)$ -values for  $^{239}\text{Pu}(n_{\text{th}},f)$  and  $^{240}\text{Pu}(sf)$ , measured by Wagemans *et al.* and Dematé *et al.*, for which the fissioning nucleus is the same, the only difference being  $\sim 6.5$  MeV in the excitation energy (Fig.3). In contrast to the case for  $^{237}\text{Np}(n,f)$  cited above, a substantial part of the excessive excitation energy seems to go to high-temperature LF. Is this a mischief of the *Maxwell's demon*?

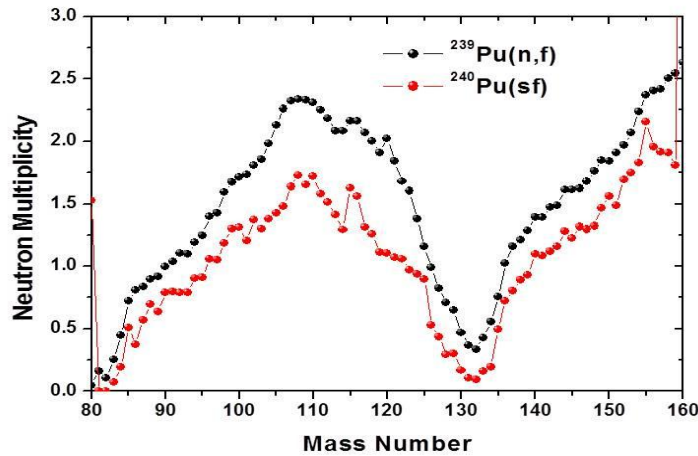


Fig. 3.  $\bar{\nu}(A)$ -values for  $^{239}\text{Pu}(n_{\text{th}},f)$  and  $^{240}\text{Pu}(sf)$  (after Serot).

• R. Vogt introduced a parameter  $x$  that adjusts the excitation energy partition according to  $\bar{E}_{\text{L}}^* = xE_{\text{L}}^*$ , where  $E_{\text{L}}^*$  is the excitation energy of LF determined by equipartition principle. Her results show that  $x > 1$  fits the saw-tooth behavior of  $\bar{\nu}(A)$ , which would imply that LF has more excitation energy than required from equipartition principle.

From the above overview, it seems to the author that the problem of energy partition between the nascent fragments has not been settled yet and still under discussion.

The author has been interested in the issue, since he was the first to propose the concept of temperature difference, or the temperature ratio  $R_{\text{T}} = \langle T_{\text{L}} \rangle / \langle T_{\text{H}} \rangle$ , twenty years ago<sup>3)</sup>. Of course this concept is only a makeshift, so to say, because, from physics point of view, the fragment excitation energy is the sum of intrinsic excitation energy and deformation energy *at the scission point*, and the

non-equitemperature concept used in the PFNS calculation concerns only the nuclear temperature *at the moment of neutron emission, i.e.*, after the initial deformation energy has been dissipated into the intrinsic excitation energy. The nuclear temperatures at the scission point and at the moment of neutron emission should be clearly distinguished. The saw-tooth structure shown in Fig.2 reflects the excitation energies of fragments at the moment of neutron emission, and *not* at scission.

According to Hamsch *et al.*<sup>4)</sup>, who studied the fragment mass and TKE distributions of  $^{237}\text{Np}(n,f)$  for incident neutron energies  $E_{in}=0.3$  to 5.5 MeV, the branching ratio to Standard-2 (S2) mode increased from 68.3% to 72.9% when going from  $E_{in}=0.7$  MeV to 5.5 MeV. Considering that the S2-mode corresponds to the 88-neutron deformed shell with  $\beta=0.65$ <sup>5)</sup> (Fig.4), and  $v_H$  is proportional to  $\beta$ , as was shown in Fig.9 of Ref.5, the increase in  $v_H$  might be accounted for by modal change at higher energies. The decrease of  $\sim 16$  MeV in the measured TKE between S1 ( $\sim 185$  MeV) and S2 ( $\sim 169$  MeV) modes corroborates this inference, since smaller TKE connotes longer charge-center distance.

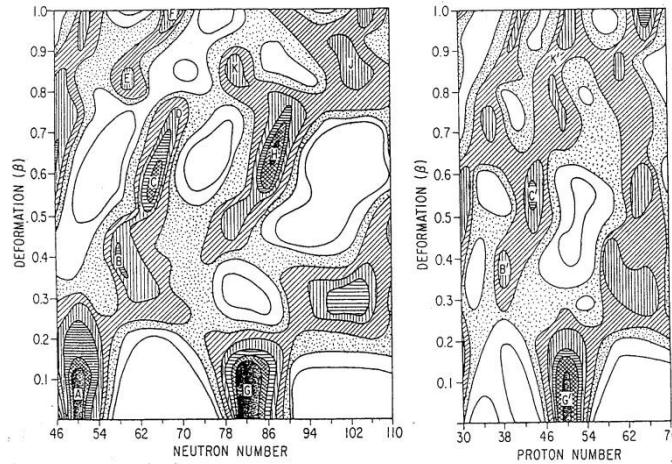
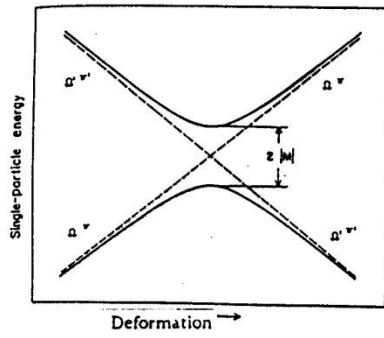


Fig. 4. Spherical shells (basins A, G, G') and deformed shell (basin H) (after Wilkins *et al.*<sup>5)</sup>). The deformed shell H is considered to be responsible for the deformation path S2.

In contrast, Schillebeeckx *et al.*<sup>6)</sup> showed that, in the case of  $^{239}\text{Pu}(n_{th},f)$  and  $^{240}\text{Pu}(sf)$ , the mode branching ratio to S2 and the corresponding TKE remain almost unchanged (74.2%, 174.2 MeV for  $^{239}\text{Pu}(n_{th},f)$  and 73.8%, 174.8 MeV for  $^{240}\text{Pu}(sf)$ ). This means that the fissioning nucleus  $^{240}\text{Pu}$  proceeds along the same deformation paths for the two cases, thus the excessive energy is shared between the two fragments.

Now, returning to thermodynamical consideration, *is it self-evident that nucleons move from high-temperature to low-temperature fragment at the scission point?* Is it stupid to ask if there is a possibility that the Maxwell's demon come into play in the quantum superfluid system? Considering that Cooper pairs of nucleons are more easily and swiftly transported between the nascent fragments than single nucleons, due to smaller energy required in transferring from one Nilsson orbit to another (Fig.5), and also the coupled pairs are less restricted by angular momentum conservation, because the intrinsic spins are coupled to be zero, there seems to be a possibility that nucleons move from low-temperature (superfluid) fragment to high-temperature (less superfluid) fragment under some condition. This situation might be realized in a transient stage from superfluid to normal state.

Thermodynamical principles apply exactly to classical statistical systems consisting of a number of particles, say, the Avogadro's number  $\sim 10^{23}$ . However, do nuclear systems consisting only of  $\sim 240$  fermions exactly follow the principles? At least, we can say that the principles entail larger fluctuations or variances for nuclear systems.



$$E = a\alpha + c$$

Non-transfer probability  
(Landau-Zener's relation)

$$E' = b\alpha + c$$

$$P = \exp\left[-\frac{2\pi|M|^2 / \eta |a-b|}{|\alpha'|}\right]$$

Fig. 5. Schematic of nucleon transfer between Nilsson orbits. The greater the strength  $|M|^2$  of the residual interaction, the greater the transfer probability.

This is simply a speculation of the author, stimulated and inspired by the ideas discussed in the meeting. It would, however, be intriguing to ask what is the driving force of nucleon transfer between the fragments, whether temperature difference or the shell effect on the deformation.

The author is thankful to the colleagues of the RCM for illuminating discussions and providing much food for thoughts.

### References

- 1) T. von Egidy and D. Bucurescu, Phys. Rev. **C72**, 044311 (2005).
- 2) A.A. Naqvi *et al.*, Phys. Rev. **C34**, 218 (1986).
- 3) T. Ohsawa, Proc. of a Consultants' Meeting on Nuclear Data for Neutron Emission in the Fission Process, INDC(NDS)-251, p.17 (1991).
- 4) F.-J. Hambsch *et al.*, Nucl. Phys. **A679**, 3 (2000).
- 5) B.D. Wilkins *et al.*, Phys. Rev. **C14**, 1832 (1976).
- 6) P. Schillebeeckx *et al.*, Nucl. Phys. **A545**, 623 (1992).

## Prompt-neutron spectra from a general description of the fission process<sup>a</sup>

Karl-Heinz Schmidt<sup>b</sup> and Beatriz Jurado<sup>c</sup>

**Abstract:** A new semi-empirical model of the fission process is described, which covers most of the properties of the fission fragments and the emitted neutrons and photons in a global and consistent way. The model is based on fragment shells that are deduced from measured fission-fragment mass distributions, assuming that the macroscopic contribution of the compound nucleus and the microscopic contributions of the nascent fragments in the potential-energy surface are separable. The distributions of the collective coordinates are attributed to the motion of the quantum oscillators in their respective potential pockets perpendicular to the fission path. Different contributions to the excitation energies of the final fragments and their division at scission are described with the help of statistical mechanics. Intrinsic excitation energies of the fragments at scission are consistently described together with the even-odd effect in fission-fragment  $Z$  distributions. Mass-dependent equilibrium deformations of the nascent fragments are adjusted to measured average prompt-neutron multiplicities. A unique set of parameters is found, which reproduces a large variety of measured data for all fissioning systems with a good precision. In contrast to most available models, this approach is applicable to fissioning systems, for which no experimental data are available.

### Introduction

Global parametrisations and very elaborate models have been developed for calculating the energy spectra of prompt fission neutrons and their multiplicity distributions. Most of them are based on measured mass-TKE distributions of the fission fragments. With the help of the  $Q$  values for specific nuclear-charge and mass splits and by considering the initial excitation energy, the total excitation energy TXE of the fragments can directly be deduced. With an assumption on the division of the TXE between the fragments, which needs to be consistent with the observed mass-dependent neutron multiplicities, the initial conditions of both fragments for a statistical de-excitation code of the Weisskopf or Hauser-Feshbach type are determined.

The task is appreciably more difficult when this experimental basis, the measured mass-TKE distribution, is not available. In this case, this information must be provided by a model calculation. The GEF code has been developed for this purpose. It is a semi-empirical model of the fission process, which covers most of the properties of the fission fragments and the emitted neutrons and photons in a global and consistent way. In addition to the mass-TKE distribution it also calculates the division of the TXE between the fragments and the angular momenta of the fragments. Moreover, the specific initial conditions of each individual fragment are given. This report gives an overview on the underlying physics ideas and the technical features of the code and presents some preliminary results.

### Fission channels

#### Experimental systematics

Figure 1 gives an overview on the measured mass and nuclear-charge distributions of fission products from low-energy fission. Fission of target nuclei in the actinide region, mostly induced by neutrons, shows predominantly asymmetric mass splits. A transition to symmetric mass splits is seen around mass 258 in spontaneous fission of fission residues. Electromagnetic-induced fission of relativistic secondary beams covers the transition from asymmetric to symmetric fission around mass 226 [1]. A pronounced fine structure close to symmetry appears in  $^{201}\text{Tl}$  [2] and in  $^{180}\text{Hg}$  [3]. It is difficult to observe low-energy fission in this mass range. Thus,  $^{201}\text{Tl}$  could only be measured down to 7.3 MeV above the fission barrier due to its low fissility, which explains the filling of the minimum between the two peaks. Only  $^{180}\text{Hg}$  was measured at energies close to the barrier after beta decay of  $^{180}\text{Tl}$ . Considering the measured energy dependence of the structure for  $^{201}\text{Tl}$  [2], the

---

a Part of this work has been performed in the frame of a consultant contract of K.-H. S. with the NEA of OECD

b E-mail: [schmidt-erzhausen@t-online.de](mailto:schmidt-erzhausen@t-online.de), URL: <http://www.khs-erzhausen.de>

c E-mail: [jurado@cenbg.in2p3.fr](mailto:jurado@cenbg.in2p3.fr), CENBG, CNRS/IN2 P3, Chemin du Solarium B.P. 120, F-33175 Gradignan, France

fission characteristics of these two nuclei are rather similar. Also other nuclei in this mass region show similar features, which have been attributed to the influence of fragment shells [4]. These shells are different from those governing the asymmetric fission of the actinides. They are not considered in the present model.

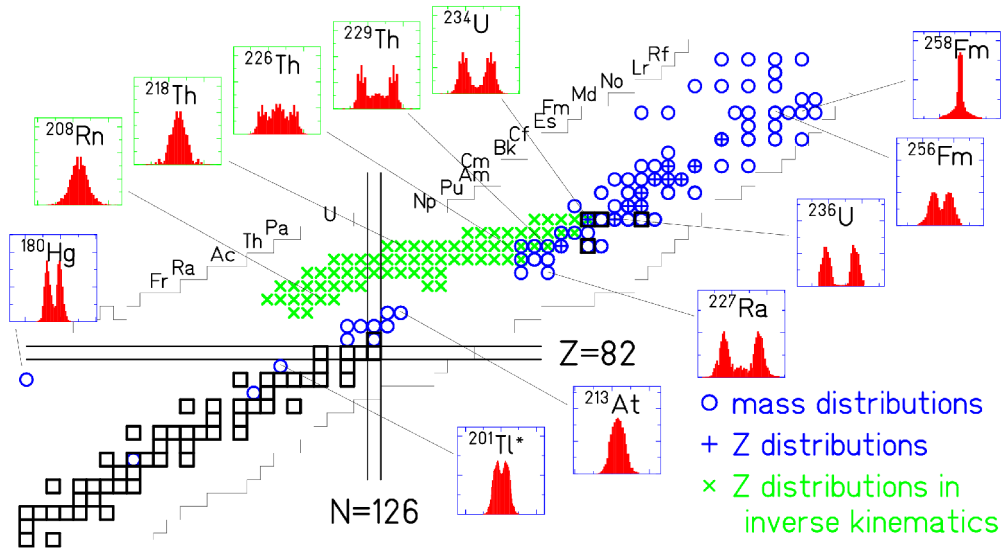


**Figure 1.** General view on the systems for which mass or nuclear-charge distributions have been measured. The distributions are shown for 12 selected systems. Blue circles (blue crosses): Mass (nuclear-charge) distributions, measured in conventional experiments [2, 3], and references given in [1]. Green crosses: Nuclear-charge distributions, measured in inverse kinematics [1].

### Size of the heavy fragment in asymmetric fission

In the range where asymmetric fission prevails, e.g. from  $^{227}\text{Ra}$  to  $^{256}\text{Fm}$ , the light and the heavy fission-product components gradually approach each other, see figure 1. A quantitative analysis reveals that the mean mass of the heavy component stays approximately constant [5] at about  $A=140$ . This has been explained by the influence of a deformed ( $\beta \approx 0.6$ ) fragment shell at  $N=88$  and the spherical shell at  $N=82$  [6], suggesting that the position of the heavy fragment is essentially constant in neutron number.

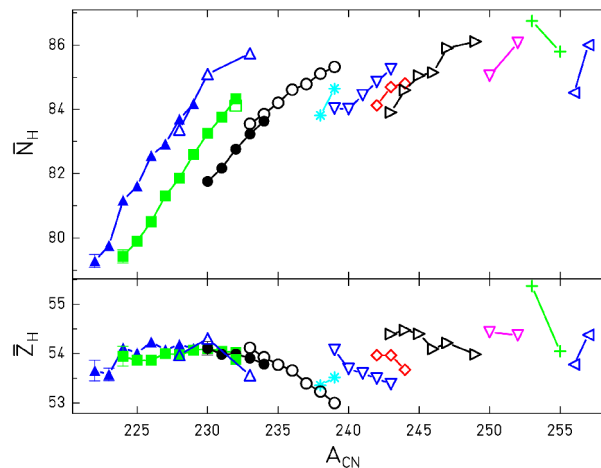


**Figure 2.** Mean neutron and proton number of the heavy component in asymmetric fission in the actinide region. The values were deduced from measured mass and nuclear-charge distributions using the semi-empirical GEF code [7] for the correction of charge polarization and prompt-neutron emission. Open symbols denote results from conventional experiments, full symbols refer to an experiment with relativistic projectile fragments of  $^{238}\text{U}$  [1]. Data points for the same  $Z_{\text{CN}}$  are connected (See [7] for references of the underlying experimental data.)

New data on  $Z$  distributions over long isotopic chains [1], however, reveal very clearly that the position in neutron number varies systematically over more than 7 units, while the position in proton number is approximately constant at  $Z=54$ , see figure 2. The rather short isotopic sequences covered in former experiments did not show this feature clearly enough and gave the false impression of a constant position in mass.

This finding represents a severe puzzle to theory, since shell-model calculations do not show any shell stabilization near  $Z=54$  at  $\beta \approx 0.6$  [6,<sup>8</sup>].

### Separability principle

The microscopic-macroscopic approach has proven to be very useful for calculating nuclear properties, in particular in applications to fission [9]. The early influence of fragment shells on the fission path, deduced from two-centre shell-model calculations [10], makes its application to fission even more powerful. It means that the microscopic properties of the fission observables are essentially determined by the shells of the fragments, and only the macroscopic properties are specific to the fissioning system [11].

This “separability principle” was exploited in the GEF code [7], which relies on an empirical description of the macroscopic stiffness parameters in the relevant normal modes and empirically deduced fragment shells, which are valid for all fissioning systems. Figure 3 demonstrates that the mass distributions over a large range of systems can be described very well with the same parameter set.

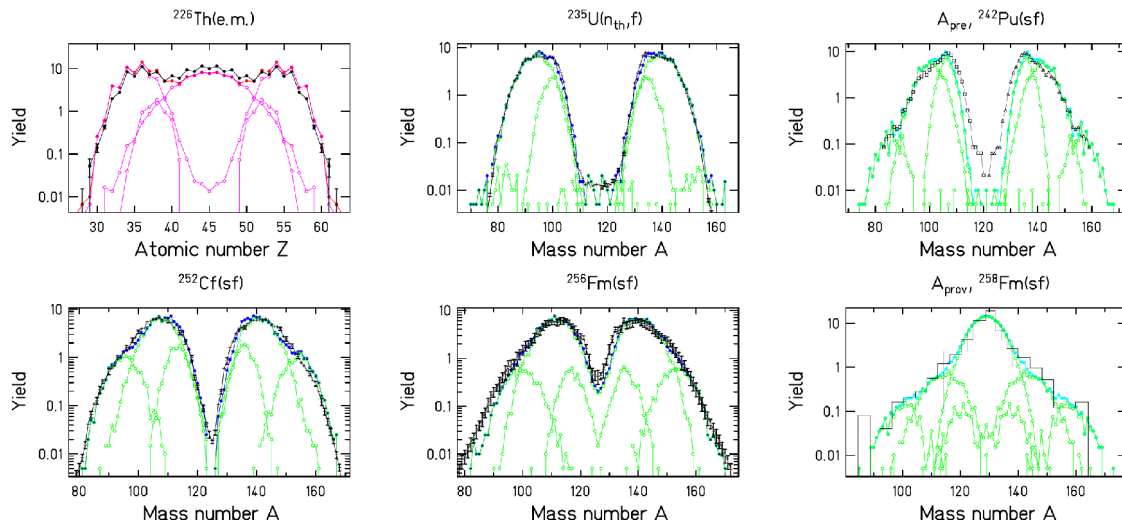


**Figure 3.** Nuclear-charge and post-neutron mass distributions of fission fragments. (For  $^{258}\text{Fm}(sf)$  the “provisional mass”  $A_{prov}$  is shown, which is directly deduced from the ratio of the kinetic energies of the fragments and thus not corrected for neutron emission.) Experimental data (black lines, respectively histogram) for electromagnetic-induced (e.m.), thermal-neutron-induced ( $n_{th},f$ ) and spontaneous fission (sf) are compared with predictions of the GEF code [7] (red and green lines). The contributions of different fission channels are shown. (See [7] for references of the data.)

### Dynamical effects

Statistical scission-point models, e.g. ref. [6], suffer from the neglect of dynamical effects. Stochastic calculations revealed that, depending on the nature of the collective degree of freedom, dynamical effects induce a kind of memory on the fission trajectory, which may be accounted for by an early freeze-out that depends on the influence of inertia. Mass-asymmetric distortions have a large inertia, and thus the mass distribution is already essentially determined slightly behind the outer fission saddle [12]. Charge polarization has a small inertia, and the distribution is determined close to scission [13].

## Fluctuations

Most fission observables form bell-shaped distributions around a mean value. This suggests treating the corresponding collective degree of freedom as an harmonic quantum oscillator coupled to a heat bath of temperature  $T$ . Especially for the charge-polarization degree of freedom there is a long discussion about the importance of the zero-point motion [14, 15]. Nix estimated the level spacing in the oscillator corresponding to mass-asymmetric distortions at saddle with the liquid-drop model to 1-2 MeV in the actinide region [16]. According to the smaller widths of the corresponding components to the mass distribution, the level spacing for oscillations in the two asymmetric fission valleys (Standard 2 and Standard 1) is about 5 and more than 10 MeV, respectively. Also for oscillations in the charge-polarization degree of freedom, the level spacing is in the order of 10 MeV. These values are appreciably larger than the temperature values of actinides, which are about 0.5 MeV in the constant-temperature regime [17]. Thus, in a statistical approach these degrees of freedom are essentially not excited, and the widths of the corresponding distributions are essentially determined by the zero-point motion.

Also the angular-momentum distributions of the fragments have been explained by “orientation pumping” due to the uncertainty principle [18]. Experimental indications for thermal excitations of spherical fragments [19] have also been explained by the compensation of the orbital angular momentum, which itself is induced by the zero-point motion [20]. Here it is the operator of the orbital angular momentum which does not commute with the angle that characterizes the direction of particle motion. Thus, all fragment angular momenta measured in low-energy fission [21] are explained by the quantum-mechanical uncertainty principle. There is no room for excitations of the angular-momentum-bearing modes [22].

Due to the strong influence of quantum-mechanical effects it is mandatory to explicitly consider these quantum-mechanical effects, as it is e.g. done in the self-consistent microscopic approach of ref. [23]. Stochastic approaches with classical models [24] seem to be inadequate.

## Comparison with previous ideas

Several descriptions of the fission observables with applications of the statistical model have been proposed in the past. The present approach is rather close to the outline of a scenario proposed by Jensen and Døssing [25], although the present model covers a larger variety of observables. More importantly, it also tries to better exploit available empirical information.

Jensen and Døssing presented a statistical calculation of the mass distribution in fission with some ideas about the dynamics of the process. The most important modifications applied in the GEF code are: (i) The shell effects that were calculated from single-particle energy spectra in a Woods-Saxon potential with the Strutinsky method in ref. [25] are replaced by global fragment shells, which are adjusted to the measured mass distributions. The separability principle simplifies this task considerably, since the fragment shells are assumed to depend only on the fragment, and, thus, they are the same for all fissioning systems. (ii) The nuclear level density that was calculated from the same single-particle spectrum including pairing correlations using the BCS approximation in ref. [25] is replaced by an empirical constant-temperature formula [17], which seems to be in good agreement with recent experimental results [26]. (iii) The influence of quantum-mechanics, in particular the zero-point motion, has been considered to model the distributions of collective coordinates. They are attributed to the motion of the quantum oscillators in their respective potential pockets perpendicular to the fission path. The parameters of these oscillators are deduced from experimental data. In addition, the shapes of the fragments at scission, the charge polarization, the angular momenta, and other properties of the fragments are calculated on the basis of similar ideas.

## Prompt-neutron yields

### Transformation of energy – the different contributions

In low-energy fission, the  $Q$  value of the reaction ends up either in the total kinetic energy (TKE) or the total excitation energy (TXE) of the fragments. The TKE is closely related to the distance of the

centres of the two nascent fragments at scission, but it cannot give information on the shapes of the individual fragments. The TXE, however, can be attributed to the individual fragments by a kinematical measurement of the prompt-neutrons. Still, there is no direct experimental information on the processes, which are responsible for the transformation of part of the Q value into the excitation energies of the separated fragments. The situation is schematically illustrated in figure 4. Before scission, dissipation leads to intrinsic excitations, collective modes perpendicular to the fission direction (“normal modes” [16]) may be excited, and, finally, some energy is stored in deformation of the nascent fragments that is induced by the Coulomb repulsion. The remaining part is found as pre-scission kinetic energy [27]. After scission, collective excitations and deformation energy are transformed and add up to the intrinsic excitations of the separated fragments. The situation at scission is important for the understanding of fission dynamics, e.g. the magnitude of dissipation and the coupling between the different collective degrees of freedom, but without additional information, the repartition of the different contributions between the fragments remains ambiguous.

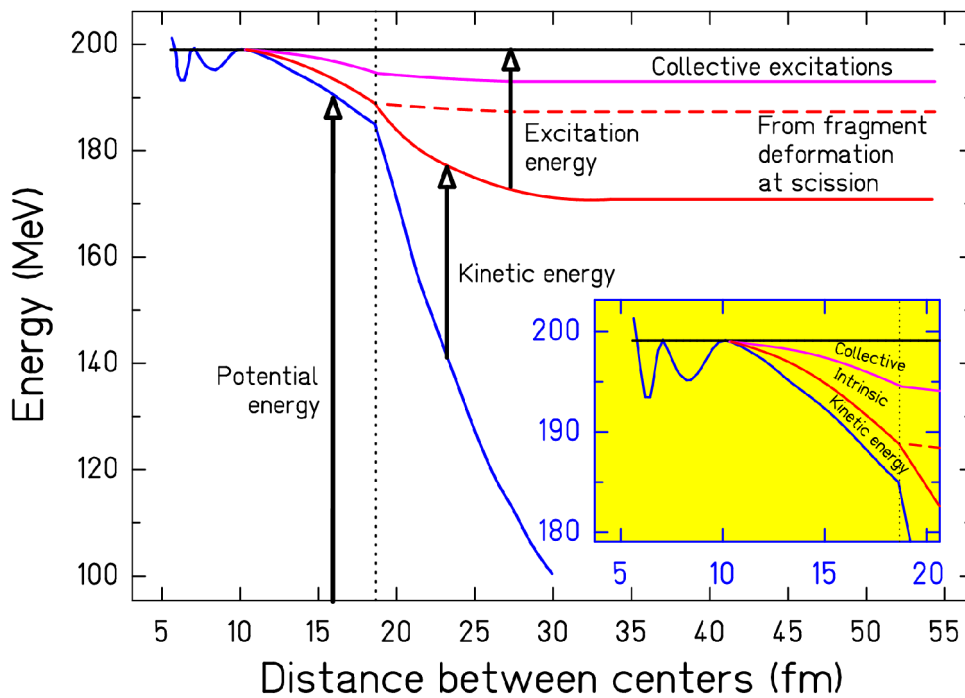


**Figure 4.** Schematic drawing of the transformation of energy during the fission process of  $^{236}\text{U}$  with an initial excitation energy equal to the height of the fission barrier.

### Origin of the saw-tooth shape

There is widespread agreement that the saw-tooth shape of the prompt-neutron yields, see figure 5, is caused by the deformation energies of the nascent fragments at scission. The scission-point model of ref. [6] attributes it to the influence of fragment shells, the random-neck-rupture model [28] links it to the location of the rupture, and also microscopic calculations predict large deformation energies of the fragments near scission [29]. Large even-odd effects in the fragment Z distributions indicate that the intrinsic excitation energy at scission is generally much too low to account for the variation of the prompt-neutron yield by several units over the different fragments.

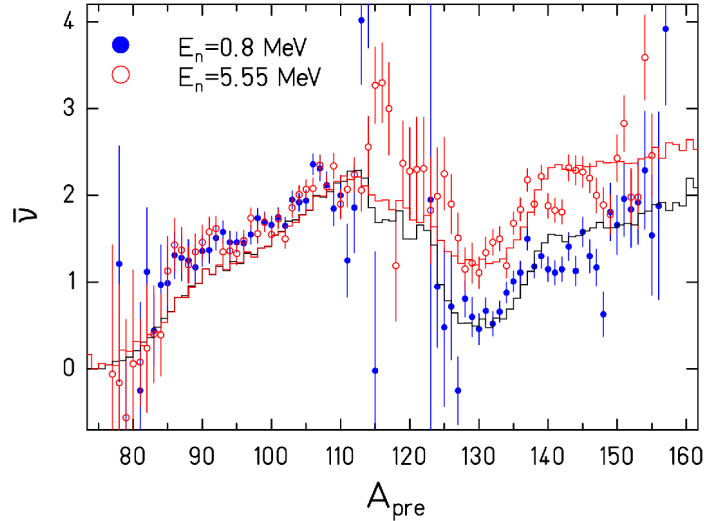


**Figure 5.** Measured prompt-neutron yield in  $^{237}\text{Np}(n,f)$  as a function of pre-neutron mass at two different incident-neutron energies  $^{[30]}$  (data points) in comparison with the result of the GEF code  $^{[7]}$  (histograms).

#### Differential behaviour – energy sorting

Recent experimental results reveal that nuclei exhibit an essentially constant temperature, may be up to excitation energies of 20 MeV  $^{[31]}$  with a temperature parameter that is grossly proportional to  $A^{-2/3}$   $^{[17]}$ . This behaviour is explained by the breaking of pairs in the so-called superfluid regime  $^{[32]}$ . This leads to a considerable increase of the heat capacity  $^{[33]}$  and consequently to a slow variation of temperature as a function of excitation energy. Note that the BCS approximation severely underestimates the pairing condensation energy and consequently also the magnitude of the heat capacity in the so-called superfluid regime  $^{[34]}$ . Thus, the assumption of a constant nuclear temperature becomes a good approximation. This implies that the intrinsic excitation energy of the two nascent fragments at scission is subject to energy sorting  $^{[35, 36, 37]}$ : The hotter light fragment transfers essentially all its intrinsic excitation energy to the colder heavy fragment. This energy sorting manifests itself in the mass-dependent neutron yields. Fig. 5 shows data for neutron-induced fission of  $^{237}\text{Np}$  with  $E_n = 0.8$  MeV and  $E_n = 5.55$  MeV as an example. The additional initial energy leads to an increased neutron yield from the heavy fragments, only. The behaviour is well reproduced by the GEF code, which includes a model for the process of energy sorting.

## Even-odd effect in Z yields

### Experimental systematics

A systematic view on the local even-odd effect in fission-fragment Z distributions  $^{[38]}$  reveals a regular pattern and a general dependence on the fissioning system, see figure 6. The magnitude of the even-odd effect is small at symmetry, and it increases strongly with increasing asymmetry. At the same time, the even-odd effect generally decreases for heavier systems. The even-odd effect in the light fragment group of nearby even-Z and odd-Z systems is essentially identical, except at symmetry, where the even-odd effect in odd-Z systems is exactly zero. Electromagnetic excitations lead to slightly higher excitation energies, thus reducing the magnitude of the even-odd effect. The large number of systems investigated revealed that the appearance of a large even-odd effect at large asymmetry is a general phenomenon, also in odd-Z fissioning systems  $^{[39]}$ . In any case, there is an enhancement of even-Z fragments in the light fragment group, indicating that it is the enhanced production of even-Z light fragments in their ground state, which is at the origin of the large even-odd effect at extreme asymmetry.

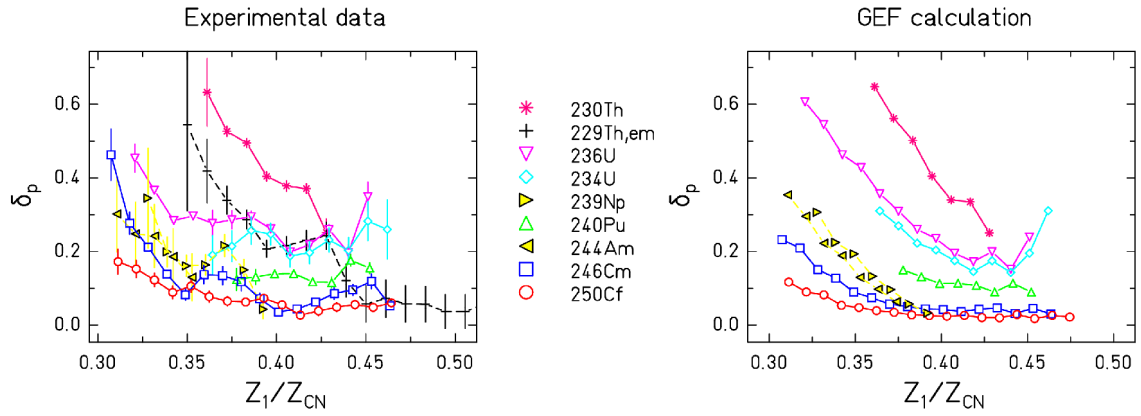


**Figure 6.** Measured (left) and calculated (right) local even-odd effect in fission-fragment  $Z$  distributions in  $(n_{th},f)$  reactions. The fissioning nuclei are indicated. Data for fission of  $^{229}\text{Th}$ , induced by electromagnetic excitations are included. See ref. [38] for references of the data.

### Final stage of energy sorting

It seems straightforward to attribute the enhanced production of even- $Z$  light fragments to the energy-sorting mechanism [40] that explained already the differential behaviour of the prompt-neutron yields. If the time until scission is sufficient for the energy sorting to be accomplished, the system can still gain an additional amount of entropy by predominantly producing even-even light fragments. Compared to the production of odd-odd light fragments, the excitation energy of the heavy fragment increases by two times the pairing gap, and its entropy increases due to the increasing number of available states in the heavy fragment. The right part of figure 6 shows a calculation with the GEF code, where this idea is included in a schematic way. The basic features are: (i) The excitation energy induced by dissipation grows with the Coulomb parameter  $Z^2/A^{1/3}$ , and the time needed for complete energy sorting is correspondingly increased. This explains the observed reduction of the even-odd effect for heavier systems. (ii) The thermal pressure grows with increasing asymmetry, which accelerates the energy-sorting process. This explains the strong increase of the even-odd effect at large asymmetry.

The asymmetry-driven even-odd effect is thus a threshold phenomena, which sets in when the time needed for reaching the scission configuration is sufficiently long for complete energy sorting. Fluctuations in the energy-sorting process are responsible for the smooth onset of the even-odd effect with increasing asymmetry.

## Charge polarization

### Experimental information

Most experimental information on charge polarization at scission is indirect, because only the fragment masses after the emission of prompt neutrons can be measured with good resolution. Thus, the influence of prompt-neutron emission has to be corrected. This correction introduces some uncertainties, because most data on mass-dependent prompt-neutron multiplicities are not very precise, and for many systems such data are not available.

Figure 7 shows the measured deviation of the mean nuclear charge from the UCD (unchanged charge distribution) value for a fixed post-neutron mass and the standard deviation of the corresponding nuclear-charge distribution for the thermal-neutron-induced fission of  $^{235}\text{U}$  [41]. The influence of the even-odd staggering of the  $Z$  yields is clearly visible in both quantities.

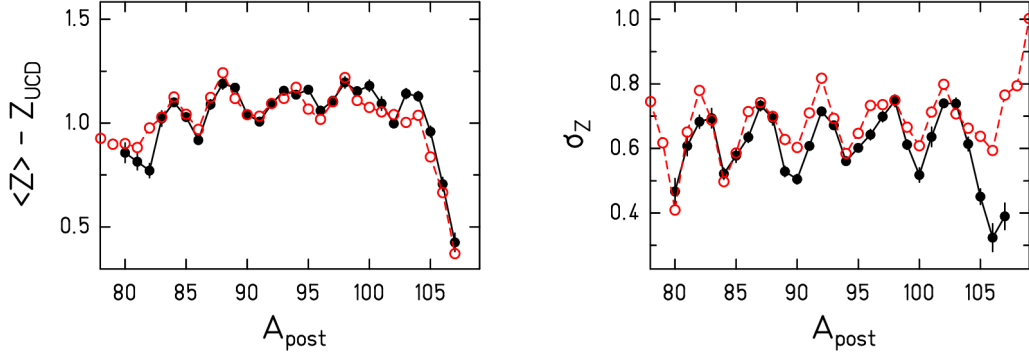


**Figure 7.** Indirect information on the charge polarization in  $^{235}\text{U}(n_{th},f)$ . Left part: Deviation of the mean nuclear charge from the UCD (unchanged charge distribution) value for a fixed post-neutron mass  $A_{post}$ . Experimental data [41] (full points) are compared with the result of the GEF code [7] (open points). Right part: Standard deviation of the nuclear-charge distribution for a fixed post-neutron mass  $A_{post}$ . Experimental data [41] (full points) are compared with the result of the GEF code [7] (open points).

### Simulation

The simulation of the nuclear-charge distributions for fixed post-neutron mass starts from the calculated pre-neutron nuclide distribution and the excitation energy of each individual fragment. The emission of prompt neutrons must be considered, which is constrained by measured mass-dependent prompt-neutron multiplicity distributions. The good agreement with post-neutron fragment distributions shown in figure 7 was obtained by minimizing the potential energy of the scission configuration, approximated by quadrupole-deformed fragments with a tip distance of 3 fm with respect to their  $N/Z$  ratios. However, for the asymmetric fission channels, the value of  $\langle Z \rangle - Z_{UCD}$  had to be increased (decreased) by 0.3 units in the light (heavy) fragment. The mean deformation of the fragments at scission is linked to the mean prompt-neutron multiplicity, considering the amount of intrinsic excitation energy at scission, which is consistent with the description of the even-odd effect in the  $Z$  distributions.

### Fragment kinetic energies

In the GEF code, the total kinetic energy of the fission fragments is given by subtracting the total excitation energy of the separated fragments from the sum of the initial excitation energy of the fissioning nucleus and the  $Q$  value of the fission process. The resulting distribution for  $^{235}\text{U}(n_{th},f)$  is shown in figure 8. The overall behaviour is in agreement with expectations from systematics. In the model, the shape of the energy distribution for a fixed mass is mainly defined by the distribution of fragment deformations at scission, which is taken as a Gaussian distribution with a maximum in the respective potential minimum. These shapes are assumed to be decisive for the amount of deformation energy of the separated fragments with respect to their respective ground state, which finally adds up to their intrinsic excitation energy. This explains the skewness of the distributions, which seem to be slightly larger than found in experiment.

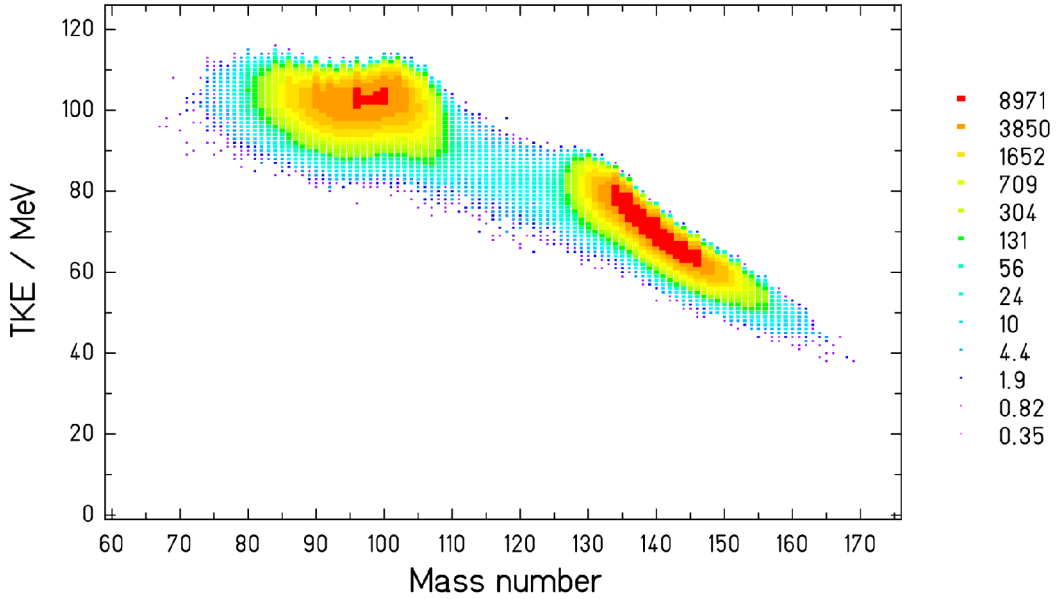


**Figure 8.** Two-dimensional distribution of kinetic energies and fission-fragment masses before emission of prompt neutrons for  $^{235}\text{U}(n_{\text{th}},f)$ . The colour scale refers to the counts of the Monte-Carlo calculation.

## Neutron multiplicities

Besides the mass-dependent mean prompt-neutron yields, see figure 5, there exist two other experimental results, which have been determined with high accuracy: The mass-integrated neutron-multiplicity distribution and the mean number of prompt fission neutrons.

The measured mean number of prompt-fission neutron yields is compared in table 1 with the values given by the GEF code for some selected systems. The same parameter set was used for all systems. However, the TXE had to be increased by 1.6 MeV, equally shared between the fragments, for odd- $Z$  fissioning systems, just as an empirical parameterisation. This is a general effect, found on the average over the whole range of fissioning systems. In contrast, there is no even-odd fluctuation in the neutron number of the fissioning nucleus.

**Table 1.** Selected values of mean prompt-neutron multiplicities. The measured values are compared with the result of the GEF code.

System	$E_n$	Exp.	GEF
$^{235}\text{U}(n,f)$	thermal	2.41 [42]	2.36
$^{235}\text{U}(n,f)$	0.5 MeV	2.46 [43]	2.47
$^{235}\text{U}(n,f)$	5.55 MeV	3.19 [43]	3.19
$^{237}\text{Np}(n,f)$	0.8 MeV	2.73 [30]	2.71
$^{237}\text{Np}(n,f)$	5.55 MeV	3.46 [30]	3.41
$^{239}\text{Pu}(n,f)$	thermal	2.88 [42]	2.93

Figure 9 demonstrates the excellent agreement of the calculated neutron-multiplicity distributions for  $^{235}\text{U}(n_{\text{th}},f)$  and  $^{239}\text{Pu}(n_{\text{th}},f)$  with the experimental data. Like in the case of the fragment kinetic energies, the width is mostly caused by the distribution of fragment deformations at scission. The shape of the distribution is very well reproduced for both systems.

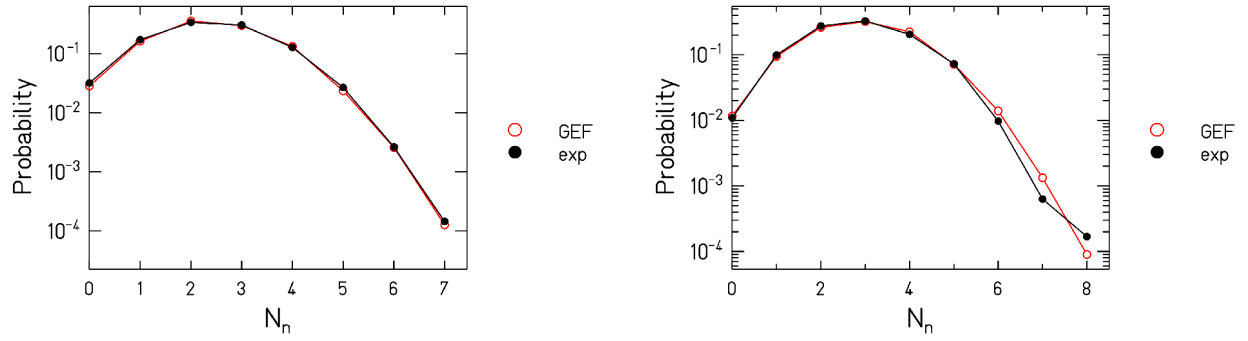


**Figure 9.** Measured prompt-neutron multiplicity distributions [42] for  $^{235}\text{U}(\text{nth},\text{f})$  (left part) and  $^{239}\text{Pu}(\text{nth},\text{f})$  (right part) are compared to the results of the GEF code.

### Prompt-neutron spectrum

The revised experimental prompt-fission-neutron spectrum for the system  $^{235}\text{U}(\text{nth},\text{f})$  [44] is compared with the result of the GEF code in figure 10. In order to better visualize the slight deviations, figure 11 shows this comparison in a reduced presentation with both spectra normalized to a Maxwellian distribution with the parameter  $T = 1.32$  MeV.

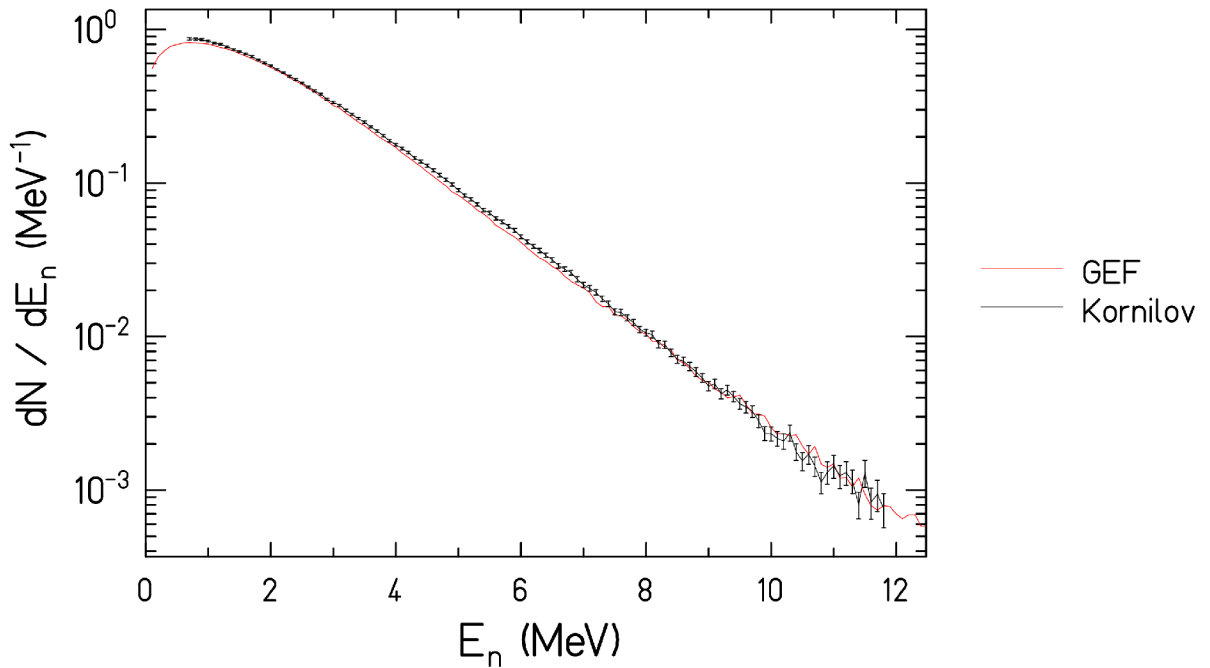


**Figure 10.** Experimental prompt-fission-neutron spectrum for  $^{235}\text{U}(\text{nth},\text{f})$  [44] in comparison with the result of the GEF code.

In this calculation, the de-excitation of the separated fragments has been obtained with a statistical model. It is assumed that both the emission of neutrons and the emission of E1 gammas does not change the angular momentum on the average, which seems to be a good approximation in the relevant angular-momentum range [45]. The angular momentum is carried away by a cascade of E2 gammas when the yrast line is reached. The angular momentum is connected with the experimental isomeric-yield ratios, e.g. ref. [12]. Inverse total neutron cross sections from a calculation of ref. [46] have been used. Gamma competition at energies above the neutron separation energy was considered. The gamma strength in the relevant energy range in the tail of the giant dipole

resonance (GDR) has been approximated by a power law  $\sim E_\gamma^{4.4}$  according to ref. [47]. Gamma competition has an important role in creating an even-odd effect in the fission-fragment neutron distributions [48, 49] but it has only a minor influence on the prompt-neutron emission. The nuclear level density was consistently modelled in the GEF code by the constant-temperature description of Bucurescu and Egidy [17] at low energies. The temperature value was normalized to the value determined for  $^{172}\text{Yb}$  in ref. [47]. The level density was smoothly joined with a Fermi-gas formula at an excitation energy  $E_{trans} = 4.5 \text{ MeV} + n \cdot \Delta_0$ ,  $\Delta_0 = 12/\sqrt{A}$ ,  $n = 0$  for odd-odd nuclei,  $n = 1$  for even-odd nuclei, and  $n = 2$  for even-even nuclei.

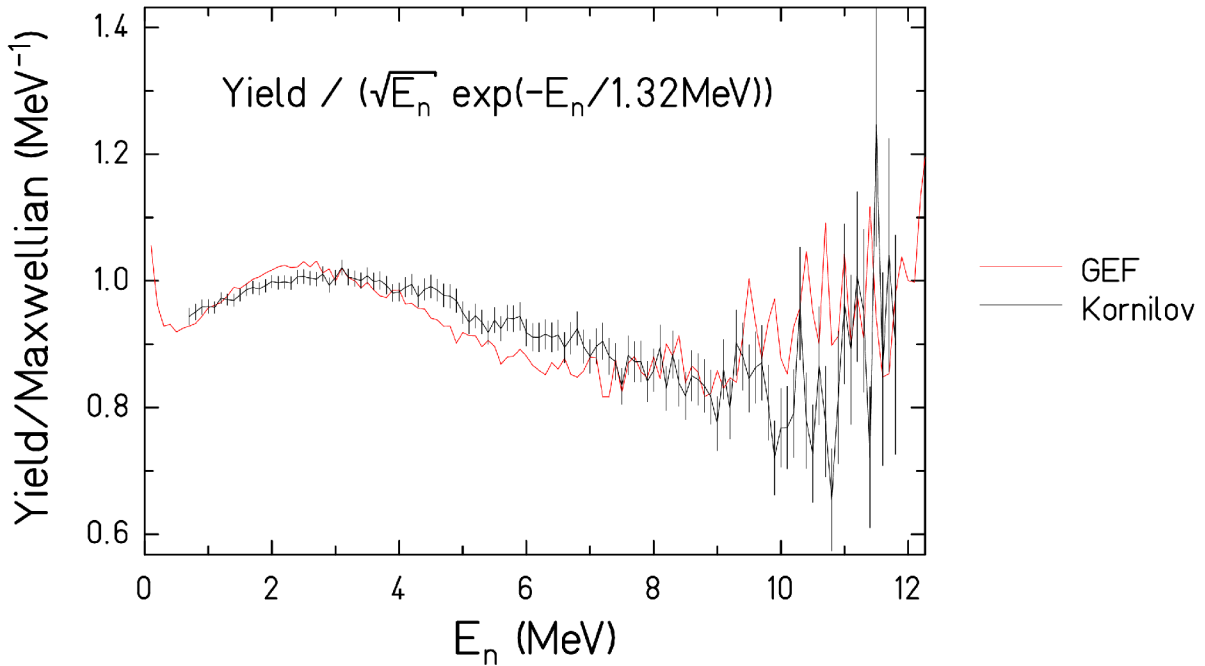


**Figure 11.** Experimental prompt-fission-neutron spectrum for  $^{235}\text{U}(n_{th},f)$  [12] in comparison with the result of the GEF code. Both spectra have been normalized to a Maxwellian with  $T = 1.32 \text{ MeV}$ .

## Conclusion

The semi-empirical fission model, implemented in the GEF code, reproduces a large variety of observables with a good precision in a consistent way without further adjustment to specific fissioning systems. With this global approach one is able to predict several characteristic quantities of the fission process, e.g. the energy and multiplicity distribution of prompt-fission neutrons, without the need for specific experimental information of the respective system, e.g. measured mass-TKE distributions. All properties of the fission fragments that are considered in the code (e.g. nuclear charge, mass, excitation energy, angular momentum) are sampled in the corresponding multi-dimensional parameter space by a Monte-Carlo technique. Thus, all respective correlations are preserved. Moreover, correlations between all observables considered in the code are provided on an event-by-event basis.

**Part of this work has been supported by the NEA of the OECD (<http://www.oecd-nea.org/>), by the EFNUDAT (<http://www.efnudat.eu/>) and by the ERINDA (<http://www.erinda.org/>) project.**

- 1 K.-H. Schmidt et al., Nucl. Phys. A 665 (2000) 221
- 2 M. G. Itkis et al., Sov. J. Nucl. Phys. 52 (1990) 601
- 3 A. N. Andreyev et al., Phys. Rev. Lett. 105 (2010) 252502
- 4 S. I. Mulgin, K.-H. Schmidt, A. Grewe, S. V. Zhdanov, Nucl. Phys. A 640 (1998) 375
- 5 J. P. Unik et al., Proc. Symp. Phys. Chem. Fission, Rochester 1973, IAEA Vienna (1974), vol. 2, p. 19
- 6 B. D. Wilkins, E. P. Steinberg, R. R. Chasman, Phys. Rev. C 14 (1976) 1832
- 7 <http://www.cenbg.in2p3.fr/GEF>, <http://www.khs-erzhausen.de>
- 8 I. Ragnarsson, R. K. Sheline, Phys. Scr. 29 (1984) 385
- 9 M. Brack et al., Rev. Mod. Phys. 44 (1972) 320
- 10 U. Mosel, H. Schmitt, Phys. Rev. C 4 (1971) 2185
- 11 K.-H. Schmidt, A. Kelic, M. V. Ricciardi, Europh. Lett. 83 (2008) 32001
- 12 A. V. Karpov, P. N. Nadtochy, D. V. Vanin, G. D. Adeev, Phys. Rev. C 63 (2001) 054610
- 13 A. V. Karpov, G. D. Adeev, Eur. Phys. J. A 14 (2002) 169
- 14 H. Nifenecker, J. Physique Lett. 41 (1980) 47
- 15 B. Bouzid et al., J. Phys. G: Nucl. Part. Phys. 24 (1998) 1029
- 16 J. R. Nix, Ann. Phys. 41 (1967) 52
- 17 D. Bucurescu, T. von Egidy, Phys. Rev. C 72 (2005) 06730
- 18 L. Bonneau, P. Quentin, I. N. Mikhailov, Phys. Rev. C 75 (2007) 064313
- 19 F. Gönnewein, I. Tsekhanovich, V. Rubchenya, Intern. J. Mod. Phys. E 16 (2007) 410
- 20 S. G. Kadmsky, Phys. Atom. Nuclei 71 (2008) 1193
- 21 H. Naik, S. P. Dange, R. J. Singh, A. V. R. Reddy, Eur. Phys. J. A 31 (2007) 195
- 22 L. G. Moretto, G. F. Peaslee, G. J. Wozniak, Nucl. Phys. A 502 (1989) 453c
- 23 H. Goutte, J. F. Berger, P. Casoli, D. Gogny, Phys. Rev. C 71 (2005) 024316
- 24 J. Randrup, P. Möller, A. J. Sierk, Phys. Rev. C 84 (2011) 034613
- 25 A. S. Jensen, T. Døssing, Proc. Symp. Phys. Chem. Fission, Rochester 1973, IAEA Vienna (1974), vol. 1, p. 40
- 26 A. V. Voinov et al., Phys. Rev. C 79 (2009) 031301
- 27 V. M. Kolomietz, S. Åberg, S. V. Radionov, Phys. Rev. C 77 (2008) 014305
- 28 U. Brosa, S. Grossmann, A. Müller, Phys. Rep. 197 (1990) 167
- 29 N. Dubray, H. Goutte, J.-P. Delaroche, Phys. Rev. C 77 (2008) 014310
- 30 A. A. Naqvi, F. Käppeler, F. Dickmann, R. Müller, Phys. Rev. C 34 (1986) 21
- 31 A. V. Voinov et al., Phys. Rev. C 79 (2009) 031301
- 32 M. Guttormsen et al., Phys. Rev. C 68 (2003) 034311
- 33 Y. Alhassid, G. F. Bertsch, L. Fang, Phys. Rev. C 68 (2003) 044322
- 34 G. G. Dussel, S. Pittel, J. Dukelsky, P. Sarriguren, Phys. Rev. C 76 (2007) 011302
- 35 K.-H. Schmidt, B. Jurado, Phys. Rev. Lett. 104 (2010) 21250
- 36 K.-H. Schmidt, B. Jurado, Phys. Rev. C 82 (2011) 014607
- 37 K.-H. Schmidt, B. Jurado, Phys. Rev. C 83 (2011) 061601
- 38 M. Caamaño, F. Rejmund, K.-H. Schmidt, J. Phys. G: Nucl. Part. Phys. 38 (2011) 035101
- 39 S. Steinhäuser et al., Nucl. Phys. A 634 (1998) 89
- 40 K.-H. Schmidt, B. Jurado, arXiv:1007.0741v1[nucl-th] (2010)
- 41 W. Lang et al., Nucl. Phys. A 345 (1980) 34
- 42 M. S. Zucker, N. E. Holden, Report BNL-38491 (1986)
- 43 R. Müller, A. A. Naqvi, F. Käppeler, F. Dickmann, Phys. Rev. C 29 (1984) 885
- 44 <http://www-nds.iaea.org/pfns/expdata/Kornilov/>
- 45 J. R. Huizenga, R. Vandenbosch, Phys. Rev. 120 (1960) 130
- 46 J. Blatt and V. F. Weisskopf, Theoretical Physics (John Wiley & Sons, New York, 1952)
- 47 A. Schiller et al., Nucl. Instrum. Methods A 447 (2000) 498
- 48 M. V. Ricciardi et al., Nucl. Phys. A 733 (2004) 299
- 49 M. V. Ricciardi et al., arXiv:1007.0386v1 [nucl-ex] (2010)

# Preliminary remarks on some correlations of prompt-neutron multiplicities with properties of the fission fragments

Contribution to the IAEA  
Coordinated Research Program on Prompt Fission Neutron Emission

Karl-Heinz Schmidt, 27. 5. 2012

**Abstract:** The differential behaviour of prompt-neutron multiplicities in the system  $^{235}\text{U}(n_{\text{th}},f)$  as a function of the total kinetic energy of the fission fragments and as a function of the emission angle relative to the direction of the light fragment are calculated with the GEF code. The results deviate from previous calculations by Nikolay Kornilov and are closer to the experimental data. The possible role of approximations and the neglect of correlations in the multi-dimensional coordinate space that characterizes the fission process are discussed.

In the report JEF/DOC 1423 [1] it has been shown that the average multiplicities, the multiplicity distributions and the energy spectra of the prompt neutrons of several systems are rather well reproduced by the GEF code by assuming statistical emission from the fragments, only. Also the details of the model and a comparison with other fission observables can be found in this report. One of the most important features of this model is the full treatment of all essential coordinates of the fissioning system along the fission process as given by the theoretical assumptions and the parameters of the model, without any averaging. In particular, all correlations are preserved.

In a long-standing discussion, difficulties in reproducing some correlations of prompt-neutron properties with specific properties of the fission fragments have been quoted as an indication that the physics behind the emission of prompt neutrons is not yet fully understood. As a possible solution of these problems, a contribution of prompt-neutron emission at scission (“scission neutrons”) has been considered.

One of these correlations is the neutron multiplicity versus the direction of the light fragment. Figure 1 shows the experimental data of ref. [2] in comparison with the result of the GEF code. There are some deviations: The GEF code overestimates the neutron multiplicity in the direction of the heavy fragment by about 10 % and underestimates the neutron multiplicity very close to the direction of the light fragment. This result differs considerably from the result of the calculation of N. Kornilov [3] that underestimates the neutron multiplicity in half the solid angle towards the heavy fragment by up to 37 %.

Another correlation that has been investigated is the variation of the mean prompt-neutron multiplicity as a function of the total kinetic energy ( $TKE$ ) of the fission fragments. Figure 2 shows a comparison of the result of the GEF code with experimental data [4, 5] and a previous calculation of N. Kornilov [3]. The different sets of data show rather diverging slopes  $d\langle\nu\rangle/dTKE$ . While the experimental data show rather high values (17.0 [4] and 21.1 [5]), the calculation of N. Kornilov [3] has a slope of 9.1, which is only about 1/2 of the experimental values. The slope of the result of the GEF code (15.5) is much closer to the experimental values.

The differential behaviour of the prompt-neutron multiplicity as a function of the emission angle and as a function of the fission-fragment  $TKE$  is obviously strongly model dependent. The result of the GEF code is much closer to the experimental data than the calculation of N. Kornilov. This is a strong motivation to carefully study the origin of the disagreement between the results of the different models in order to have a better basis for interpreting the discrepancies between a specific model calculation and the experimental data.

One can imagine that it is important for reproducing correlations between different fission observables that the model explicitly treats all essential coordinates of the fissioning system along the whole fission process for each fission event separately. Any averaging, e.g. introducing average velocities of light and heavy fragments (e.g. [2]), may distort the correlations and risks to lead to erroneous conclusions. Whether this is an explanation for the discrepancies between the two model calculations considered above needs further investigations.

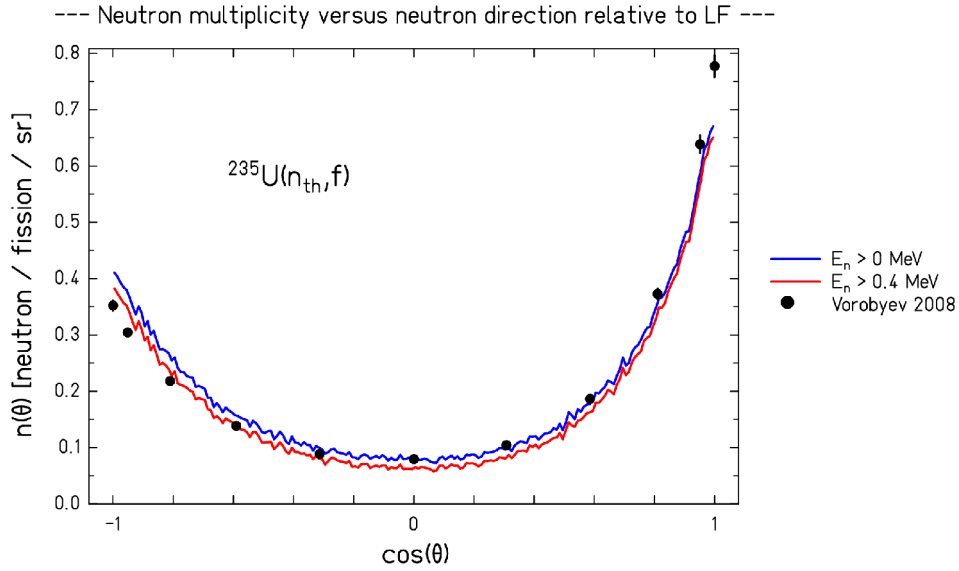


Figure 1: Variation of the prompt-neutron multiplicities versus the neutron direction relative to the light fission fragment. The result of the GEF code with two different neutron-energy thresholds is compared with experimental data from ref. [2]. The energy threshold in the experiment was 0.15 to 0.2 MeV.

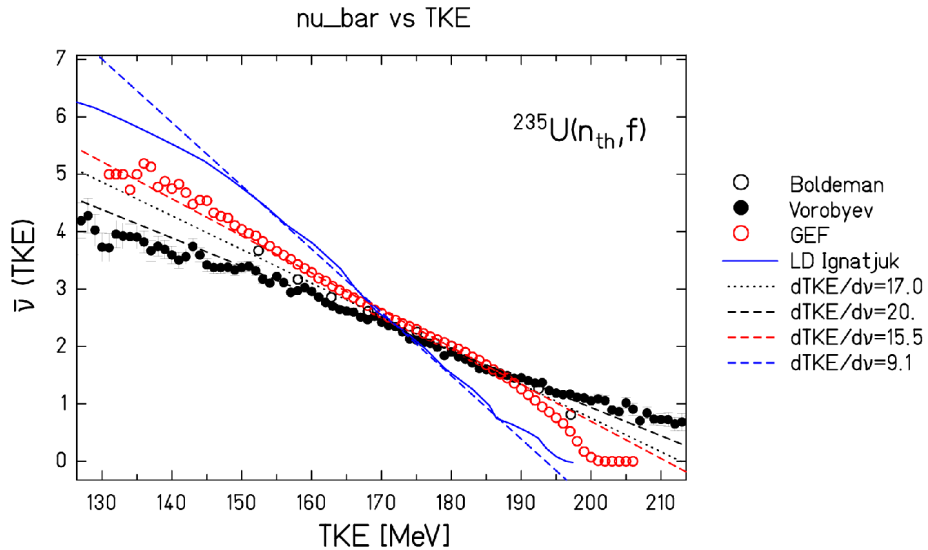


Figure 2: Variation of the mean prompt-neutron multiplicity as a function of the total kinetic energy of the fission fragments in the system  $^{235}\text{U}(n_{th}, f)$ . The experimental data of Boldeman et al. [4] and Vorobyev et al. [5] are compared with a calculation of N. Kornilov [3] (labeled as “LD Ignatjuk”) and the result of the GEF code. Linear fits to the different correlations are shown in addition. The symbols and line styles are explained in the legend.

- 1 K.-H. Schmidt, B. Jurado, JEF/DOC 1423, OECD-NEA, Paris, 2012 (available at [www.khs-erzhausen.de](http://www.khs-erzhausen.de) )
- 2 A. S. Vorobyev et al., Nucl. Instrum. Methods A 598 (2009) 795
- 3 N. Kornilov, private communication, 20. 4. 2012
- 4 J. W. Boldeman et al. , Aust. J. Phys. 24 (1971) 821
- 5 A. S. Vorobyev, EXFOR41516

## Correlation between prompt-neutron multiplicities and fission-fragment total kinetic energies further investigated with the GEF code.

Karl-Heinz Schmidt, June 5, 2012

Figure 1 shows a comparison of some results of the GEF code with experimental data [1, 2] and a previous calculation of N. V. Kornilov [3]. The first GEF calculation has been performed using the Thomas-Fermi masses of Myers and Swiatecki [4] with recommended shell corrections and schematic even-odd fluctuations. The variation of the prompt-neutron yields from the light and the heavy fragment were assumed to be uncorrelated for a given split in  $Z$  and  $N$ . In the second calculation the anti-correlation of the variation of the prompt-neutron yields from the light and the heavy fragments found in ref. [5] has been included. In the third calculation, atomic masses from the 2003 data evaluation have been used.

All GEF calculations are rather close to the data of the two experiments near the maximum of the  $TKE$  distribution (around 175 MeV). There is some influence of the anti-correlation in the prompt-neutron yields of light and heavy fragments: With the anti-correlation considered, the calculation shows a smaller slope. Also the mass model has some influence: The slope increases slightly if experimental masses are used. However, all GEF calculations, in particular the slopes, are rather close to the experimental data in the region between 155 MeV and 185 MeV. Also the low-energy point of Boldeman is well reproduced. For energies higher than 185 MeV all calculations, also the calculation of Kornilov, are appreciably below the experimental data. The cut-off slightly below 200 MeV is probably realistic, because even for the splits with the highest  $Q$  values the excitation energies of the fragments fall below the corresponding neutron separation energy.

One should not forget that scattering phenomena can considerably disturb experimental data in regions of low yield as e.g. demonstrated in ref. [6]. Such processes would tend to flatten the variation of the prompt-neutron yield as a function of  $TKE$ . In this context it is interesting to note that the data of Boldeman et al. have a steeper slope than the data of Vorobyev et al., especially in the wings of the  $TKE$  distribution. The data of Vorobyev et al. even extend to  $TKE$  values, where there is hardly any yield expected, and neutrons are still seen above  $TKE = 200$  MeV, where neutron emission is suppressed in the GEF code due to the  $Q$ -value limit. This puts also doubts on the data of Vorobyev et al. for total kinetic energies below 150 MeV, where the yield is low and scattering phenomena may have an important influence.

The GEF code reproduces also well the measured mean prompt-neutron yields as a function of the total fission-fragment total kinetic energy for spontaneous fission of  $^{252}\text{Cf}$  of ref. [7].

As a conclusion one may speculate that the “transport” of a multitude of correlations along the fission process in the GEF code without any intermediate averaging has an important influence on correlations between different fission observables. The calculations with the GEF code do not give strong hints for additional phenomena; the data of figure 1 can rather well be reproduced with the assumption of prompt neutron emission from the fragments after scission.

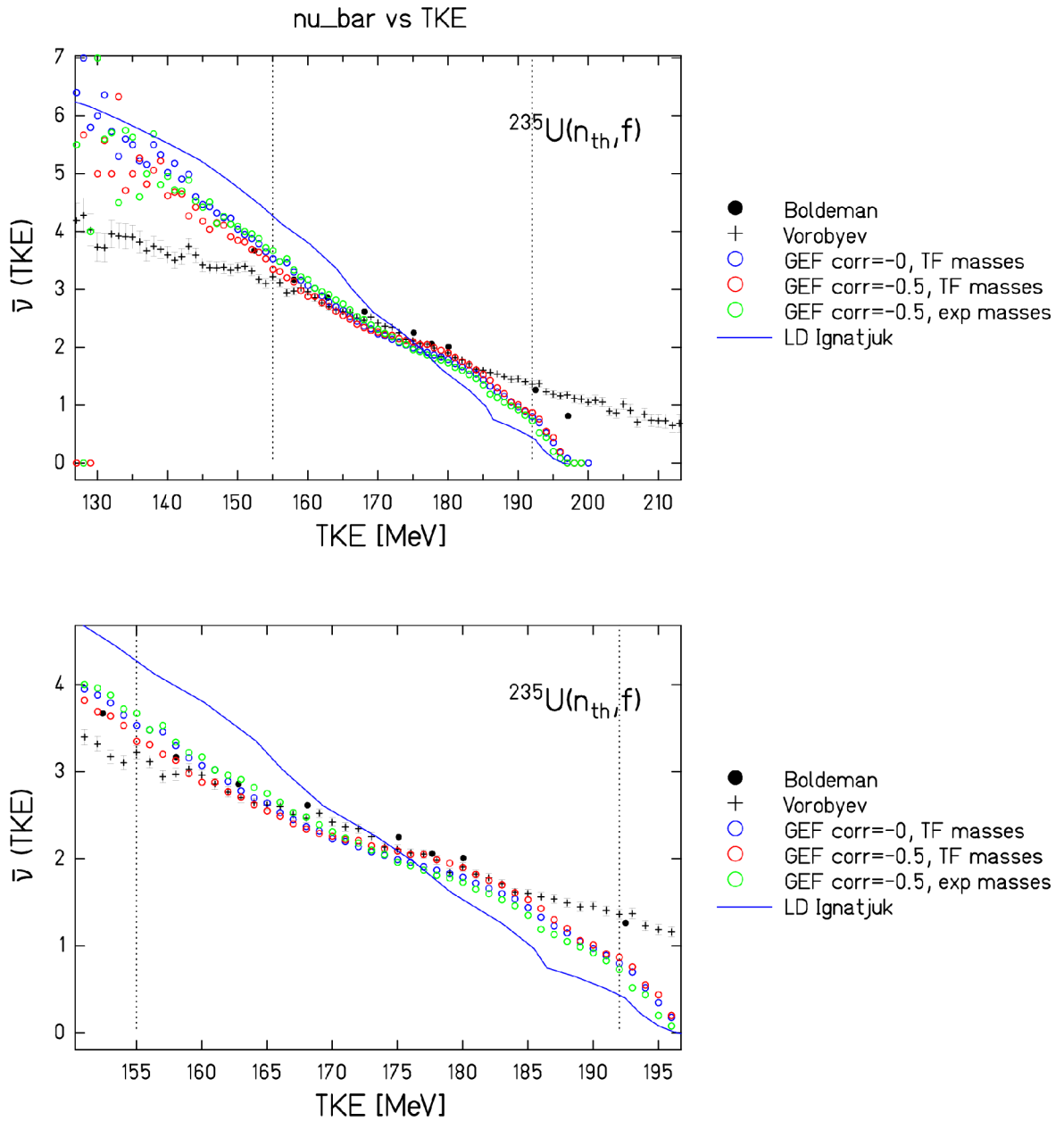


**Figure 1:** Mean prompt-neutron yield as a function of fission-fragment total kinetic energy for the system  $^{235}\text{U}(n_{th}, f)$ . The experimental data of Boldeman et al. [1] and Vorobyev et al. [2] are compared with a calculation of N. V. Kornilov [3] (labeled as “LD Ignatjuk”) and different results of the GEF code. The lower part shows a zoom on the central part of the TKE distribution. The dotted vertical lines denote the region which contains 95% of the fission events.

- 1 J. W. Boldeman et al. , Aust. J. Phys. 24 (1971) 821
- 2 A. S. Vorobyev, EXFOR41516
- 3 N. V. Kornilov, private communication, 20. 4. 2012
- 4 W. D. Myers, W. J. Swiatecki, Nucl. Phys. A 601 (1996) 141
- 5 A. S. Vorobyev, V. N. Dushin, F.-J. Hamsch, V. A. Jakovlev, V. A. Kalinin, A. B. Laptev, B. F. Petrov, O. A. Shcherbakov, AIP Conference Proceedings, Vol. 798, Issue 1 (2005) p. 255
- 6 F.-J. Hamsch, S. Oberstedt , Nucl. Phys. A 617 (1997) 347
- 7 C. Budtz-Jorgensen, H.-H. Knitter, Nucl. Phys. A 490 (1988) 307

## Comments about the partition of excitation energy between complementary fission fragments in connection with “A Chairman’s Note” of T.Ohsawa

Anabella Tudora

*University of Bucharest, Faculty of Physics, Bucharest-Magurele, RO-077125, Romania*

The very interesting Chairman’s Note of mister T.Ohsawa [1] regarding the question of excitation energy partition pushed me to write some comments about this theme that maybe can give “much food for thoughts”.

Regarding the energy sorting mechanism proposed by K-H.Schmidt and B.Jurado in Ref.[2], affirming that the nascent fragments cannot share the same temperature at scission, in Ref.[3] P.Talou and co-workers have written: this “stems from one assumption and one observation:

i) it is assumed that the nascent fragments near scission are already in their equilibrated ground-state shape and

ii) a formula for the temperature of the fragments is inferred from observed level densities.

The assumption of a constant temperature formula is best suited to low excitation energies and is part of the Gilbert-Cameron level density composite representation. However, the distribution of excitation energies in the fission fragments extends to higher energies for which the Fermi-gas formula might be a better representation” [3], as it was considered by a great part of physicists, for instance research groups from Dresda (A.Ruben et al), Los Alamos (P.Talou et al.), CEA-Cadarache (O.Serot and O.Litaize), Bucharest (A.Tudora et al.) and so on.

Concerning the energy sorting mechanism, as T.Ohsawa mentioned in [1]: “K-H Schmidt discussed, on the base of Egidy’s formula [4]:

$$T = A^{-2/3}(17.45 - 0.515S + 0.051S^2) \quad (1)$$

that the temperature of heavy fragments (HF) is lower than that of light fragments (LF) unless the shell effect S is large, which can explain the behaviour of experimental  $v(A)$  of Naqvi et al. [5] at 0.8 MeV and 5.5 MeV...the increase in  $v_{\text{tot}}$  is totally accounted for only by  $v_{\text{H}}$ .” This experimental fact is “interpreted by energy sorting in a superfluid system due to temperature difference  $T_{\text{L}} > T_{\text{H}}$ .”

**I.** A very simple exercise is to apply the Egidy-Bucurescu formula of Eq.(1), without to neglect the shell effects, to nuclei forming the fission fragment range of any fissioning system. Two examples of low-energy fission,  $^{252}\text{Cf}(\text{SF})$  and  $^{235}\text{U}(\text{n}_{\text{th}},\text{f})$ , are given in **Fig.1** where the temperatures of complementary fragments are plotted on the same grid line (with red circles for HF and blue squares for LF).

It can be observed in this figure that  $T_{\text{L}}$  is higher than  $T_{\text{H}}$  only for fragment pairs with  $A_{\text{H}}$  above 139-140. In the  $A_{\text{H}}$  region below 140 where shell effects are important,  $T_{\text{H}}$  is lower than  $T_{\text{L}}$ . As result of this fact, for fragment pairs with  $A_{\text{H}} < 140$ , the energy sorting fails to explain the behaviour of experimental  $v(A)$  of Naqvi et al. [5] showing an increase of only  $v_{\text{H}}$  over the entire  $A_{\text{H}}$  range, including the fragment pairs with  $A_{\text{H}}$  less than 140, for which, obviously, the shell effects are large.

Consequently at least a question arises: in order to support the energy sorting mechanism to explain the behaviour of experimental  $v(A)$  at 0.8 MeV and 5.5 MeV *it is possible to neglect the shell effects?*

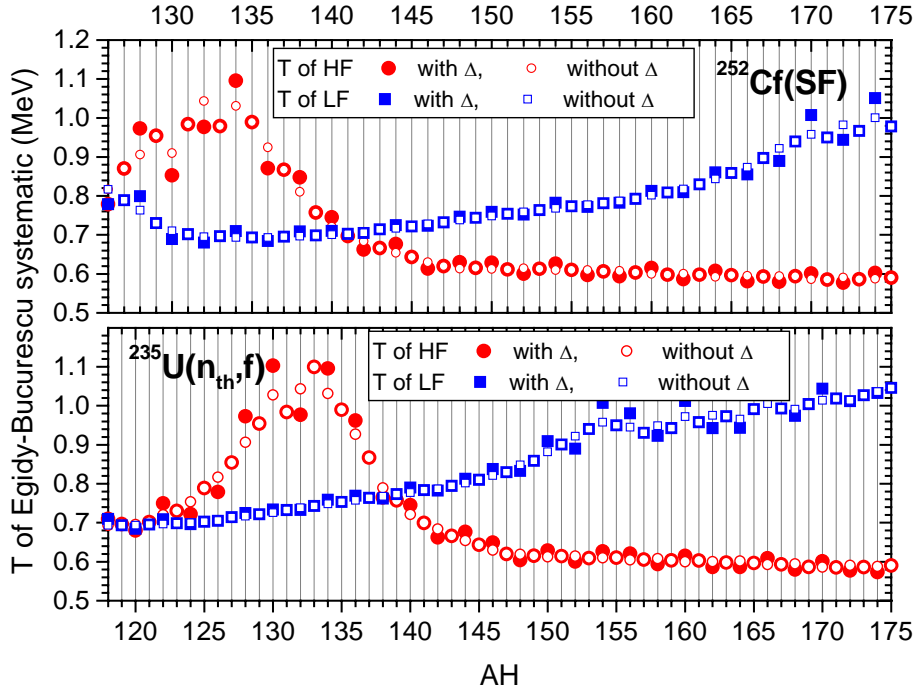


**Fig.1:** Constant  $T$  calculated by using the systematic Egidy-Bucurescu for the FF range of  $^{252}\text{Cf}(\text{SF})$  (upper part) and of  $^{235}\text{U}(n_{\text{th}},f)$  (lower part) as a function of the HF mass number.  $T$  values of HF are plotted with red circles and  $T$  of LF with blues squares (full symbols when shell corrections with pairing effects are taken into account, open symbols without pairing corrections). Temperatures of complementary fragments are placed on the same grid line.

**II.** More research groups consider that at scission the Fermi-Gas description of fragment level densities is more appropriate. In this case a straightforward assumption is to consider the nascent fragments in statistical equilibrium (equal nuclear temperatures  $\tau_L = \tau_H$  at scission). Under the Fermi-Gas assumption the excitation energy can be expressed as the product  $a\tau^2$  ( $a$  being the level density parameter). Consequently the available excitation energy at scission  $E_{sc}^*$  (or the intrinsic energy component, as in the work of Litaize and Serot [6]) can be shared between complementary nascent fragments according to the ratio:

$$E_L^*/E_H^* = a_L/a_H \quad \text{with } E_{sc}^* = E_L^* + E_H^* \quad (2)$$

(underlying again that this relation is valid and it is applied only at scission and not at full acceleration).

It is interesting to compare the ratio of level density parameters  $a_L/a_H$  provided by different models (for instance effective level density parameters given by the Gilbert-Cameron systematic and level density parameters provided by the generalized super-fluid model) with the inverse ratio  $T_H/T_L$  of constant temperatures provided by the Egidy-Bucurescu systematic, see **Fig.2** (where the ratios  $a_L/a_H$  are plotted with blue symbols and the ratio  $T_H/T_L$  with red symbols). The similar behaviour of the ratios  $a_L/a_H$  (blue symbols) and  $T_H/T_L$  (red symbols) is visible.

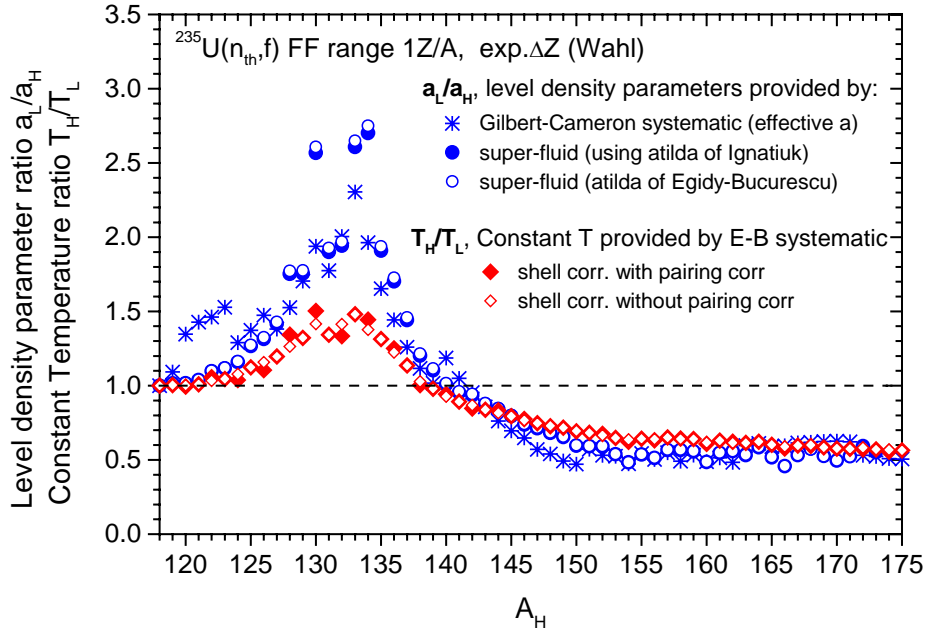


**Fig.2:** FF range of  $^{235}\text{U}(n_{th},f)$ : Ratio  $a_L/a_H$  provided by the super-fluid model (full and open blue circles) and by an effective level density parameter systematic (black stars). Ratio  $T_H/T_L$  provided by the systematic of Egidy-Bucurescu with and without pairing corrections (full and open red diamonds, respectively)

This fact *can lead to thoughts in connection with the two opposite assumptions at scission:*

a) level density description by the constant T formula and the use of the Egidy systematic of Eq.(1) *with the neglect of shell effects*, in order to support the energy sorting mechanism based on  $T_L > T_H$ .

b) level density description by the Fermi-gas formula and fragments in statistical equilibrium at scission leading to the possibility to share the excitation energy (or intrinsic energy) at scission according to the level density ratio of Eq.(2).

Regarding the fragment level density description by constant T and Fermi-gas, see also **Appendix 1**.

**III.** Maybe some additional comments regarding the fragment temperatures at scission and at full acceleration can be useful.

It was already established by many authors that at full acceleration the residual temperatures of complementary fragments are not equal. In this sense, 20 years ago T Ohsawa introduced the nice concept of average residual temperature ratio ( $RT = \langle T_L \rangle / \langle T_H \rangle$ ). We can speak about statistical equilibrium (equal temperatures) only at scission.

Consequently in the original Los Alamos (LA) model of Madland and Nix [7], taking into account the neutron emission from fully accelerated fragments and only one fragmentation (the so-called most probable one), it seems that the consideration of equal temperatures is wrong. In my opinion, the consideration in [7] of equal residual temperatures (or more precisely equal maximum values of the triangular residual temperature distributions  $P(T)$  of LF and HF) is not so wrong. Why? Because Madland and Nix take into account only the most probable fragmentation (usually placed around  $A_H = 140$ ). Or all experimental  $v(A)$  data of neutron induced fission at low energies exhibit almost equal number of neutrons emitted by fragment pairs with  $A_H$  around 140. In other words, taking into account that almost all prompt neutrons are emitted at full acceleration, this

means almost equal excitation energies of fully accelerated fragments of the most probable fragmentation. The level density parameters of LF and HF forming the most probable fragmentation calculated at full acceleration in the frame of the generalized super-fluid model have also close values (more details can be found in [8]). So, when only the most probable fragmentation is taken into account the consideration of equal residual temperature distributions at full acceleration is not a so bad assumption. Moreover Madland and Nix used the assumption of equal number of neutrons emitted by the LF and HF also in the calculation of the total prompt neutron spectrum and that is OK for the case of the most probable fragmentation.

When more fragmentations are taken into account (multi-modal approach or PbP model or other models based on Monte-Carlo treatments) the consideration of equal residual temperatures at full acceleration (as in the case of the hypothesis H2 of Ref.[9]) is a rough approximation and it is not true for the physical point of view (more details and comparative results are given in [8]).

In order to avoid the ambiguities related to models and assumptions at scission, we have developed a method of TXE partition (at fully acceleration) that is based on the systematic behaviour of experimental  $\nu(A)$  data of spontaneous and neutron induced fission at low energies, allowing parameterizations of  $\nu_H/(\nu_L+\nu_H)$  as a function of  $A_H$ . Assuming that in the low energy fission all prompt neutrons are emitted at full acceleration, the TXE was partitioned according to the ratio  $\nu_L/\nu_H$  using the parameterization mentioned above. This method is described in [8]. The ratios  $RT(A_H)$  resulted from the use of this method are in good agreement with the RT ratio proposed by Litaize and Serot in [6].

Another method of TXE partition recently published (see Ref.[10]) accounts of assumptions and models at scission and consists in two steps as following:

1) the calculation of the additional deformation energy of nascent LF and HF at scission considering that at scission the fragments are more deformed than at full acceleration (this additional deformation energy being dissipated into excitation energy at full acceleration)

2) the available excitation energy at scission is obtained by subtracting the additional deformation energies (obtained in the step 1) from TXE, and it is shared between the nascent fragments assuming the statistical equilibrium (equal nuclear temperatures  $\tau_L=\tau_H$  at scission) and the Fermi-gas description of the level density of fragments.

Finally the excitation energy of a fragment at full acceleration is obtained as a sum of the additional deformation energy (step1) and the excitation energy at scission (step2).

Using this new method of TXE partition the resulted residual temperature ratios  $RT(A_H)$  [10] are in agreement with the ratios  $RT(A_H)$  reported in Refs. [6, 8].

The nice and very simple ratio proposed by Talou et al. in Ref.[3] (Eq.(9)):

$$d_{LH} = \frac{[(d-r)/r]_L}{[(d-r)/r]_H} = \frac{(N - N_L) + (P - Z_L)}{(N - N_H) + (P - Z_H)} \quad (3)$$

(where N and P have values 28, 50 or 82 depending on their proximity to the corresponding spherical closed shells)

also can help in the effort to predict  $RT(A_H)$  by avoiding complicate calculations at scission. The  $RT(A_H)$  of  $^{239}\text{Pu}(n_{th},f)$  given by Talou et al. in Fig.9 of [3] has a shape almost similar with  $RT(A_H)$  reported in Refs. [6, 8, 10].

Consequently it is interesting to observe that even if the ways to obtain the residual temperature ratio  $RT(A_H)$  at full acceleration used by 3 teams (Serot&Litaize, Tudora et al, Talou et al.) are different, the results are practically similar.

IV. The interesting behaviour of  $\nu(A)$  consisting in the increase of  $\nu_H$  only (proved experimentally by the Naqvi data at 0.8 MeV and 5.5 MeV) was predicted six years ago and reported in Ref.[11] where PbP calculations of  $\nu(A)$  at many En exhibit this behaviour, as it can be seen in the lower part of Fig.13 of Ref.[11] reproduced here as Fig.3.

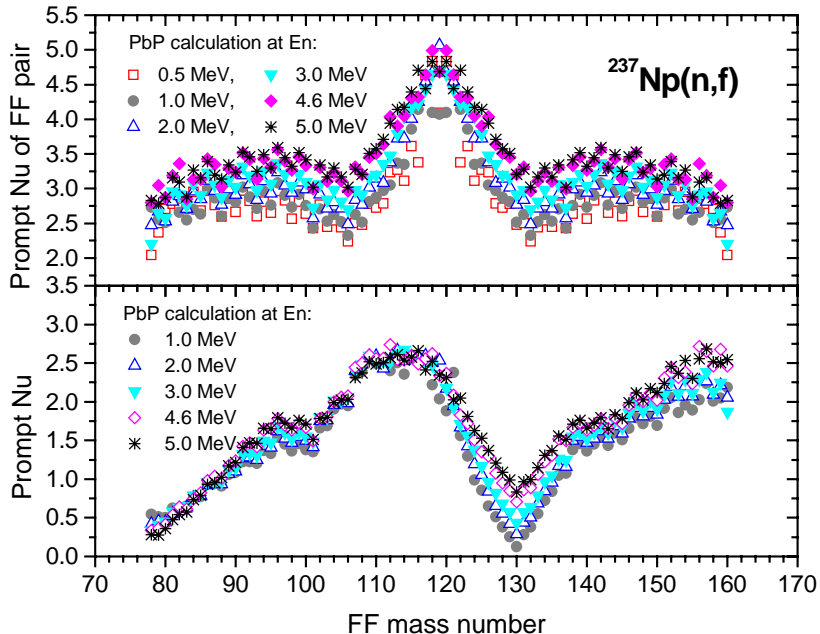


**Fig.3:** PbP calculation of the FF pair multiplicity and  $\nu(A)$  for  $^{237}\text{Np}(n,f)$  at more incident energies. Reproduction of Fig.13 of Ref.[11]

In the case of  $^{240}\text{Pu}$ , fissioning from the ground state (the case of  $^{240}\text{Pu}(\text{SF})$ ) and from the excitation energy  $B_n=6.5335$  MeV (the case of  $^{239}\text{Pu}(n_{\text{th}},f)$ ) the  $\nu(A)$  calculations performed by O.Serot and given in Fig.3 of [1] do not show the behaviour mentioned above.

In my knowledge *experimental  $\nu(A)$  data for  $^{240}\text{Pu}(\text{SF})$  do not exist*. So, the behaviour of  $\nu(A)$  with increasing of excitation energy cannot be proved experimentally in the case of the fissioning nucleus  $^{240}\text{Pu}$ . The data plotted in Fig.3 of [1] are the results of Monte-Carlo calculations (made with the code Fifrelin developed by the group of Cadarache) using as input the experimental fragment distributions of Wagemans et al., and cannot be validated by comparison with experimental data.

In the GEF code description given in Ref.[12] the following very nice and simple global expressions for the deformation of the nascent fragments in the light and heavy groups are reported:

$$\beta_{LF} = 0.04(Z_{LF} - 26.6), \quad \beta_{HF} = 0.035(Z_{HF} - 48) \quad (4)$$

These global expressions of  $\beta_2$  deformation parameters are used in the following exercises to calculate the additional deformation energy of nascent fragments in the frame of the TXE partition method described in [10].

The  $E^*(A)$  results at full acceleration for  $^{235}\text{U}(n_{\text{th}},f)$  and  $^{252}\text{Cf}(\text{SF})$ , obtained by using the  $\beta_2$  parameterizations of K-H.Schmidt and B.Jurado [12] (given in Eqs.(4)), plotted with blue stars in

**Figs. 4 and 5**, respectively, are in agreement with the “indirect” experimental data and are rather close to the  $E^*(A)$  results reported in [10] (red circles).

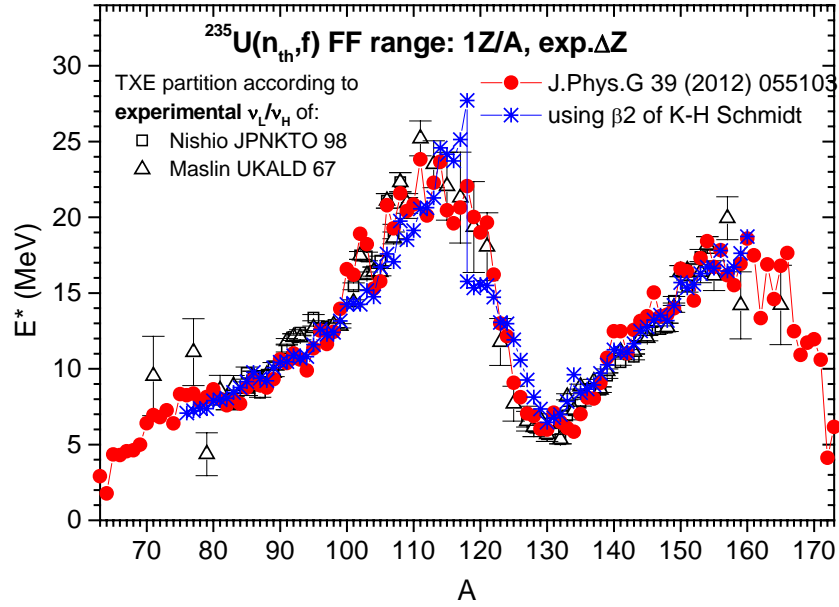


**Fig.4:**  $^{235}\text{U}(n_{th}, f)$   $E^*(A)$  obtained by using the  $\beta_2$  parameterizations of [12] in the frame of the same method as in [10] (blue stars) in comparison with  $E^*(A)$  reported in [10] (red circles) and “indirect” experimental data obtained as described in [10] (open symbols).

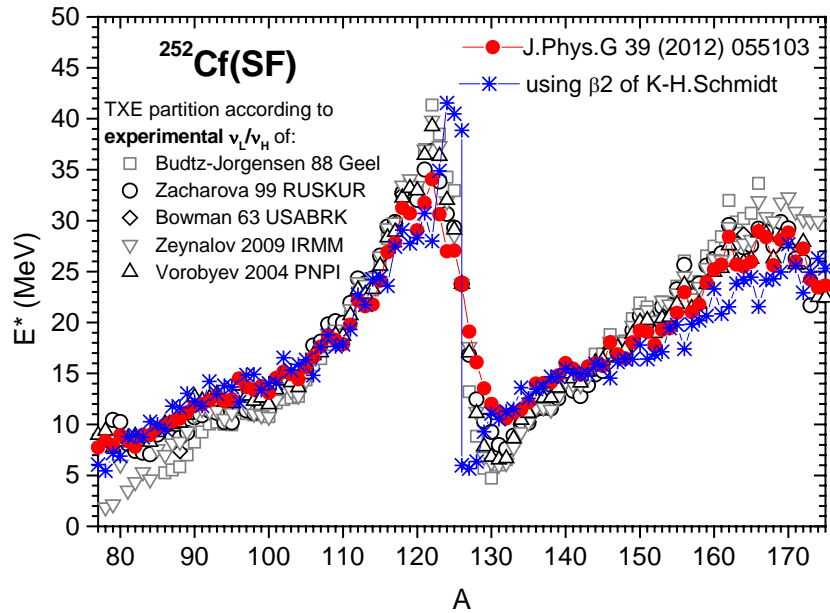


**Fig.5:**  $^{252}\text{Cf}(\text{SF})$ :  $E^*(A)$  obtained by using the  $\beta_2$  parameterizations of [12] in the frame of the same method as in [10] (blue stars) in comparison with  $E^*(A)$  reported in [10] (red circles) and “indirect” experimental data obtained as described in [10] (open symbols).

This fact encouraged me to consider the simple parameterizations proposed by K.H.Schmidt and B.Jurado [12] as an appropriate global description of the  $\beta_2$  deformation parameters of nascent fragments. Moreover the use of the global expressions (4) in the frame of the TXE partition method of [10] has the advantage to reduce significantly the amount of calculations.

Consequently I extended this exercise to the case of  $^{237}\text{Np}(n,f)$  at  $E_n = 0.8$  MeV and 5.5 MeV. The  $E^*(A)$  results obtained by using the  $\beta_2$  of Eqs.(4) are plotted with magenta and cyan symbols connected with lines in **Fig.6** in comparison with the  $E^*(A)$  reported in [10] (red and blue symbols connected with lines) and the “indirect” experimental  $E^*(A)$  of Naqvi and Mueller (black and gray symbols). Especially for  $E_n = 0.8$  MeV the use of these global  $\beta_2$  leads to  $E^*(A)$  results close to the ones previously reported (see in Fig.6 the red and magenta points connected with lines that are very close each other in the ranges  $A_L < 105$  and  $A_H > 130$ ).

As it can be seen, in the case of present  $E^*(A)$  results the increase with the incident energy is visible for heavy fragments. Though an increase of  $E^*(A)$  is observed for light fragments with  $A_L$  between 100-119, while for the other light fragments with  $A_L < 100$   $E^*(A)$  can be considered practically constant with  $E_n$ . So, the use of  $\beta_2$  global expressions of [12] in the frame of the TXE partition method [10] can support the behaviour of experimental  $v(A)$  at  $E_n = 0.8$  and 5.5 MeV.

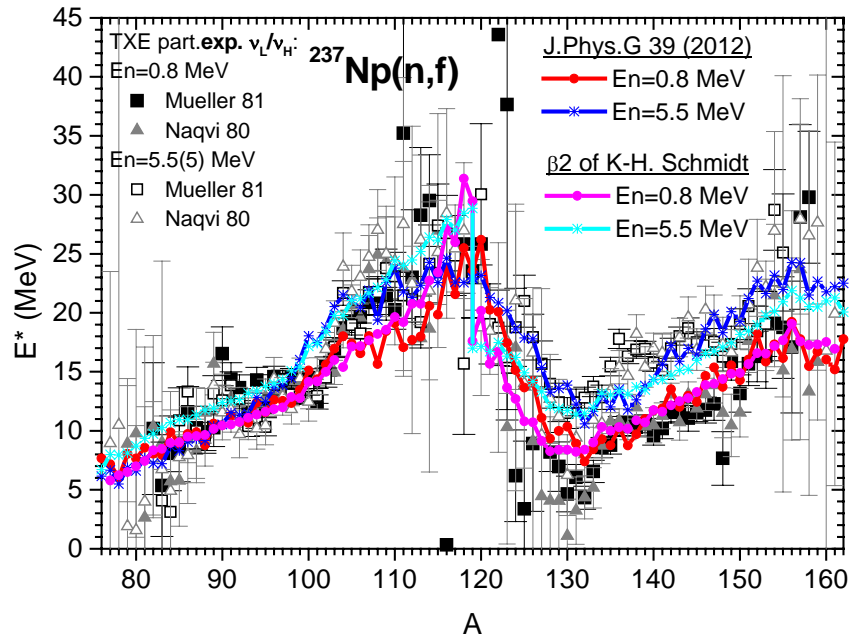


**Fig.6:**  $^{237}\text{Np}(n,f)$ :  $E^*(A)$  obtained by using the  $\beta_2$  of [12] in the frame of the same method as in [10] (magenta circles for  $E_n=0.8$  MeV and cyan stars for  $E_n=5.5$  MeV) in comparison with  $E^*(A)$  calculations reported in [10] (red circles for  $E_n=0.8$  MeV and blue stars for  $E_n=5.5$  MeV) and “indirect” experimental data obtained as described in [10] (black and gray full symbols for  $E_n=0.8$  MeV and open symbols for  $E_n=5.5$  MeV).

In the case of  $^{239}\text{Pu}(n_{th},f)$   $E^*(A)$  resulted by using the global expressions of  $\beta_2$  proposed by K.H.Schmidt and B.Jurado [12] in the frame of the TXE partition method of [10] are plotted with blue circles in **Fig.7**. As it can be seen the present  $E^*(A)$  are close to our results of [10] (red circles) and describe rather well the “indirect” experimental data (different open symbols). So, in the case of  $^{239}\text{Pu}(n_{th},f)$  the  $\beta_2$  parameterizations of [12] are working well, too.

For this reason I have extended the same calculation ( $\beta_2$  of [12] in the frame of the method of [10]) in the case of  $^{240}\text{Pu}(\text{SF})$ , the results being given with blue stars in the same figure. As observation, in this exercise in both cases,  $^{239}\text{Pu}(\text{n}_{\text{th}},\text{f})$  and  $^{240}\text{Pu}(\text{SF})$ , the same experimental TKE(A) distribution of Wagemans et al. was used. Taking into account that the fission fragment range is the same in both cases, the difference in TXE for each pair of fragments is given only by Bn.

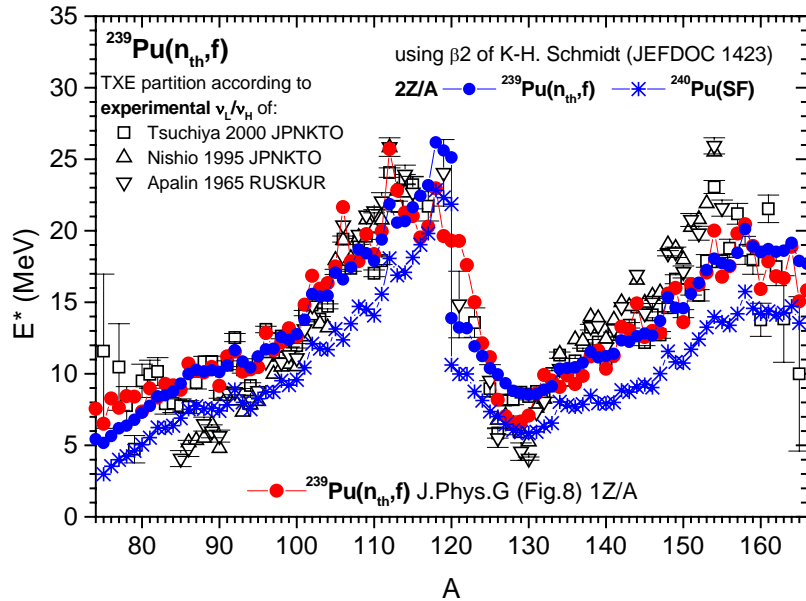


**Fig.7:**  $^{239}\text{Pu}(\text{n}_{\text{th}},\text{f})$ :  $E^*(A)$  obtained by using the  $\beta_2$  of [12] in the frame of the same method as in [10] (blue circles) in comparison with  $E^*(A)$  reported in [10] (red circles) and “indirect” experimental data of [10] (open symbols).  $E^*(A)$  of  $^{240}\text{Pu}(\text{SF})$  obtained by using the  $\beta_2$  parameterizations of [12] in frame of the method [10] are plotted with blue stars.

Looking at the behaviour of present  $E^*(A)$  results in Fig.7 (blue circles and stars), the  $E^*(A)$  increase with the excitation energy of the fissioning nucleus  $^{240}\text{Pu}$  is visible for both heavy and light fragments, being a little bit more pronounced for the heavy fragments, especially for  $A_{\text{H}} > 135$ .

In the case of  $^{240}\text{Pu}$  undergoing fission from the ground state (SF) and from the excitation energy  $B_n = 6.5335$  MeV ( $\text{n}_{\text{th}},\text{f}$ ) the  $E^*(A)$  results of the present simple exercise as well as the  $\nu(A)$  calculations reported by O.Serot (given in Fig.3 of the Chairman’s note [1]) do not exhibit the behaviour of  $E^*(A)$  and  $\nu(A)$  obtained in the case of  $^{237}\text{Np}(\text{n},\text{f})$  at  $E_n$  of 0.8 and 5.5 MeV. **Why ?**

In the present exercise more aspects can be suspected, as following:

i) the TXE partition method of [10]. But it is not the case because this method was successfully verified in many cases as it was reported in [10].

ii) the global parameterizations of  $\beta_2$  proposed by Schmidt and Jurado [12]. But again it is not the case because these parameterizations were also verified and are working well in the frame of the method [10], see the present results in good agreement with the experimental data and the results of [10] for  $^{235}\text{U}(\text{n}_{\text{th}},\text{f})$ ,  $^{242}\text{Cf}(\text{SF})$ ,  $^{237}\text{Np}(\text{n},\text{f})$  at 0.8 and 5.5 MeV and  $^{239}\text{Pu}(\text{n}_{\text{th}},\text{f})$ .

iii) The use of the same experimental TKE(A) distribution for both  $^{239}\text{Pu}(\text{n}_{\text{th}},\text{f})$  and  $^{240}\text{Pu}(\text{SF})$ . But again it is not the case because all experimental TKE(A) data sets for  $^{239}\text{Pu}(\text{n}_{\text{th}},\text{f})$  and  $^{240}\text{Pu}(\text{SF})$  are very close each other and the use of different TKE(A) data does not change significantly the results.

It remains to suspect a mischief of the Maxwell’s demon (as mister T.Ohsawa said [1])?

Thanks to colleagues of the RCM for suggestions and answers in connections with the present comments.

## References:

1. T. Ohsawa “*A Chairman’s Note*” (2012)
2. K.H. Schmidt and B.Jurado, *Phys.Rev.Lett.* 104 (2010) 212501
3. P.Talou, B.Becker, T.Kawano, M.B.Chadwick, Y.Danon, *Phys.Rev.C* 83 (2011) 064612
4. T. von Egidy and D.Bucurescu, *Phys.Rev.C* 72 (2005) 044311
5. A.A.Naqvi et al., *Phys.Rev.C* 34 (1986) 218 and electronic files retrieved from EXFOR.
6. O.Litaize, O.Serot, *Phys.Rev.C* 82 (2010) 054616
7. D.G.Madland, J.R.Nix, *Nucl.Sci.Eng.* 81 (1982) 213-271
8. C.Manailescu, A.Tudora, F-J.Hambsch, C.Morariu, S.Oberstedt, *Nucl.Phys.A* 867 (2011) 12-40
9. S.Lemaire, P.Talou, T.Kawano, M.B.Chadwick, D.G.Madland, *Phys.Rev.C* 72 (2005) 024601
10. C.Morariu, A.Tudora, F-J.Hambsch, S.Oberstedt, C.Manailescu, *J.Phys.G: Nucl.Part Phys.* 39 (2012) 055103
11. A.Tudora, *Ann.Nucl.Energy* 33 (2006) 1030-1038
12. K-H. Schmidt, B.Jurado, “Prompt-neutron and prompt-gamma emission from a general description of the fission process”, *JEF/DOC 1423* (2012). GEF code OECD-NEA-Data Bank (CPC), package *NEA-1864/03*.

## Appendix 1

As I was already mentioned during the RCM, the level density description by constant T and Fermi-gas formulae gives practically the same results at excitation energy values emerging at scission. This fact is exemplified here for two nuclei ( $^{138}\text{Xe}$  and  $^{95}\text{Sr}$ ), appearing as fission fragments and having level schemes with enough levels to allow the comparison of cumulative numbers.

As it can be seen in **Fig.A1** the cumulative number of levels obtained by using the composite Gilbert-Cameron formula (constant T up to the matching energy  $E_m$  and Fermi-gas above  $E_m$ ), plotted with red line, and the cumulative number obtained by using only the constant T formula, plotted with blue dashed line, are practically the same up to a few MeV above  $E_m$  (indicated by arrows, too).

Not only the cumulative numbers but also the total level densities  $\rho(E^*)$  exhibit the same behaviour, constant T and Fermi-gas giving practically the same total level density in the energy range of about 2-3 MeV above the matching energy value, see **Fig.A2**.

This known fact, valid for many nuclei appearing as fission fragments, can be the basis of a possible prolongation of the energy range where the constant T function is working. As observation, in this example we have used the T-values provided by the Egidy systematic Eq.(1) in order to be under the same assumption used to support the energy sorting mechanism [2].

So, both formulae, constant T and Fermi-gas, giving practically the same cumulative number and total level density in the excitation energy range of interest at scission, can be taken as appropriate descriptions of fragment level densities at scission...

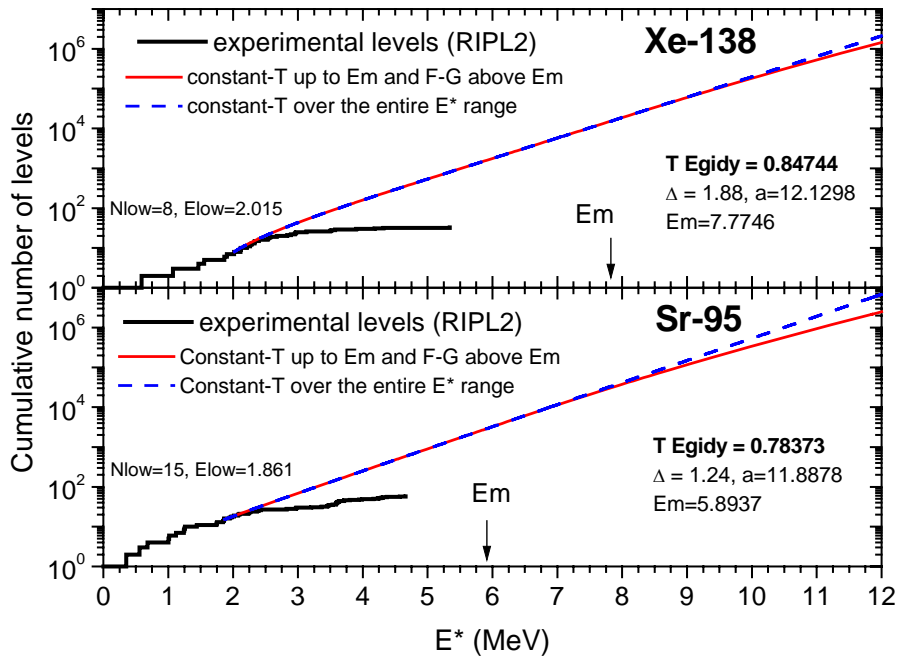


**Fig.A1:** cumulative number of levels for  $^{138}\text{Xe}$  (upper part) and  $^{95}\text{Sr}$  (lower part): obtained from level schemes with black line, calculated by using the composite Gilbert-Cameron formula with red line and only the constant T formula with blue dashed line.

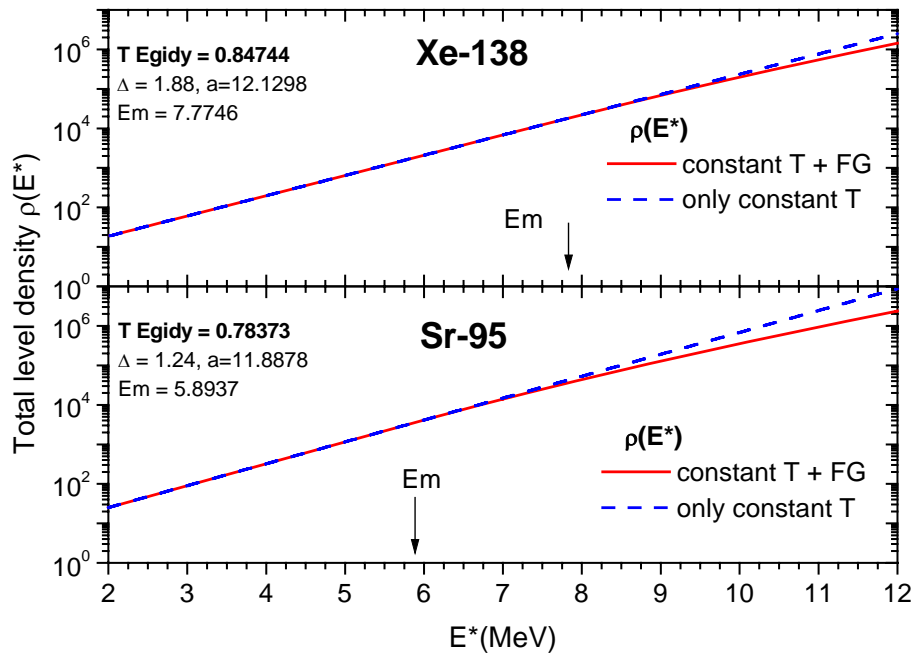


**Fig.A2:** Total level density for  $^{138}\text{Xe}$  (upper part) and  $^{95}\text{Sr}$  (lower part) calculated by using the composite Gilbert-Cameron formula with red line and only the constant T formula with blue dashed line.



---

Nuclear Data Section  
International Atomic Energy Agency  
Vienna International Centre, P.O. Box 100  
A-1400 Vienna  
Austria

e-mail: [NDS.Contact-Point@iaea.org](mailto:NDS.Contact-Point@iaea.org)  
fax: (43-1) 26007  
telephone: (43-1) 2600-21725  
Web: <http://www-nds.iaea.org>

---